Dielectric relaxation study of the cellulose solvent system LiCl/N,N-dimethylacetamide

Dissertation
zur Erlangung des Grades
Doktor der Naturwissenschaften
(Dr. rer. nat.)
der Naturwissenschaftlichen Fakultät IV
Chemie und Pharmazie
der Universität Regensburg

vorgelegt von
Sarka Fernandez

Regensburg 2003

Promotionsgesuch eingereicht am:	17. November 2003
Tag des Kolloquiums:	18. Dezember 2003
Die Arbeit wurde angeleitet von:	Prof. Dr. W. Kunz
Prüfungsausschuss:	Prof. Dr. N. Korber Prof. Dr. W. Kunz PD Dr. R. Buchner Prof. Dr. B. König

Patrick und meinen Eltern

Contents

Vorwort

Diese Doktorarbeit entstand in der Zeit von November 2000 bis November 2003 am Institut für Physikalische und Theoretische Chemie – der naturwissenschaftlichen Fakultät IV – Chemie und Pharmazie – der Universität Regensburg.

An erster Stelle möchte ich mich besonders bei Herrn Prof. Dr. Kunz für die Erteilung des Themas, seine großzügige Unterstützung und sein Interesse am Fortschreiten der Arbeit bedanken.

Weiterhin gilt mein Dank vor allem Herrn Dr. R. Buchner und Herrn Dr. D. Touraud für ihre stete Bereitschaft zur wissenschaftlichen Diskussion, ihre wertvollen Ratschläge und ihren freundschaftlichen Umgang nicht nur während der Arbeitszeit. Mein Dank gebührt auch meinem Mitarbeiter aus der Mikrowellen-Gruppe Herrn Dipl.-Chem. S. Schrödle für seine außerordentliche Hilfsbereitschaft und Kollegialität, die das Fertigstellen meiner Doktorarbeit erleichtert haben.

Bei allen anderen Mitarbeitern des Lehrstuhls möchte ich mich für die gute Atmosphäre und zahlreiche Hilfe bedanken. Namentlich möchte ich Herrn Dr. N. Papaiconomou, Frau Dr. M-L. Touraud-Navarro, Herrn Dipl.-Chem. P. Bauduin, Frau Dipl.-Chem. A. Renoncourt, Herrn Dipl.-Chem. J. De Roche, Herrn Dipl.-Biophys. D. Zimin, Frau Dipl.-Chem. B. Widera, Herrn W. Simon und den Gastwissenschaftler Herrn Dr. T. Sato hervorheben.

Da ein Teil dieser Arbeit in Kooperation mit dem Christian-Doppler-Labor der Universität für Bodenkultur in Wien durchgeführt wurde, möchte ich dessen Mitarbeitern Herrn Dr. T. Rosenau und Frau Dr. A. Potthast für ihre Einführung in das Thema Cellulose, ihre große Hilfsbereitschaft, und schließlich auch für die Celluloseproben selbst danken.

Nicht zuletzt möchte ich allen Mitarbeitern der Werkstätten (insbesondere Herrn Dipl.-Ing. H. Frey) für die schnelle und gewissenhafte Erledigung der Aufträge meinen Dank aussprechen.

Am Ende möchte ich mich vom ganzen Herzen bei meinem Mann, ehemaligem Mitglied der Mikrowellen-Gruppe, Herrn Dr. P. Fernandez, nicht nur für seine Hilfe bei der Einarbeitung in das MW-Gebiet bedanken, sondern vor allem für seine Geduld und Unterstützung während der Endphase meiner Doktorarbeit.

Constants and symbols

Constants

Elementary charge	e_o	$= 1.60217739 \cdot 10^{-19}\,\mathrm{C}$
Electric field constant	ε_o	$= 8.854187816 \cdot 10^{-12}\,\mathrm{C^2(Jm)^{-1}}$
Avogadro's constant	N_A	$= 6.0221367 \cdot 10^{23}\,\mathrm{mol^{-1}}$
Speed of light	c	$= 2.99792458 \cdot 10^{8}\,\mathrm{m\,s^{-1}}$
Boltzmann's constant	k_B	$= 1.380658 \cdot 10^{-23}\,\mathrm{J\,K^{-1}}$
Permittivity of vacuum	μ_0	$= 4\pi \cdot 10^{-7}\,\mathrm{(Js)^2(C^2m)^{-1}}$
Planck's constant	h	$= 6.6260755 \cdot 10^{-34}\,\mathrm{Js}$

Symbols

$\vec{B}$	magnetic induction ($\mathrm{Vs\,m^{-2}}$)	$\vec{D}$	electric induction ($\mathrm{C\,m^{-2}}$)
ω	angular frequency ($\mathrm{s^{-1}}$)	$\vec{j}$	current density ($\mathrm{A\,m^{-2}}$)
$\vec{E}$	electric field strength ($\mathrm{V\,m^{-1}}$)	$\hat{\varepsilon}$	complex dielectric permittivity
$\vec{H}$	magnetic field strength ($\mathrm{A\,m^{-1}}$)	ε'	real part of $\hat{\varepsilon}$
$\vec{P}$	polarization ($\mathrm{C\,m^{-2}}$)	ε''	imaginary part of $\hat{\varepsilon}$
τ	relaxation time (s)	ε_∞	$\lim_{\nu\to\infty}(\varepsilon')$
η	viscosity (Pa s)	ε	$\lim_{\nu\to 0}(\varepsilon')$
T	temperature (K)	μ	dipole moment (C m)
t	time (s)	ν	frequency (Hz)
c	molarity ($\mathrm{mol\ dm^{-3}}$)	m	molality ($\mathrm{mol\ kg^{-1}}$)
κ	conductivity ($\mathrm{S\ m^{-1}}$)	ρ	density ($\mathrm{kg\,m^{-3}}$)
CIP	contact ion pair	SIP	solvent-shared ion pair
PSIP	penetrating solvent-shared ion pair	2SIP	solvent-separated ion pair
DMA	N,N-dimethylacetamide	DMF	N,N-dimethylformamide
AGU	Anhydroglucose unit	M	molecular weight ($\mathrm{g\ mol^{-1}}$)

Chapter 1

Introduction

1.1 General comments

Cellulose, with its annual photosynthetic production estimated to 10^{11} - 10^{12} t, belongs to the most abundant natural polymers on earth [1]. From the very beginning cellulose has played an important role in the development of human civilization. It has been used in the form of wood as energetic source, construction material or for the manufacture of textile fibers from plants like flax, cotton, etc. The industrial revolution and the development of organic chemistry in the 19th century enabled the isolation, identification of the structure and later modification of this highly interesting polymer [2]. In present it is used for the production of paper, board, the manufacture of textile fibers and the pure forms of cellulose for the synthesis of cellulose derivatives. Many of them serve as textile fibers but can be utilized also as membranes, additives for colloidal suspensions, in the food industry, etc. [3]. The future prospects of cellulose as renewable resource for many industrial branches in comparison to finite reserves of oil, natural gas or coil are good. Also the ecological aspect of the biodegradability of most cellulose-based products should be mentioned. In order to use better the outstanding properties of this polymer some optimization of the industrial processes (especially regarding the isolation of cellulose from wood sources and its further modification) is required [2]. However, the number of solvents able to dissolve cellulose is limited and the majority of them reacts with the hydroxyl groups of cellulose which leads to the degradation of cellulose samples [1].

LiCl/DMA (N,N-dimethylacetamide) solutions belong to a small group of nondegrading solvents of cellulose [1]. They were first applied for the solubilization of cellulose in 1979 by McCormick et.al. [4] and since then established as a powerful solvent system for polysaccharides in general. Especially its use in the analysis [5] and its application in the preparation of cellulose derivatives seems to be promising [6]. However, there is still some disagreement about the conditions under which this solvent should be applied [7, 8] and to which extent water is involved in the solubilization process. Because a literature survey revealed that the information about the LiCl/DMA system itself is rather scarce, a major part of this work concentrated on the solvent system itself.

As the experimental technique dielectric relaxation spectroscopy (DRS) was chosen. This method operating in a broad frequency range (from 10^{-3} to 10^{11} Hz) enables the investigation of a large number of processes related to the molecular structure of the studied material. It determines the magnitude and time-dependency of electric polarization by measuring the changes of the polarizability of the material placed into a weak electromagnetic field. Depending on the equipment samples in all forms from solids to liquids can be investigated. DRS is applied e.g. in polymer research [9] for the interpretation of the conformation or configuration of polymers, in pharmaceutical and biological sciences [10, 11] for quality control, in the determination of structural characteristics of gels, proteins, emulsions, or various states of water in the samples. With the help of the DRS also such complex systems as biological membranes, colloidal suspensions and other heterogenous systems can be studied [12]. Besides these applications this technique proved to be a convenient and appropriate tool for studies of solvents and electrolyte solutions [13]. Its working frequency range in the GHz-scale corresponds well to relaxation processes resulting from the molecular reorientation, ion-cloud and ion-pair relaxation. In our laboratory the combination of the time domain reflectometry (TDR) and frequency-domain interferometry (FDI) is used in order to cover sufficient frequency range. The combination of both methods was in the past successfully applied to the investigation of different amides [14] and electrolyte/amide solutions [15].
In the first part of this work a short introduction into the field of cellulose dissolution is presented. The advantages and disadvantages of the LiCl/DMA system as a solvent for cellulose are presented and commented there as well. Since temperature seems to play an important role in the solubilization process, temperature dependent DRS-measurements of LiCl/DMA solutions were carried out during this work. Further DRS-spectra of aqueous LiCl solutions and in the presence of both solvents were recorded. Additionally phase diagrams investigating the solubilization of cellulose in LiCl/DMA solutions were provided and the influence of temperature and water content was demonstrated.

1.2 Cellulose

Each year hundreds of publications and plenty of patents are released dealing with this polymer. The following chapter does not intend to cover the whole spectrum of this research field as cellulose was only in a specific way involved in this work. Only aspects relevant to our study are listed here. The majority of the following information can be obtained in various monographs reporting on cellulose chemistry, see [1, 2, 16].

1.2.1 Sources

The main source of cellulose represent various woody plants (soft and hard woods, wheat, straw, bamboo) where cellulose is present as a composite with lignin and other polysaccharides (hemicelluloses) in their cell wall. In this case cellulose can be obtained by delignification with different processes (sulfite, sulfate or Organocell method) in the form of pulp. Rather pure form of cellulose can be obtained from the hair or seeds of textile plants like cotton, ramie, jute or flax. The content of cellulose in these sources strongly depends on their origin and the isolation procedure. In the case of cotton the cellulose content is about 95 %, in wood about 40 %. For scientific purposes cellulose produced extracellularly by some bacteria can be used (e.g. *Acetobacter xylinum*).

1.2.2 Structure

Due to its different functions in nature the structure of cellulose is very complex and has a deciding influence on its reactivity and availability for chemical modifications. For the correct interpretation of cellulose properties, the structure has to be considered on three structural levels: the molecular, supramolecular and morphological level [1, 2].
Pure cellulose is composed of D-anhydroglucopyranose units (AGU), linked together by β-(1,4)-glycosidic bonds as shown in figure 1.1.

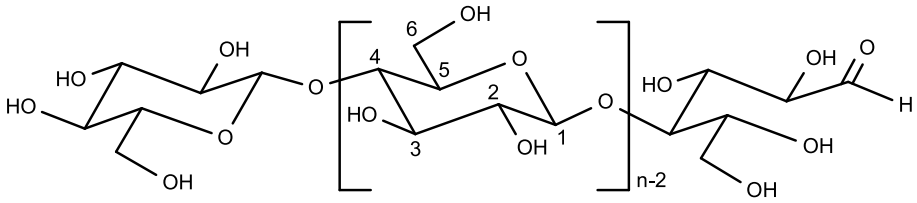

Figure 1.1: Molecular structure of cellulose with the reducing and non-reducing end group.

Each of the AGUs possesses hydroxyl groups at C-2, C-3 and C-6 positions, showing the typical behavior of primary and secondary alcohols. A different behavior can be expected from the hydroxyl groups at the end of the chains: the C-1 end possesses reducing and the C-4 non-reducing properties. The conformation of the AGU is $^4C_1$ chair as derived from NMR and X-ray diffraction studies [17]. The free hydroxyl groups are positioned in the

ring plane (equatorial) and the hydrogen atoms in vertical position (axial) which represents the conformation with the lowest energy for β-D-glucopyranose, see [18].
The number of AGUs in the cellulose, n, represents the so called average degree of polymerization (DP) and is used as characteristics for cellulose samples. The average molecular mass can be then obtained as product of the DP and the molecular mass of AGU. The DP strongly depends on the origin of the cellulose, the isolation method and the technique used for measurement [2]. It should be noted that the native cellulose samples are always polydisperse consisting of macromolecules with differing chain lengths which is typical for all native polymers [1].
The present hydroxyl groups form an network of intra- and intermolecular hydrogen bonds (H-bonds) which is responsible for the stiffness and stability of the cellulose chains. The most common crystalline modifications of cellulose are cellulose I and II. According to X-ray measurements two intramolecular H-bonds are formed in cellulose I between the neighboring AGUs (O-3-H and O-5' and O-2'-H and O-6) and so only one intermolecular hydrogen-bond is present [19].

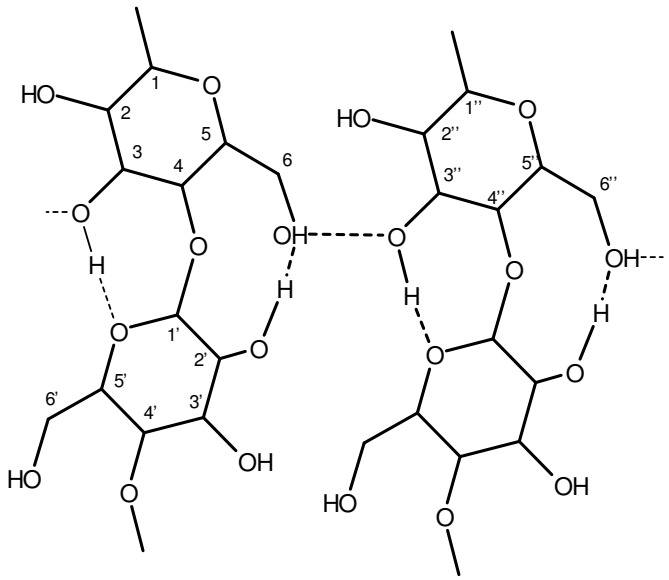

Figure 1.2: Schematic presentation of the probable intra- and intermolecular hydrogen-bonds situated in the cellulose I crystal lattice (as suggested in ref. [19]).

In fig. 1.2 the possible hydrogen-bond pattern of cellulose I is shown. In the case of cellulose II only one intramolecular H-bond is expected between O-3-H and O-5' due to the different conformation of the primary hydroxyl group [20]. The chains form in both cases a 1,2-helix [19, 21]. The intermolecular H-bond between O-6-H and O-3" of another chain seems to be the strongest hydrogen bond, having the largest cohesion effect [22].

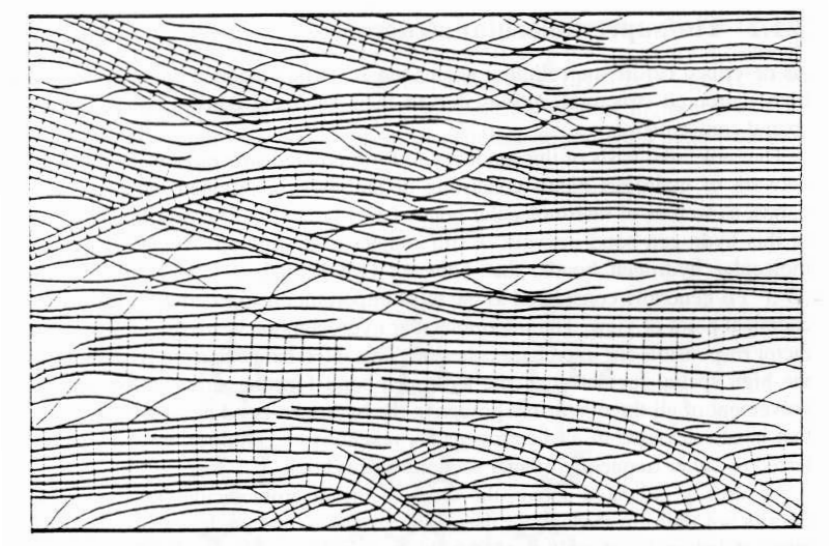

Figure 1.3: Fringed fibril model of cellulose supramolecular structure according to Hearle [23], adopted from [1].

The ability of the hydroxyl groups to form secondary valence hydrogen bonds with one another is also responsible for the tendency of cellulose chains to form highly ordered aggregates. When considering the structure of cellulose on the supramolecular level it is important to keep in mind that the local order of the macromolecules in cellulose is not uniform throughout the whole structure. Cellulose chains aggregate to elementary fibrils which are then the basis of the morphological structures. Their structure can be described by a two-phase model as composed of low ordered ('amorphous') and highly ordered ('crystalline') regions [23]. This is the main principle of the so called fringed fibril model shown in fig. 1.3. Cellulose samples can be characterized by the so called degree of crystallinity representing the relative amount of polymer within the highly ordered regions. These values are usually obtained by the wide-angle X-ray scattering technique and their size depends strongly on the origin of the material, see [24]. The relationship between the degree of crystallinity and the dissolution of cellulose samples is not yet clear.

As mentioned in the previous paragraph cellulose represents a polymorphic material which can exist in four different crystal modifications: cellulose I, cellulose II, cellulose III and cellulose IV. Cellulose I is the crystalline structure of native cellulose. Cellulose II is obtained by alkaline treatment of cellulosic material or by precipitating cellulose from solution into aqueous medium. It is also called mercerized or regenerated cellulose. Treatment of celluloses I or II with liquid ammonia at temperatures below -30 °C and the subsequent evaporation of the solvent yields cellulose III, which exists in two submodifications depending on the starting material. It can be turned into the starting modifications by application of water. The fourth modification, cellulose IV, is formed from previous celluloses at high temperatures. Its importance for practical purposes is rather low.

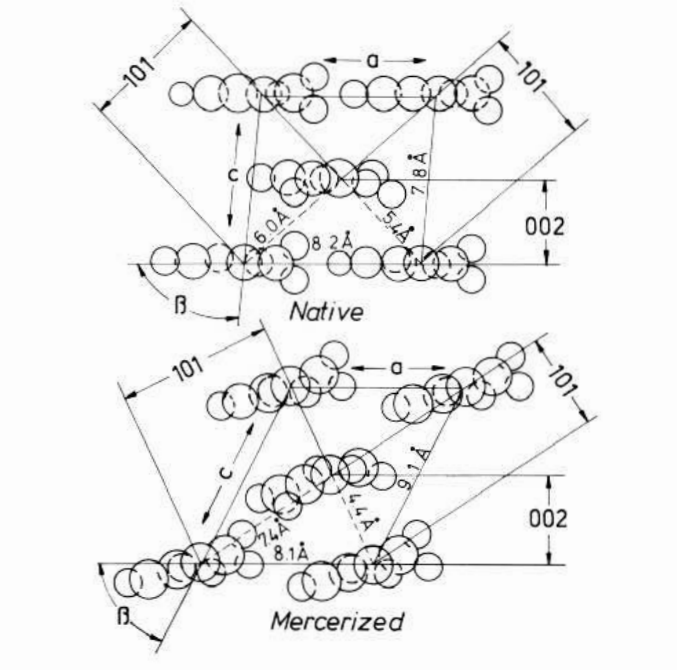

Figure 1.4: Lattice plane distances of cellulose I (native and cellulose II (mercerized) as proposed by Meyer, Mark and Misch and Andress respectively (adopted from ref. [2]) .

As the first two modifications are the most important for practical purposes, they will be shortly discussed further. For cellulose I originally a monoclinic unit cell with the space group $P2_1$ was proposed. This so called Meyer-Mark-Misch [25] model is presented in fig. 1.4, together with the unit cell of cellulose II as proposed by Andress [26]. Later a triclinic cell was suggested for the description of the crystalline state of cellulose I [27]. The newest measurements suggest that there are two modifications of cellulose units: the monoclinic unit cell seems to represent the thermodynamically stable state whereas the triclinic cell is metastable [28]. For cellulose I a parallel chain arrangement is assumed whereas for cellulose II an antiparallel chain arrangement seems to be more probable [29]. In cellulose II the hydrogen-bond pattern is different from cellulose I as the center cellulose chain seems to have different conformation of the primary hydroxyl group than the corner chains [29].

The morphological structure deals with the fibrillar structure of cellulose and the structure of cell walls. As the basis elementary fibril [30] is considered whose length, diameter and characteristic properties vary depending on the source and type of material [2]. However, some authors consider microfibrils to be the smallest morphological entities (even though non-uniform) [31] which aggregate to macrofibrils. The practical consequence of the fibrillar structure of cellulose fibers is the presence of the pore system. This represents an network of capillaries, cavities and interspaces among the microfibrils. The pore structure and inner surface of the fiber cell wall play an important role in the availability and reactivity

of cellulose. The knowledge about size, volume or shape of the pores is also helpful in the description of heterogenous reactions of cellulose. These properties can be obtained from sorption data, from small-angle X-ray scattering or mercury porosimetry measurements [1]. The effective surface is in the dry or swollen state very often different which has consequences for the accessibility of cellulose.

1.2.3 Dissolution of cellulose

For the dissolution of cellulose samples the accessibility of the hydroxyl groups in the sample is crucial. It is mainly given by the supramolecular structure of the fibrils and the properties of the pore system as mentioned in the previous paragraph. It does not represent a structural parameter as it is dependent also on the type of interaction considered. It can be characterized e.g. by the interaction with water, sorption of various inert gases, or interactions with solvents [1]. It can be considerably increased by pretreatment (activation) of the sample.
The application of an appropriate solvent can either result in swelling or in dissolution of the sample. Both the processes require the loosening or even the breakdown of the present supramolecular structure. However, in the case of swelling a two-phase system is formed and the reaction takes place only on a limited surface, whereas the dissolution results in a single phase formation. Very often both principles are combined in order to enhance the reactivity of cellulose samples. For this purpose also different degradation methods (mechanical, chemical, thermal, radiation) can be used.
The swelling principles can be divided into two groups: inter- and intracrystalline swelling. In the first case only easily accessible regions are attacked by the solvent which leads to the rupture of the interfibrillar bonds. This is caused e.g. by the following solvents: water, ethanol, DMF, DMSO. Especially the swelling with water has important industrial applications [1, 16]. The so called intracrystalline swelling leads to changes in the pore size, their volume and of the inner surface of the fibers (changes of the morphological structures). It increases also the lattice dimensions in the crystalline regions. This is achieved by the use of polar protic systems e.g. aqueous alkali hydroxide solutions or liquid ammonia. The changes of the corresponding cellulose crystalline modifications were mentioned in the previous section. In the case of aqueous NaOH solutions the impact on all three structural levels can be observed and this system can be be used as an example of a swelling agent and solvent at the same time.

Solvents for cellulose

For a long time nearly no true solvents of cellulose were available with the exception of aqueous cuprammonium hydroxide (Cuam) solutions. Later other aqueous metal transition-complex systems were discovered like cupriethylenediamine chelate (Cuen), the corresponding cadmium chelate (Cadoxen) or ferric tartaric acid in alkali solutions (FeTNa) which can be used also for analytical purposes as no modification of the cellulose hydroxyl groups in these solvents proceeds although the interaction with the polymer itself is very strong.

Table 1.1: Some examples of nonderivatizing and derivatizing systems for cellulose (adapted from [1]).

nonderivatizing	derivatizing
anhydrous hydrazine	CS_2/NaOH/water
sec. or tert. aliphatic amine/SO_2	HCOOH/H_3PO_4
methylamine/DMSO	$(CH_2O)_3$/DMSO
N-oxides e.g. NMMO·H_2O	N_2O_4/DMF
	H_3PO_4/water

They can be accepted as nonderivatizing solvents of cellulose. In the case of derivatizing solvents the dissolution is accompanied by the formation of an unstable derivative (e.g. ether, ester, acetal). By the change of pH or the medium the regenerated cellulose can be obtained.

As can be seen from table 1.1, sometimes quite exotic solvents were chosen for the purpose of cellulose dissolution. Many of them have no chance of being used on a large scale because of their toxic or aggressive components like e.g. SO_2. Some, however, proved to be appropriate for industrial applications like e.g. NMMO·H_2O (N-methylmorpholine-N-oxide monohydrate) in the Lyocell process.

Several dissolution principles are discussed in the literature. In the case of aqueous systems the dissolution probably takes place due to acid-base interaction between the hydroxyl groups in cellulose and the solvent [32]. For other solvent systems the concept of electron donor-acceptor interaction resulting in complex formation seems to be more applicable, see [33]. Another possibility represents the model of the formation of crypto-ionic hydrogen-bonds suggested for the dipolar aprotic solvent systems [34].

The solvents presented in table 1.1 are mostly composed from two or more solvents or/and organic salts. However, also concentrated aqueous solutions of inorganic salts can be applied on the dissolution of cellulose e.g. $Ca(SCN)_2$, $ZnCl_2$. From the various salts especially lithium salts lead to good results (e.g. LiSCN). Their combinations with other inorganic compounds in the form of molten salts could represent a promising solvent for future applications [35]. Quite recently also the use of ionic liquids as nonderivatizing solvent for cellulose was reported [36]. A different use for the inorganic salts was found in combination with aprotic dipolar solvents. Their complexes often act as nonderivatizing systems for cellulose. Some examples are shown in table 1.2.

Table 1.2 demonstrates that LiCl or LiBr can be used with a number of different aprotic systems for cellulose dissolution. The use of urea derivatives like DMEU (dimethylethylene urea) and DMPU (dimethylpropylene urea) [37] or the combination with HMPT (hexamethylphosphoric acid triamide)[38] do not seem to be very practical. The situation is different for LiCl/DMA [4, 6, 39] and LiCl/NMP (N-methylpyrrolidinone) [38] systems.

Table 1.2: Some examples of nonderivatizing salt-containing systems (from [1]).

nonderivatizing salt-containing systems
tetraalkylammonium halides /DMSO
aqueous tetraalkylammonium hydroxide
KSCN/DMSO
NH_3/NaSCN; NaI; $NaNO_3$
DMA/LiCl(LiBr); NMP/LiCl; DMF/LiCl
HMPT/LiCl
DMEU/LiCl; DMPU/LiCl
pyridine/LiCl; choline/LiCl
ethylendiamine/NaI/DMF

Abbreviations explained in the text.

Both of them proved to be valuable for the analysis and derivatization of cellulose. A similar system, LiCl/DMF (N,N-dimethylformamide), can be used for the dissolution either but its solubilization potential is much smaller than in the case of LiCl/DMA [40]. The further text concentrates only on the used LiCl/DMA system.

Dissolution in LiCl/DMA

Since its first use for cellulose dissolution in 1979 [4] this solvent system has become a common solvent of cellulose and polysaccharides in general [1]. It is applied in the homogenous synthesis of further cellulose derivatives, see [41], which allows often full substitution of the free hydroxyl groups under the minimization of the danger of side effects and byproducts. Another field of application represents the analysis of polysaccharides by various chromatographic techniques e.g. the size-exclusion chromatography (SEC) [5] where LiCl/DMA solutions can be used directly as the mobile phase. However, the composition and conditions used for the dissolution vary from group to group and have not yet been unified. The drawback of this system presents the necessity of the pretreatment of the cellulose samples. Without activation no dissolution takes place.
For the pretreatment the previously mentioned activation techniques can be utilized [7]. The activation can proceed by polar solvent exchange: swelling in water is followed by the solvent exchange to methanol or acetone, and then to DMA. A further technique represents treatment with liquid ammonia, see [39]. Refluxing of cellulose samples in low-concentrated LiCl/DMA solutions, see [41], or DMA, see [39, 42, 43], represents the most spread method. However, those activation processes connected with refluxing or heating of cellulose samples in DMA or LiCl/DMA seem to result in chemical modification of the solvent itself [8, 44] and subsequently lead to the degradation of the cellulose sample

(accompanied by a coloration of the probe). For this reason recently the activation by solvent exchange in polar media at room temperature is preferred e.g. [45–49]. The effect of the different activation procedures is discussed e.g. in the following study [45].
Not only the activation of the samples but even the LiCl content in the system necessary for the dissolution is still subject of discussion. The LiCl concentration in the solutions can vary from 3 to 12 wt% [6]. Since the solubilization limit of LiCl in DMA at 25 ^{o}C is 8.46 wt% [50] the presence of water in the solvent system has to be considered as probable. The widely preferred LiCl concentration is about 8-9 wt% in DMA. The ratio between LiCl and cellulose seems to be deciding for the dissolution process [6] and in some cases the pulp samples were not dissolved completely at lower LiCl concentrations [51]. It has also influence on the aggregation in cellulose solutions. This was demonstrated e.g. by some light-scattering studies [46, 51, 52] and in phase diagrams [42, 53]. At lower LiCl concentrations in DMA (even 6wt%) cellulose chains do not seem to be fully disintegrated and the formation of large particles is favored [51]. Depending on the sample and the used activation technique up to 17 wt% of cellulose should dissolve [6]. The solutions are supposed to be extremely stable also upon standing for a long time. Some authors found that no degradation took place even after months [45, 52], in other cases small decrease in intristic viscosity during 30 days was reported [43].
For the dissolution the interaction of the $[Li(DMA)_x]Cl$ complex (or ion-pair) with the hydroxyl groups of cellulose is made responsible [6, 7]. McCormick [6] suggests direct interaction between the chloride and hydrogen in the H-bond system. According to El-Kafrawy [54] the chloride is left free whereas the lithium cation coordinates with the oxygen from the hydroxyl group of cellulose as well as with the oxygen from the amide group. A similar model was proposed by Turbak [39] but the lithium cation is unrealistically coordinated also with the nitrogen from the amide group. Another concept was introduced by Herlinger [37] based on the formation of a cyclic complex where both chloride and lithium cation were involved in the interaction with the hydroxyl group. Morgenstern [55] proposed a different model based on the presence of a stable LiCl/DMA complex, where one DMA molecule from the coordination sphere of lithium is substituted by the cellulose hydroxyl whose hydrogen was attacked by the present chloride before. Until now there is no agreement about the real dissolution mechanism [1].
In order to sum up it should be repeated that one of the largest advantages of this system is the variety of possible cellulose samples which can be dissolved, reaching from the soft and hardwood pulps to microcrystalline cellulose, bacterial cellulose and to mixed samples with other polymers (for details see some of previously named studies). The maximum soluble amount of cellulose in the solutions depends on the used conditions, preparation and activation of the sample. In this work some phase diagrams were performed demonstrating the influence of temperature and water on specific cellulose sample (beech sulfite pulp and degenerated beech sulfite pulp) activated by the solvent exchange method.

Chapter 2

Theoretical background

2.1 Basics of electrodynamics

2.1.1 Maxwell and constitutive equations

The properties of static electromagnetic fields are described by means of the four Maxwell equations [56, 57]

$$\vec{\mathrm{rot}}\,\vec{H} = \vec{j} + \frac{\partial}{\partial t}\vec{D} \tag{2.1}$$

$$\vec{\mathrm{rot}}\,\vec{E} = -\frac{\partial}{\partial t}\vec{B} \tag{2.2}$$

$$\mathrm{div}\,\vec{D} = \rho_{el} \tag{2.3}$$

$$\mathrm{div}\,\vec{B} = 0 \tag{2.4}$$

where $\vec{H}$ accounts for the magnetic field strength, $\vec{E}$ electric field strength, $\vec{D}$ electric induction (or dielectric displacement), $\vec{B}$ magnetic induction, $\vec{j}$ current density and ρ_{el} electric charge density.
These equations are supported by the three constitutive equations which are valid for the ideal case of homogenous isotropic bodies at low magnetic field strengths

$$\vec{D} = \varepsilon\varepsilon_0\vec{E} \tag{2.5}$$

$$\vec{j} = \kappa\vec{E} \tag{2.6}$$

$$\vec{B} = \mu\mu_0\vec{H} \tag{2.7}$$

and define the following material properties: the relative static permittivity, ε, specific conductivity, κ, and relative magnetic permeability, μ. The symbols ε_0 and μ_0 stand for the absolute permittivity of vacuum and the permeability of vacuum respectively.

The constitutive equations (2.5-2.7) are valid only for the special case of static field. In the dynamic case the electric field, $\vec{E}$, harmonically oscillates with the amplitude, $\vec{E}_0$, and angular frequency $\omega = 2\pi\nu$

$$\vec{E}(t) = \vec{E}_0 \cos(\omega t). \tag{2.8}$$

When the frequency of the external field exceeds some value (in molecular solutions typically 0.1 GHz) the motion of the dipoles cannot follow the changes of the field without some phase delay, $\delta(\omega)$, between the electric field and the electric induction so that

$$\vec{D}(t) = \vec{D}_0 \cos(\omega t - \delta(\omega)) \tag{2.9}$$

which can be transformed into

$$\vec{D}(t) = \vec{D}_0 \cos(\delta(\omega)) \cos(\omega t) + \vec{D}_0 \sin(\delta(\omega)) \sin(\omega t) \tag{2.10}$$

and by introducing of

$$\vec{D}_0 cos(\delta(\omega)) = \varepsilon'(\omega)\varepsilon_0 \vec{E}_0 \tag{2.11}$$

$$\vec{D}_0 sin(\delta(\omega)) = \varepsilon''(\omega)\varepsilon_0 \vec{E}_0 \tag{2.12}$$

the electric induction can be then written as follows

$$\vec{D}(t) = \varepsilon'(\omega)\varepsilon_0 \vec{E}_0 \cos(\omega t) + \varepsilon''(\omega)\varepsilon_0 \vec{E}_0 \sin(\omega t) \tag{2.13}$$

The relation between $\vec{D}(t)$ and $\vec{E}(t)$ can be expressed by the means of ε' and ε'' that are both frequency dependent replacing the amplitude $\vec{D}_0$ and the phase delay $\delta(\omega)$. The relationship to the phase delay is defined as

$$\tan(\delta(\omega)) = \frac{\varepsilon''(\omega)}{\varepsilon'(\omega)}. \tag{2.14}$$

In eq.(2.13) the electric induction is separated into a dispersive part and a dissipative part. The dispersive part, $\varepsilon'(\omega)\varepsilon_0 \vec{E}_0 \cos(\omega t)$, with the frequency-dependent relative permittivity, ε', is in phase with the outer electric field whereas the dissipative part, $\varepsilon''(\omega)\varepsilon_0 \vec{E}_0 \sin(\omega t)$, with ε'' representing the dielectric loss (or absorption) is phase delayed by $\pi/2$ with respect to the electric field. For non-conductive systems the following relation between the frequency-dependent absorption energy and time can be drawn

$$\frac{\partial W}{\partial t} = \frac{\omega}{2}\varepsilon''(\omega)\varepsilon_0 E_0^2 = \frac{\omega}{2} E_0 D_0 \sin(\delta(\omega)). \tag{2.15}$$

The field vectors $\vec{E}(t)$ and $\vec{D}(t)$ can be described by the use of complex quantities as exponential functions

$$\hat{\vec{E}}(t) = \vec{E}_0 \cos(\omega t) + \mathrm{i}\vec{E}_0 \sin(\omega t) = \vec{E}_0 \exp(\mathrm{i}\omega t) \tag{2.16}$$

$$\hat{\vec{D}}(t) = \vec{D}_0 \cos(\omega t - \delta) + \mathrm{i}\vec{D}_0 \sin(\omega t - \delta) = \vec{D}_0 \exp[\mathrm{i}(\omega t - \delta)] \tag{2.17}$$

Also the constitutive equations (2.5) to (2.7) can be rewritten in this form [58]:

$$\hat{\vec{D}}(t) = \hat{\varepsilon}(\omega)\varepsilon_0 \hat{\vec{E}}(t) \tag{2.18}$$

$$\hat{\vec{j}}(t) = \hat{\kappa}(\omega)\hat{\vec{E}}(t) \tag{2.19}$$

$$\hat{\vec{B}}(t) = \hat{\mu}(\omega)\mu_0 \hat{\vec{H}}(t) \tag{2.20}$$

By comparison of eq.(2.18) with (2.13) the complex dielectric permittivity

$$\hat{\varepsilon}(\omega) = \varepsilon'(\omega) - \mathrm{i}\varepsilon''(\omega) \tag{2.21}$$

can be obtained. Similar relations can be introduced for the complex conductivity, $\hat{\kappa}$

$$\hat{\kappa}(\omega) = \kappa'(\omega) - \mathrm{i}\kappa''(\omega) \tag{2.22}$$

and the complex relative magnetic permittivity, $\hat{\mu}$

$$\hat{\mu}(\omega) = \mu'(\omega) - \mathrm{i}\mu''(\omega) \tag{2.23}$$

The transformation of the equations into the above forms is necessary so that all the electric and magnetic properties of a system can be described.

2.1.2 Wave equations

In the case of harmonic oscillating fields the Maxwell equation (2.1) can be written as

$$\hat{\vec{E}}(t) = \vec{E}_0 \cos(\mathrm{i}\omega t) \tag{2.24}$$

$$\hat{\vec{H}}(t) = \vec{H}_0 \cos(\mathrm{i}\omega t) \tag{2.25}$$

and transformed with the help of complex constitutive equations (2.18) - (2.20) into

$$\vec{\mathrm{rot}}\, \vec{H}_0 = (\hat{\kappa}(\omega) + \mathrm{i}\omega\hat{\varepsilon}(\omega)\varepsilon_0)\vec{E}_0 \tag{2.26}$$

For equation (2.2) the same procedure results in

$$\vec{\mathrm{rot}}\, \vec{E}_0 = -\mathrm{i}\omega\hat{\mu}(\omega)\mu_0 \vec{H}_0. \tag{2.27}$$

When the rotation operator is applied on eq.(2.26) and Legendre vectorial identity and eq.(2.27) are taken into account then

$$\vec{\mathrm{rot}}\, \vec{\mathrm{rot}}\, \vec{H}_0 = \vec{\mathrm{grad}}\, \mathrm{div}\, \vec{H}_0 - \triangle \vec{H}_0 = \vec{\mathrm{grad}}\, (0) - \triangle \vec{H}_0 = - \triangle \vec{H}_0, \tag{2.28}$$

and the reduced form of the wave equation of magnetic field for homogenous isotropic media can be obtained

$$\triangle \vec{H}_0 + \hat{k}^2 \vec{H}_0 = 0 \tag{2.29}$$

with propagation coefficient, $\hat{k}$. The latter can be written as follows

$$\hat{k}^2 = k_0^2 \left(\hat{\mu}(\omega)\hat{\varepsilon}(\omega) + \frac{\hat{\mu}(\omega)\hat{\kappa}(\omega)}{\mathrm{i}\omega\varepsilon_0} \right) \tag{2.30}$$

The propagation coefficient of the vacuum, k_0, is defined in the following manner

$$k_0 = \omega\sqrt{\varepsilon_0\mu_0} = \frac{2\pi}{\lambda_0} \tag{2.31}$$

$$c_0 = \frac{1}{\sqrt{\varepsilon_0\mu_0}}. \tag{2.32}$$

where c_0 represents the speed of light and λ_0 the wavelength of a monochromatic wave in vacuum. For a source-free medium ($\mathrm{div}\,\vec{E} = 0$) a reduced wave equation for $\vec{E}$ can be used

$$\triangle \hat{\vec{E}}_0 + \hat{k}^2 \hat{\vec{E}}_0 = 0 \tag{2.33}$$

In the case of non-magnetizable substances ($\hat{\mu} = 1$) the eq.(2.30) can be simplified in

$$\hat{k}^2 = k_0^2 \left(\hat{\varepsilon}(\omega) + \frac{\hat{\kappa}(\omega)}{\mathrm{i}\omega\varepsilon_0} \right) \equiv k_0^2 \hat{\eta}(\omega). \tag{2.34}$$

with the generalized complex permittivity $\hat{\eta} = \eta' - \mathrm{i}\eta''$. Its real part is described as

$$\eta'(\omega) = \varepsilon'(\omega) - \frac{\kappa''(\omega)}{\omega\varepsilon_0} \tag{2.35}$$

and the imaginary part as

$$\eta''(\omega) = \varepsilon''(\omega) - \frac{\kappa'(\omega)}{\omega\varepsilon_0} \tag{2.36}$$

The practical consequence of equations (2.34) to (2.36) is that the dielectric properties and the conductivity of the system can never be measured separately. In electrolyte systems the theory [59] suggests that some dispersion of the complex conductivity, $\hat{\kappa}$, happens, however, in the microwave range this effect can be neglected [60].
So generally it is possible to suppose for simple electrolyte solutions that

$$\kappa'(\omega) = \kappa \tag{2.37}$$

and

$$\kappa''(\omega) = 0 \tag{2.38}$$

When the dispersion resulting from the conductivity is neglected the real and imaginary part of the frequency-dependent relative permittivity can be expressed as

$$\varepsilon'(\omega) = \eta'(\omega) \tag{2.39}$$

and

$$\varepsilon''(\omega) = \eta''(\omega) - \frac{\kappa}{\omega\varepsilon_0} \tag{2.40}$$

These equations serve for the calculation of ε' and ε'' from the experimentally accessible values of η', η'' and κ. The experimental value ε'' is always corrected for the Ohmic loss according to the equation (2.40).

2.2 Dielectric relaxation

2.2.1 Polarization

Polarization, $\hat{\vec{P}}$, presents the actual observable quantity in DRS experiments. It can be described from a macroscopic and a microscopic point of view. The comparison of both principles makes it possible to interpret macroscopic quantities on molecular level [58].
Macroscopically $\hat{\vec{P}}$ is defined as

$$\hat{\vec{P}} = (\hat{\varepsilon} - 1)\varepsilon_0 \hat{\vec{E}} \tag{2.41}$$

whereas microscopically

$$\hat{\vec{P}} = \hat{\vec{P}}_\mu + \hat{\vec{P}}_\alpha \tag{2.42}$$

Both interpretation can be combined as follows in order to express the overall polarization

$$\hat{\vec{P}} = (\hat{\varepsilon} - 1)\varepsilon_0 \hat{\vec{E}} = \hat{\vec{P}}_\mu + \hat{\vec{P}}_\alpha \tag{2.43}$$

where $\hat{\vec{P}}_\alpha$ represents the induced and $\hat{\vec{P}}_\mu$ the orientational polarization. The orientational polarization defined in eq.(2.44) results from the reorientation of the molecular dipole moments, $\vec{\mu}_k$, with number density, ρ_k, of species k caused by the external electric field.

$$\hat{\vec{P}}_\mu = \sum_k \rho_k \langle \vec{\mu}_k \rangle \tag{2.44}$$

with $\langle \vec{\mu}_k \rangle$ representing the ensemble average of the permanent dipole moments of species k. The involved processes contain information about intermolecular interactions in the measured systems e.g. about solvent-solvent, ion-solvent or interionic interactions in electrolyte systems. The time scale of these processes is in the nano- and picosecond range which corresponds to the microwave frequency range. The measurements of condensed phases usually result in broad absorption bands because the energy levels lie very close to each other.
The molecular polarizability, α_k, resulting from the electron and the atomic polarization leads to formation of induced dipole moments and so to the induced polarization

$$\hat{\vec{P}}_\alpha = \sum_k \rho_k \alpha_k (\hat{\vec{E}}_i)_k \tag{2.45}$$

where $(\hat{\vec{E}}_i)_k$ is the internal field acting on the components. The value of $\hat{\vec{P}}_\alpha$ leads to information about the intramolecular dynamics of the system and is usually not observable in the microwave range but in the infra red (atomic polarization) and ultra violet range (electron polarization). The absorption peaks are in this case sharper [13].

Because the time scales of $\hat{\vec{P}}_\mu$ and $\hat{\vec{P}}_\alpha$ are very different both polarizations can be treated as linearly independent [61]. They can be described with the help of the so called infinite frequency permittivity, ε_∞

$$\hat{\vec{P}}_\mu = \varepsilon_0(\hat{\varepsilon} - \varepsilon_\infty)\hat{\vec{E}} \tag{2.46}$$

$$\hat{\vec{P}}_\alpha = \varepsilon_0(\varepsilon_\infty - 1)\hat{\vec{E}} \tag{2.47}$$

2.2.2 Response functions of the orientational polarization

At high frequencies the changes of the electric field become so quick that the dipoles cannot follow the field variation any more without delay. The polarization cannot reach its equilibrium value. The relation between $\hat{\vec{E}}$ and $\hat{\vec{P}}$ can be then established by the help of the response functions. This can be only realized when the superposition principle and the conditions of linear media are valid. If one field $\vec{E}_1$ produces polarization $\vec{P}_1$ and another field $\vec{E}_2$ polarization $\vec{P}_2$, then the field $\vec{E}_1 + \vec{E}_2$ leads to following polarization $\vec{P}_1 + \vec{P}_2$. The response functions enable us to describe the polarization of a dielectric in any time scale. If an isotropic linear dielectric is exposed to a jump through the applied field, $\vec{E}$, at time $t = 0$, it causes polarization, $\vec{P}$. When we consider that the induced polarization, $\vec{P}_\alpha$, follows without decay, then the corresponding polarization can be written as

$$\hat{\vec{P}}_\mu(t) = \hat{\vec{P}}_\mu(0) \cdot F_P^{or}(t) \quad \text{mit} \quad F_P^{or}(0) = 1, \quad F_P^{or}(\infty) = 0. \tag{2.48}$$

with the step response function, $F_P^{or}(t)$, defined as

$$F_P^{or}(t) = \frac{\langle \vec{P}_\mu(0) \cdot \vec{P}_\mu(t) \rangle}{\langle \vec{P}_\mu(0) \cdot \vec{P}_\mu(0) \rangle}. \tag{2.49}$$

In this case, $F_P^{or}(t)$ is a monotonously decreasing function. One of the methods used in this work, the Time Domain Reflectometry (TDR), is based on this principle [62].

In the case of harmonic electromagnetic alternating fields of the form $\hat{\vec{E}}(t) = \hat{\vec{E}}_0 \exp(-\mathrm{i}\omega t)$ the polarization can be defined as

$$\hat{\vec{P}}_\mu(\omega, t) = \varepsilon_0(\varepsilon - \varepsilon_\infty)\hat{\vec{E}}(t) \int_0^\infty \exp(-\mathrm{i}\omega t') f_P^{or}(t') \mathrm{d}t' \tag{2.50}$$

with

$$\int_0^\infty \exp(-\mathrm{i}\omega t') f_P^{or}(t') \mathrm{d}t' = \mathcal{L}_{\mathrm{i}\omega}[f_P^{or}(t')] \tag{2.51}$$

where $\mathcal{L}_{iw}[f_P^{or}(t')]$ is the Laplace transformed pulse response function of orientational polarization. This can be obtained from the pulse response function

$$f_P^{or}(t') = -\frac{\partial F_P^{or}(t-t')}{\partial(t-t')} \quad \text{normalized with} \quad \int_0^\infty f_P^{or}(t')\mathrm{d}t' = 1. \tag{2.52}$$

The complex permittivity, $\hat{\varepsilon}(\omega)$, can be then calculated as follows [58]

$$\hat{\varepsilon}(\omega) = \varepsilon'(\omega) - \mathrm{i}\varepsilon''(\omega) = \varepsilon_\infty + (\varepsilon - \varepsilon_\infty) \cdot \mathcal{L}_{\mathrm{i}\omega}[f_P^{or}(t')] \tag{2.53}$$

2.3 Empirical description of dielectric relaxation

For the description of dielectric relaxation a number of different equations have been developed. As the majority of the spectra represent a sum of various relaxation processes the best description of the spectra can be reached by a combination of various equations.

2.3.1 Debye equation

The Debye equation [63] represents the simplest way of expressing dielectric relaxation. It is assumed that the decrease of the polarization in the absence of an outer electric field is directly proportional to the polarization itself [64]. It can be expressed by a time law of the first order

$$\frac{\partial}{\partial t}\vec{P}_\mu(t) = -\frac{1}{\tau}\vec{P}_\mu(t) \tag{2.54}$$

where τ represents the relaxation time and describes the dynamics of the system. From the following relation

$$\vec{P}_\mu(t) = \vec{P}_\mu(0)\exp\left(-\frac{t}{\tau}\right) \tag{2.55}$$

the part response function, $F_P^{or}(t) = \exp(-t/\tau)$, can be obtained. Application of eq.(2.52) leads to the definition of pulse response function, $f_P^{or}(t)$, as

$$f_P^{or}(t) = \frac{1}{\tau}\exp\left(-\frac{t}{\tau}\right) \tag{2.56}$$

The complex permittivity can be obtained from the application of the Fourier transformation to the pulse response function according to the eq.(2.53)

$$\hat{\varepsilon}(\omega) = \varepsilon_\infty + (\varepsilon - \varepsilon_\infty) \cdot \mathcal{L}_{\mathrm{i}\omega}\left[\frac{1}{\tau}\exp\left(-\frac{t}{\tau}\right)\right] \tag{2.57}$$

The final Debye equation can be written as

$$\hat{\varepsilon}(\omega) = \varepsilon_\infty + \frac{\varepsilon - \varepsilon_\infty}{1 + \mathrm{i}\omega\tau} \tag{2.58}$$

which can be split into the real

$$\varepsilon'(\omega) = \varepsilon_\infty + \frac{\varepsilon - \varepsilon_\infty}{1 + \omega^2\tau^2} \tag{2.59}$$

and imaginary part

$$\varepsilon''(\omega) = \omega\tau\frac{\varepsilon - \varepsilon_\infty}{1 + \omega^2\tau^2}. \tag{2.60}$$

The dispersion curve, $\varepsilon' = \varepsilon'(\ln(\omega))$, is a monotonically decreasing point-symmetric function and the absorption curve, $\varepsilon' = \varepsilon'(\ln(\omega))$, an axes-symmetric band reaching its maximum when $\omega = 1/\tau$.
Equations (2.59) and (2.60) are not always able to describe all experimental results. However, the full description of the spectrum can be reached by the superposition of more Debye equations. In this case the assumption of continuous relaxation time distribution, $g(\tau)$, is used [58]. Usually the logarithmic representation, $G(\ln\tau)$, is preferred. The complex permittivity can be then written as

$$\hat{\varepsilon}(\omega) = \varepsilon_\infty + (\varepsilon - \varepsilon_\infty)\int_0^\infty \frac{G(\ln\tau)}{(1 + \mathrm{i}\omega\tau)}\mathrm{d}\ln\tau \quad \text{with} \quad \int_0^\infty G(\ln\tau)\mathrm{d}\ln\tau = 1. \tag{2.61}$$

2.3.2 Other equations

As mentioned in paragraph 2.3.1 the Debye equation represents only one possible way of expressing dielectric relaxation. When special parameters are added other empirical distribution functions for the description of the relaxation behavior can be obtained.

Cole-Cole equation

In comparison to Debye equation includes the Cole-Cole equation an additional empirical parameter $\alpha \in [0..1]$ [65, 66]

$$\hat{\varepsilon}(\omega) = \varepsilon_\infty + \frac{\varepsilon - \varepsilon_\infty}{1 + (\mathrm{i}\omega\tau_0)^{1-\alpha}}. \tag{2.62}$$

which describes a symmetric relaxation time distribution as the principal relaxation time, τ_0. This kind of distribution results in flatter dispersion curves, and broader and flatter absorption curves.
When $\alpha = 0$ the Cole-Cole equation turns into the Debye equation.

Cole-Davidson equation

When an asymmetric time relaxation distribution is present the Cole-Davidson equation [67, 68] with parameter $\beta \in [0..1]$

$$\hat{\varepsilon}(\omega) = \varepsilon_\infty + \frac{\varepsilon - \varepsilon_\infty}{(1 + \mathrm{i}\omega\tau_0)^\beta} \tag{2.63}$$

is used. The Cole-Davidson equation describes asymmetric dispersions and absorption curves. When $\beta = 1$ this equation turns into the Debye form.

Havriliak-Negami equation

When both parameters $\alpha \in [0..1]$ and $\beta \in [0..1]$ are combined, another way for the description of a broad asymmetric relaxation time distribution is obtained [69]:

$$\hat{\varepsilon}(\omega) = \varepsilon_\infty + \frac{\varepsilon - \varepsilon_\infty}{(1 + (\mathrm{i}\omega\tau_0)^{1-\alpha})^\beta} \tag{2.64}$$

Both the dispersion and absorption curves are asymmetric. For $\alpha = 0$ and $\beta = 1$ this equation turns into the simple Debye equation.

Combination of models

In most of the systems the complex permittivity spectrum is composed of more than one relaxation process. So it is possible to write eq.(2.61) as superimposition of n separate processes

$$\hat{\varepsilon}(\omega) = \varepsilon_\infty + \sum_{j=1}^{n} (\varepsilon_j - \varepsilon_{\infty,j}) \int_0^\infty \frac{G_j(\ln \tau_j)}{1 + \mathrm{i}\omega\tau_j} \mathrm{d} \ln \tau_j \tag{2.65}$$

Each of the processes is treated separately and has its own relaxation time, τ_j, and dispersion amplitude, S_j

$$\varepsilon - \varepsilon_\infty = \sum_{j=1}^{n} (\varepsilon_k - \varepsilon_{\infty,j}) = \sum_{j=1}^{n} S_j \tag{2.66}$$

$$\varepsilon_{\infty,j} = \varepsilon_{j+1} \tag{2.67}$$

2.4 Models for the description of relaxation behavior

2.4.1 Equilibrium properties

Onsager equation

This model describing dipole orientation is based on Onsager's theory [58, 70] which assumes the interaction of the electric field with only one molecule. The environment of the molecule is then treated as a continuum characterized by the macroscopic properties of the system. In this case specific interactions are not taken into account. At first the microscopic and macroscopic polarization are compared which results in the following expression

$$\varepsilon_0(\varepsilon - 1)\vec{E} = \vec{E}_h \cdot \sum_j \frac{\rho_j}{1 - \alpha_j f_j} \left(\alpha_j + \frac{1}{3k_B T} \cdot \frac{\mu_{eff,j}^2}{1 - \alpha_j f_j} \right), \tag{2.68}$$

where ρ_j represents the charge density, α_j the polarizability, f_j the reaction field factor of the species j and $\mu_{eff,j}$ the effective dipole moment of species j. This is the usual expression used for interpretation of dielectric spectra. $\vec{E}_h$ stands for the cavity field which is defined as

$$\vec{E}_h = \frac{3\varepsilon}{2\varepsilon + 1}\vec{E} \tag{2.69}$$

under the conditions of a sphere-like cavity in dielectrics with permittivity ε.
When eq.(2.69) is introduced into eq.(2.68) the general form of Onsager equation is obtained

$$\frac{(\varepsilon - 1)(2\varepsilon + 1)\varepsilon_0}{3\varepsilon} = \sum_j \frac{\rho_j}{1 - \alpha_j f_j}\left(\alpha_j + \frac{1}{3k_BT}\cdot\frac{\mu_{eff,j}^2}{1 - \alpha_j f_j}\right) \tag{2.70}$$

and if only one dispersion step is present the eq.(2.70) can be simplified in the following way

$$\frac{(\varepsilon - \varepsilon_\infty)(2\varepsilon + \varepsilon_\infty)}{\varepsilon(\varepsilon_\infty + 2)^2} = \frac{\rho\mu_{eff}^2}{9\varepsilon_0 k_B T} \tag{2.71}$$

which represents a very important relation for the interpretation of ion-pair relaxation processes.

Cavell equation

The Cavell equation [71] represents the extension of the Onsager equation (2.70) on systems with more dispersion steps. The dispersion amplitude, $S_j = \varepsilon_j - \varepsilon_{j+1}$, of a relaxation process j depends on the concentration c_j of the species which take part on the relaxation process and its dipole moment, $\mu_{eff,j}$

$$S_j = \frac{\varepsilon}{2\varepsilon + 1}\cdot\frac{N_A c_j}{k_B T\varepsilon_0}\cdot\frac{\mu_{eff,j}^2}{(1 - f_j\alpha_j)^2} \tag{2.72}$$

This equation is valid for sphere-like species with radius, a_j, polarizability, α_j, dipole moment, μ_j and reaction field factor, f_j, [58]

$$f_j = \frac{1}{4\pi\varepsilon_0 a_j^3}\cdot\frac{2\varepsilon - 2}{2\varepsilon + 1} \tag{2.73}$$

For the evaluation of dispersion amplitudes eq.(2.72) is usually used in the following form

$$c_{j,i} = \frac{(\varepsilon_j - \varepsilon_{\infty,j})\varepsilon_0(2\varepsilon + 1)}{\varepsilon}\cdot\frac{(1 - \alpha_j f_j)^2}{\mu_j^2}\cdot\frac{k_B T}{N_A} \tag{2.74}$$

However, since usually the species are not spheres and this assumption can represent a source of errors, the previous equation was extended for ellipsoidal particles with half-axes $a_j > b_j > c_j$ [58, 72]

$$S_j = \frac{\varepsilon}{\varepsilon + A_j(1 - \varepsilon)}\cdot\frac{N_A c_j}{3k_B T\varepsilon_0}\cdot\frac{\mu_{eff,j}^2}{(1 - f_j\alpha_j)^2} \tag{2.75}$$

where

$$f_j = \frac{3}{4\pi\varepsilon_0 a_j b_j c_j} \cdot \frac{A_j(1-A_j)(\varepsilon-1)}{\varepsilon+(1-\varepsilon)A_j} \tag{2.76}$$

and

$$A_j = \frac{a_j b_j c_j}{2} \int_0^\infty \frac{\mathrm{d}s}{(s+a_j^2)^{3/2}(s+b_j^2)^{1/2}(c+c_j^2)^{1/2}} \tag{2.77}$$

For spheroids ($b_j = c_j$) eq.(2.77) can be transformed in [73]

$$A_j = -\frac{1}{p_j^2-1} + \frac{p_j}{(p_j^2-1)^{1.5}} \ln\left(p_j + \sqrt{p_j^2-1}\right), \qquad p_j = \frac{a_j}{b_j}. \tag{2.78}$$

Kirkwood-Fröhlich equation

Thanks to the application of statistical mechanics it is possible to introduce the influence of specific intermolecular interactions into the Onsager theory. In this way molecular characteristics can be interpreted in terms of macroscopic properties. The theory [74, 75] is based on a model of a dipole whose orientation is in correlation with its neighbors. The result has a form similar to the one of Onsager equation(2.68)

$$\frac{(\varepsilon-\varepsilon_\infty)(2\varepsilon+\varepsilon_\infty)}{\varepsilon(\varepsilon_\infty+2)^2} = \frac{\rho\mu^2}{9\varepsilon_0 k_B T} \cdot g \tag{2.79}$$

where g is the Kirkwood factor, representing the interactions between the particles. If the orientation between the neighbors is preferentially parallel, the value of $g > 1$. The mainly antiparallel orientation leads to $g < 1$.

2.4.2 Dynamic properties

The dynamics of the systems can be described with the help of statistical mechanics. A relation between the experimental correlation function, F_p^{or}, eq.(2.49) and the molecular dipole correlation function, $\gamma(t)$

$$\gamma(t) = \frac{\langle\vec{\mu}(0)\cdot\vec{\mu}(t)\rangle}{\langle\vec{\mu}(0)\cdot\vec{\mu}(0)\rangle} = \langle\cos(\theta(t))\rangle \tag{2.80}$$

has to be established. This function describes the probability of the existence of the orientation of the permanent dipole at $t = 0$ also in time t after the field has been switched off. θ represents the angle between the dipole orientation at time $t = 0$ and time t.
As

$$\vec{P}_\mu(t) = \frac{1}{V}\sum_j \vec{\mu}_{eff,j}(t) = \frac{1}{V}\sum_j \vec{M}(t) \tag{2.81}$$

where $\vec{\mu}_{eff,j}$ are the effective dipole moments and $\vec{M}(t)$ the macroscopic dipole moment, F_p^{or} can be obtained as

$$F_P^{or}(t) = \frac{\langle\vec{M}(0)\cdot\vec{M}(t)\rangle}{\langle\vec{M}(0)\cdot\vec{M}(0)\rangle} \equiv \Phi^M(t) \tag{2.82}$$

$\Phi^M(t)$ represents the autocorrelation function of the orientational polarization. When the macroscopic, $F_P^{or}(t)$, and molecular, $\gamma(t)$, correlation functions are equal, no interactions between the molecules take place. This is the case only at low pressures in gases. However, in condensed systems it never happens. Here the movement of the particles and their orientation do not occur separately. So under real conditions the macro- and microscopic correlation function are always different.

Microscopic and macroscopic relaxation time

The relation between the experimentally measurable relaxation time, τ, and the microscopic relaxation time, τ_s, plays an important role in the interpretation of the dielectric spectra and there are various theoretical approaches to the problem.
Debye suggested following expression [76]

$$\tau = \frac{\varepsilon + 2}{\varepsilon_\infty + 2} \cdot \tau_s \tag{2.83}$$

under the assumption of Lorentz field as inner field. However this approach is too inaccurate for polar dielectrics and so it can be used only for non-polar systems.
For the case of pure rotational diffusion Powles and Glarum combined the macroscopic and microscopic relaxation time [77, 78] in the following manner

$$\tau = \frac{3\varepsilon}{2\varepsilon + \varepsilon_\infty} \cdot \tau_s \tag{2.84}$$

Also here statistic mechanics [79–81] can be applied which leads to a generalized form

$$\tau = \frac{3\varepsilon}{2\varepsilon + \varepsilon_\infty} \cdot \frac{g}{\dot{g}} \cdot \tau_s \tag{2.85}$$

where g is the Kirkwood correlation factor and $\dot{g}$ the dynamic correlation factor. When $g/\dot{g} = 1$ expression (2.85) turns into Powles-Glarum equation (2.84).

Debye model of rotational diffusion

In this model Debye assumed that the system consists of an aggregation of sphere-like inelastic dipoles which do not interact with each other. However, this assumption is valid only under the conditions of the application of Lorentz field as inner field, when inertia and the dipole-dipole interaction can be neglected. This makes the theory applicable only for non-associated systems. Debye obtained for the dipole correlation function the following term

$$\gamma(t) = \exp\left(-\frac{t}{\tau_s}\right) \tag{2.86}$$

where the relaxation time, τ_s, can be described by the friction factor, ζ,

$$\tau_s = \frac{\zeta}{2k_B T} \tag{2.87}$$

The rotation of a sphere in viscous media according to the hydrodynamic laws described by the Stokes-Debye-Einstein equation is defined as

$$\tau_s = \frac{3V\eta}{k_B T} \tag{2.88}$$

where V represents the volume of the sphere and η the dynamic viscosity of the environment of the sphere (so called microscopic viscosity). However the application of this theory has its drawbacks as the relation between macroscopic and microscopic viscosity is not clear. This problem can be solved by introducing of various parameters into the equation [82] that leads to the following term

$$\tau_s = \frac{3V\eta}{k_B T} f_{stick} C + \tau_s^0 \tag{2.89}$$

The shape factor, f_{stick}, describes the deviation of the shape of the molecule from the ideal form of a sphere. For a sphere with *stick* boundary conditions of rotational diffusion $f_{stick} = 1$. The friction parameter, C, involves correction of the macroscopic viscosity and its value in the case of *stick* conditions is $C = 1$. For *slip* motion $C = 1 - f_{stick}^{-2/3}$. τ_s^0 is just an empirical value which is sometimes interpreted as free rotation correlation time.

2.5 Kinetic depolarization

The observed marked decrease of the solvent dispersion amplitude with increasing electrolyte concentration (see chapter 4) is supposed to result from two additive contributions [83, 84]

$$\Delta\varepsilon(c) = S(0) - S(c) = \Delta_{eq}\varepsilon(c) + \Delta_{kd}\varepsilon(c) \tag{2.90}$$

The equilibrium term, $\Delta_{eq}\varepsilon(c)$, results from the changes of the internal field caused by the dilution of the solvent dipole density by the ions. The kinetic depolarization (kd), $\Delta_{kd}\varepsilon(c)$, is caused by the relative motion of the ions and the surrounding solvent molecules in the external field. According to the Hubbard-Onsager continuum theory [85, 86] kd is directly proportional to the specific conductivity, κ,[87]

$$\Delta_{kd}\varepsilon(c) = \xi \cdot \kappa \quad \text{with} \quad \xi = p \cdot \frac{\varepsilon(0) - \varepsilon_\infty(0)}{\varepsilon(0)} \cdot \frac{\tau(0)}{\varepsilon_0} \tag{2.91}$$

where ξ represents the depolarization factor determined by the dielectric properties of the system. This definition is based on the following assumption: the ion moving in the electrical field forces the molecules of the solvent to rotation which is opposite to the outer electrical field. The solvent then decreases the speed of the ionic movement. From eq.(2.91) can be seen that ξ depends on the relaxation parameters of the pure solvent and the hydrodynamic parameter, p. This parameter characterizes conditions of kd that can be expected in the system. For $p = 1$ *stick* conditions are assumed which means that the whole solvent shell moves with the ions, for $p = 2/3$ *slip* conditions are expected and if $p = 0$, kd can be neglected.

2.6 Temperature dependence of relaxation times

2.6.1 Arrhenius equation

This equation [88] represents one of the oldest methods for the description of the temperature dependence of rate constants and so the relaxation time

$$\ln(\tau/\mathrm{s}) = \ln(\tau_0/\mathrm{s}) + \frac{E_a}{RT} \tag{2.92}$$

$$= a_0 + a_1/T \qquad \text{where} \qquad E_a = a_1 \cdot R \tag{2.93}$$

This approach is based on the idea that particles are pushed by thermic fluctuations to transition between two stable energetic levels which are divided by a temperature dependent potential barrier, E_a, the activation energy. The frequency factor, τ_0, accounts for the minimal possible relaxation time.

Chapter 3

Experimental part

3.1 Samples and their preparation

3.1.1 LiCl

LiCl (Merck, p.A.) was dried under vacuum at 180 ^{o}C for two weeks and stored in glove box. The solutions in the concentration range $0.1 < c/\text{mol L}^{-1} < 2.1$ were prepared and stored under nitrogen.

3.1.2 N,N-dimethylacetamide

DMA (Sigma Aldrich, HPLC grade) was dried with 4 Å molecular sieve (Merck) and used without any further purification. The water content in the dry DMA determined by Karl-Fischer titration was < 20 ppm. The amount of organic impurities did not exceed 50 ppm.

3.1.3 Water

As water for the LiCl/water solutions only millipore water was used (Milli-Q system from Millipore A-S, Germany). This water contained less than 0.1 ppm impurities.

3.1.4 Cellulose samples

For the phase diagrams samples from beech sulfite pulp of molecular weight 290 000 g mol^{-1} (determined by GPC/MALLS) were used. For the DRS-measurement samples were prepared from the same starting material but partly decomposed. The molecular weight was in this case only 54 000 g mol^{-1}.

3.1.5 Cellulose activation

The cellulose sample was activated by solvent exchange from water to acetone to DMA. The activated sample was shaken in DMA for one day, filtered off and freeze-dried. Then the sample was transferred into the LiCl/DMA mixture and was left in the refrigerator at 4-8 ^{o}C (samples at 5 ^{o}C) or just left standing at 25 ^{o}C for three days. In the case of water containing samples, a specific amount of water was added into the solvent and stirred. Then a certain amount of cellulose was introduced in the solutions. The resulting mixtures were kept in the refrigerator for three days. After the first measurement the samples were left standing at room temperature.

3.2 Measurements

3.2.1 Density measurements

The densities, required to calculate the molar concentrations, were determined with a vibrating-tube densimeter (Paar model DMA 60) calibrated with nitrogen ($\rho = 1.1456 \times 10^{-3}$g cm^{-3}, from van der Waals coefficients [89]) and water ($\rho = 0.997043$ g cm^{-3} [89]) according to the procedure described in [90]. For the density the following expression is valid

$$\rho = A(T^2 - B) \tag{3.1}$$

where A and B are the device constants and T the measuring temperature. The measuring cell was thermostatically controlled with the accuracy of 0.01 ^{o}C. The densities of DMA were used from ref. [14] and for the LiCl/DMA solutions at 25 ^{o}C from ref. [50]. The measured densities were fitted by a polynomial

$$\rho(m) = a + bm + cm^2 + dm^3 \tag{3.2}$$

and used also for other solutions. The parameters are listed in table 3.1.

Table 3.1: Fit parameters of the polynomial shown in eq.(3.2) resulting from the density data of LiCl/DMA solutions at different temperatures.

T	258.15	278.15	318.15	338.15
a	0.9712 ± 0.0002	0.9545 ± 0.0001	0.9191 ± 0.0003	0.9018 ± 0.0002
b	0.049 ± 0.001	0.044 ± 0.001	0.040 ± 0.001	0.037 ± 0.001
c	-0.017 ± 0.002	-0.009 ± 0.001	-0.0035 ± 0.0004	-0.004 ± 0.001
d	0.005 ± 0.001	0.0020 ± 0.0004		

units: T in K; a in kg dm^{-3}; b in kg^2 dm^{-3}mol^{-1}, c in kg^3 dm^{-3}mol^{-2} and d in kg^4 dm^{-3}mol^{-3}.

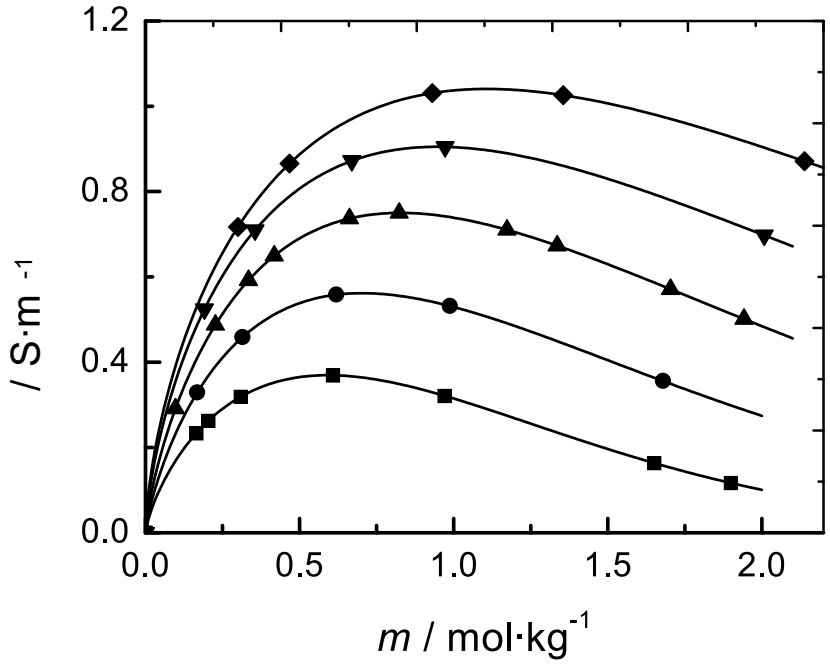

Figure 3.1: Conductivity, κ, as function of molality, m, in LiCl/DMA solutions at 258.15 K (■), 278.15 K (●), 298.15 K (▲), 318.15 K (▼) and 338.15 K (♦).

3.2.2 Conductivity measurements

The electric conductivity of the samples was measured with a set of capillary cells using frequencies $0.12 < f\,/\,\mathrm{kHz} < 11$ according to [91]. During the measurements the cells were thermostatically controlled with precision of 0.01 K. The concentration dependence of the specific conductivity was expressed by the Casteel-Amis equation [91]

$$\kappa = \kappa_{\max} \cdot \left(\frac{m}{\mu}\right)^{a} \cdot \exp\left[b\,(m-\mu)^2 - a\left(\frac{m}{\mu} - 1\right)\right] \tag{3.3}$$

with following parameters, the molal concentration of the solution, m, the maximum conductivity, κ_{max}, the corresponding molality, μ, and fit parameters a, b. The results are presented in table 3.2 and figure 3.1. Data for DMA were adopted from ref. [14] and for LiCl/DMA solutions at 25 ^{o}C from ref. [50].

3.2.3 Phase Diagrams

The samples were observed under polarized light in a special device (a thermostated bath equipped with a cross-Nicol-filter), three days and one month after their preparation. As isotropic systems only such samples were accepted where no light scattering was observed. These may be isotropic solutions or gels (empty circles). If some fibers or liquid crystals were found (opalescence), the samples were considered as non-dissolved (filled circles).

Table 3.2: Fit parameters of Casteel-Amis equation (eq. 3.3) describing the conductivity of LiCl/DMA solutions at different temperatures (κ_{max}, μ, a, b).

T	258.15	278.15	318.15	338.15
κ_{max}	0.369 ± 0.002	0.562 ± 0.002	0.905 ± 0.0001	1.12 ± 0.03
μ	0.592 ± 0.007	0.702 ± 0.008	0.947 ± 0.0004	1.22 ± 0.06
a	0.75 ± 0.04	0.77 ± 0.03	0.67 ± 0.001	0.42 ± 0.16
b	-0.21 ± 0.04	-0.06 ± 0.03	-0.01 ± 0.001	-0.22 ± 0.12

units: T in K; κ_{max} in $\mathrm{S\,m^{-1}}$; μ in $\mathrm{mol\,kg^{-1}}$; a, b without units.

Because of the high viscosity of the solutions, which made stirring at higher concentrations impossible, no clear difference between liquid crystals and non-dissolved particles in the solutions could be seen. For this reason the corresponding region is designated "liquid crystal or non-dissolved" in the diagrams. In some cases also the difference between pure solvation and phase separation is not obvious. These transition points are symbolized with circles with crosses. It should be also stressed that due to high viscosity of the samples, the phase diagrams do not necessarily reflect the thermodynamic equilibrium. In the graphs obtained, the x-axis gives weight percent, wt %, of LiCl in DMA, if not stated otherwise. Thus, the LiCl concentration in the starting solution, i.e. in the pure DMA, is given, but not the final LiCl concentration, which is slightly different by the contents of added water and cellulose. The numbers correspond to weight percent throughout. The mole numbers, n, are absolute values, not normalized to the weight or the sum of all mol numbers.

3.2.4 Rheology

The dynamic viscosity of some cellulose/LiCl/DMA samples was determined with the help of a rotational viscosimeter RVDVIII (Brookfield). For the experiments samples with increasing concentration of cellulose (0.5 - 3 %) and probes with increasing LiCl concentration in DMA (4.5 - 8.5 %) were examined. The obtained curves (time, τ, versus dynamic viscosity, η, and η versus shear stress, γ) were fitted and the data extrapolated to $\tau = 0$ s (η_0) and $\tau = \infty$ s (η_∞). Each sample was measured twice and the difference divided by two was taken as the error of the measurement.

3.3 DRS measurements

There are two main techniques used in the dielectric spectroscopy, see [9–13] - the frequency domain interferometry (FDI), see [92], and the time domain reflectometry (TDR), see [58, 93]. The measurements in the frequency domain yield directly the complex dielectric permittivity as function of the used frequency. TDR allows the determination of the

response functions and the application of Fourier transformation leads to the complex dielectric permittivity.
In this work a combination of both systems was used in order to record the complex dielectric spectra in the range $0.2 \leq \nu\ /\mathrm{GHz} \leq 89$. The precision of the measurements was better than 2 % of the static permittivity of the sample.

3.3.1 Interferometry

The method of travelling waves [94] proved to be appropriate for the determination of complex permittivity data in the microwave and millimeter region [95, 96]. The transmission line theory shows that in a waveguide filled with a dielectric of permittivity, ε', only frequencies higher than the cut-off frequency, ν_c^{mn}, are transmitted

$$\nu_c^{mn} = \frac{c_0}{2\pi\sqrt{\varepsilon'}} k_c^{mn} \tag{3.4}$$

where

$$(k_c^{mn})^2 = \left(\frac{m\pi}{a}\right)^2 + \left(\frac{m\pi}{b}\right)^2 \tag{3.5}$$

for the wave mode determined by (m, n) with $m = 1, 2, \ldots$ and $n = 0, 1, 2 \ldots$. The frequency band used for a given waveguide is defined by the so-called TE_{10}-mode representing the only transmittable wave type in the range $\nu_c^{10} \leq \nu \leq 2\nu_c^{10}$.
From the experiment the values of generalized permittivity, $\hat{\eta}$, can be obtained as follows

$$\eta'(\omega) = \left(\frac{c_0}{\nu}\right) \cdot \left[\left(\frac{1}{\lambda_M}\right)^2 - \left(\frac{p\alpha}{2\pi}\right)^2 + \left(\frac{1}{2a}\right)^2\right] \tag{3.6}$$

and

$$\eta''(\omega) = \left(\frac{c_0}{\nu}\right)^2 \cdot \left(\frac{p\alpha}{\pi\lambda_M}\right) \tag{3.7}$$

with the conversion factor

$$p = \left(20 \log \mathrm{e} \cdot \frac{dB}{Np}\right)^{-1} \tag{3.8}$$

where λ_M represents the wavelength of the transmitted radiation of certain ν and α the attenuation coefficient. Both values can be then determined by the adjusting of the interference minimum at a defined probe position, z_0

$$A(z - z_0) = A_0 + 10 \log\left[(1 + \exp(-2p\alpha(z - z_0))\right. \\ \left. - 2\cos\left[\frac{2\pi}{\lambda_M}(z - z_0)\right] \cdot \exp(-p\alpha(z - z_0))\right. \tag{3.9}$$

where A_0 represents the relative intensity of the signal.

Instrumentation

For the measurements double-beam interferometers with a measuring cell of variable path-length in the sample beam are used. A frequency stabilized signal source serves as a transmitter for both the measuring and reference branch. In the measuring branch a phase attenuator and a measuring cell are placed. A part of the reference branch is a precision phase shifter. The cell is composed of a hollow guide conductor filled with the measured solution and a measuring probe whose position is controlled by a motor. The apparatus used in our lab (for details see [92]) is composed of a set of four rectangular waveguide interferometers (Mach-Zender) working on the transmission principle in the following range: X-band $8.5 \leq \nu/\mathrm{GHz} \leq 12$, Ku-band $12.4 \leq \nu/\mathrm{GHz} \leq 18$, A-band $26.4 \leq \nu/\mathrm{GHz} \leq 40$ and E-band $60 \leq \nu/\mathrm{GHz} \leq 90$ (fig. 3.2). While the X-band interferometer operates only at (298.15 ± 0.02) K, the wave guide instruments for $12.4 \leq \nu \leq 90$ GHz were geared up for the temperature range $248.15 \leq T/\mathrm{K} \leq 338.15$ with 0.1 K accuracy[83].

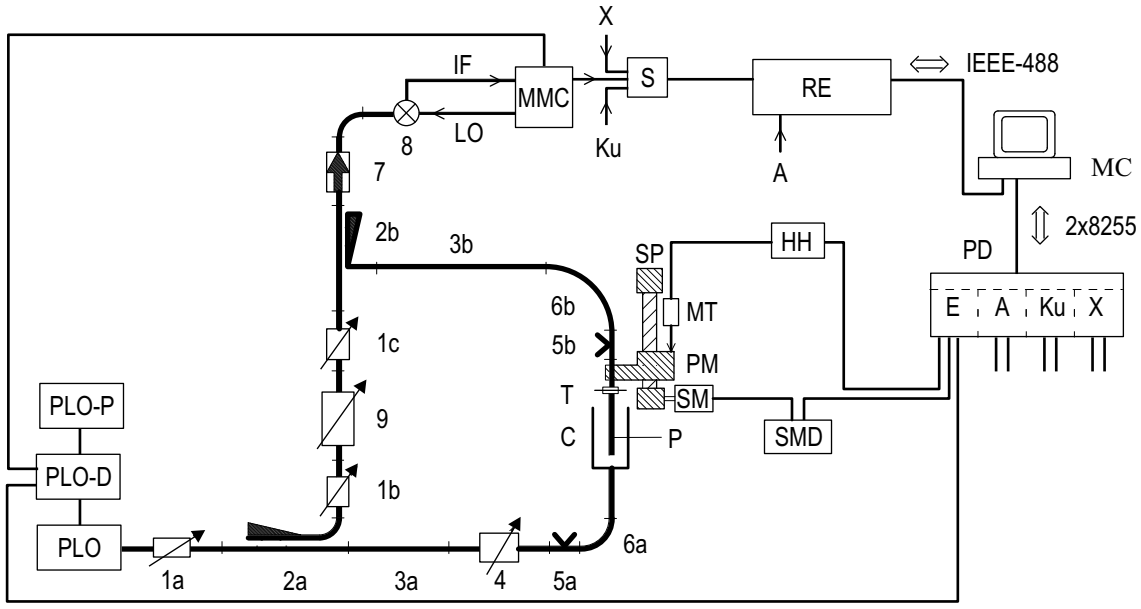

Figure 3.2: Block diagram of the E-band device[92]: **1a**, **b**, **c** represent variable attenuators; **2a**, **b** directional couplers; **3a**, **b** waveguide sections; **4** precision phase shifter; **5a**, **b** E/H tuners; **6a**, **b** flexible waveguides; **7** isolator; **8** harmonic mixer; **9** variable precision attenuator; **C** cell, **HH** bidirectional counter; **MC** microcomputer; **MMC** millimeter-wave to microwave converter; **MT** digital length gauge; **P** probe; **PD** parallel interface unit; **PLO** phase locked oscillators; **PLO-D** PLO-control unit; **PLO-P** PLO-power supply; **PM** probe mount; **RE** precision receiver; **S** electromechanical switch; **SM** stepping motor; **DMD** stepping motor control unit; **SP** spindle and spindle mount; **T** tapered transmission; double lines represent waveguides, thick lines semi-rigid microwave cables and normal lines symbolize data transfer connections (analog or digital). For detailed information see ref.[92]

3.3.2 Time Domain Reflectometry

Time domain reflectometry (TDR) or spectroscopy (TDS) was established at the end of the sixties by Fellner-Feldegg [97, 98] and further developed by Cole and his coworkers [99–101]. This technique is based on recording of the impedance in the system. The dielectric properties are then calculated from the obtained impedance values. The TDR-measurements can be based either on the reflection or transmission principle. Our device uses reflection cutoff cells [103].

Theoretical background

A fast rising voltage pulse, $V_0(t)$ (rise time t_a) generated by a tunnel diode is applied to the sample. The shape of $V_0(t)$, registered by a fast sampling scope (response time t_r), is then compared with the transients of the signal transmitted through, $V_t(t)$, or reflected by the sample cell, $V_r(t)$. The intensities of the signals are transformed by Fourier transformation which results in

$$v_0(\omega) = \mathcal{L}_{\mathrm{i}\omega}\left[\frac{\mathrm{d}}{\mathrm{d}t}V_0(t)\right] = \int_0^\infty \frac{\mathrm{d}}{\mathrm{d}t}V_0(t)\cdot\exp(\mathrm{i}\omega t)\mathrm{d}t \tag{3.10}$$

$$v_r(\omega) = \mathcal{L}_{\mathrm{i}\omega}\left[\frac{\mathrm{d}}{\mathrm{d}t}V_r(t)\right] = \int_0^\infty \frac{\mathrm{d}}{\mathrm{d}t}V_r(t)\cdot\exp(\mathrm{i}\omega t)\mathrm{d}t \tag{3.11}$$

From the transformed values $v_0(\omega)$ and $v_r(\omega)$ the absolute reflection coefficient of the cell, $\hat{\rho}(\omega)$, can be calculated

$$\hat{\rho}(\omega) = \frac{c_0}{\mathrm{i}\omega g l}\cdot\frac{v_0(\omega)-v_r(\omega)}{v_0(\omega)+v_r(\omega)} \tag{3.12}$$

where l is the electrical pin-length and g the ratio between wave resistance of the empty cell and the connection.
The complex dielectric permittivity, $\hat{\eta}(\omega)$, can be obtained from $\hat{\rho}(\omega)$ in the following manner

$$\hat{\eta}(\omega) = \hat{\rho}(\omega)\cdot\hat{z}\cot\hat{z} \tag{3.13}$$

where

$$\hat{z} = \frac{\omega l}{c_0}\sqrt{\hat{\eta}(\omega)} \tag{3.14}$$

However, the signal intensity of the incident wave cannot be obtained in the measurement and therefore has to be eliminated from the calculation. For this purpose a measurement of a reference with known permittivity is used (usually air, pure solvent, another liquid with similar dielectric properties). In this way the relative reflection coefficient can be calculated as

$$\hat{\rho}(\omega) = \frac{c}{\mathrm{i}\omega g l}\cdot\frac{\mathcal{L}_{\mathrm{i}\omega}\left[\frac{\mathrm{d}}{\mathrm{d}t}V_{rr}(t)\right]-\mathcal{L}_{\mathrm{i}\omega}\left[\frac{\mathrm{d}}{\mathrm{d}t}V_{rx}(t)\right]}{\mathcal{L}_{\mathrm{i}\omega}\left[\frac{\mathrm{d}}{\mathrm{d}t}V_{rr}(t)\right]+\mathcal{L}_{\mathrm{i}\omega}\left[\frac{\mathrm{d}}{\mathrm{d}t}V_{rx}(t)\right]}. \tag{3.15}$$

where $V_{rx}(t)$ and $V_{rr}(t)$ represent the relative time dependent reflection intensities of the sample and the reference [100, 101]. This coefficient can be written also in the following way which represents the working equation of TDR

$$\hat{\rho}_{xr} = \frac{\hat{\eta}_x \cdot \hat{z}_r \cot(\hat{z}_r) - \hat{\eta}_r \cdot \hat{z}_x \cot(\hat{z}_x)}{\hat{z}_r \cot(\hat{z}_r)\hat{z}_x \cot(\hat{z}_x) + g^2 \cdot \hat{\eta}_x \hat{\eta}_r (\omega l/c)^2} \tag{3.16}$$

with

$$\hat{z}_x = \frac{\omega l}{c}\sqrt{\hat{\eta}_x} \quad \text{and} \quad \hat{z}_r = \frac{\omega l}{c}\sqrt{\hat{\eta}_r} \tag{3.17}$$

In order to obtain the complex dielectric permittivity of the sample only some approximations can be used as eq.(3.16) does not have a real mathematical solution. For this purpose Taylor-series of the term $z \cdot \cot z$ or the Newton-Raphson-procedure [102] are applied.

Device

As can be seen from fig. 3.3 the time-domain reflectometer in our lab is composed of a sampling scope (TEK 11802; Tektronix) and two sampling heads (SD24) of maximum time resolution of 0.02 ps. Each of the sampling heads has two independent channels which are able to conduct four reflection or two transmission experiments simultaneously. For the experiments a set of cutoff reflection cells is used. Each of the cells is adapted to certain frequency range so that a good signal-to-noise ratio can be reached. For details of cell construction please see [83, 103].
The majority of the measurements presented in this work was recorded with the cells T1 and T2 (the lowest ν reached was 0.2 GHz). These was considered as sufficient as no further relaxation at lower ν was expected. Later some additional measurements with the cell T11 were done. However, the application of this cell is strongly limited by the conductivity of the measured sample and so T11 could not be used for all the samples. In the case of cellulose samples the combination of all three cells was applied as the conductivity of the used LiCl/DMA solution was convenient. The characteristics of the cells used in this study are listed in table 3.3. As the electrical pin length, l_{el}, of the T1 cell is dependent on the properties of the measured system, it was adjusted to the T2 cell. The l_{el} of the T2 cell proved to be slightly different for systems with different static permittivity. This was quantified in one calibration measurement with different solvents and evaluated as $l_{\mathrm{el}} = f(\varepsilon)$ (see fig. 3.4). The scatter of the data can be probably explained by the large sensitivity of the parameters.

Measurement procedure

Note that the following procedure is described in detail in ref. [103]. A voltage pulse $V_0(t)$ is transmitted from the pulse generator integrated into the sampling heads SH1 and SH2 (fig. 3.3) to the cell. From a certain point, t_{start}, voltage-time transients of the reflected signal (usually $n = 5120$ equidistant data pairs (t, V_r)) are recorded. These are sampled in the time window $t_{\max} = t_{\mathrm{stop}} - t_{\mathrm{start}}$ with a resolution $\Delta t = t_{\max}/n$. Theoretically the

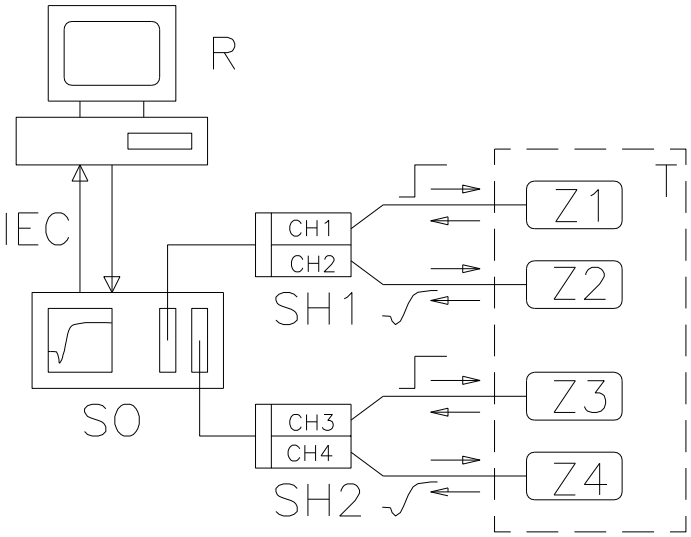

Figure 3.3: Diagram[103] describing the time-domain reflectometer used in our group: **SO** digital sampling scope; **SH1,SH2** SD-24 sampling heads; **Z1-Z4** cutoff cells; **T** precision thermostat; **R** personal computer with access to other computers for data analysis.

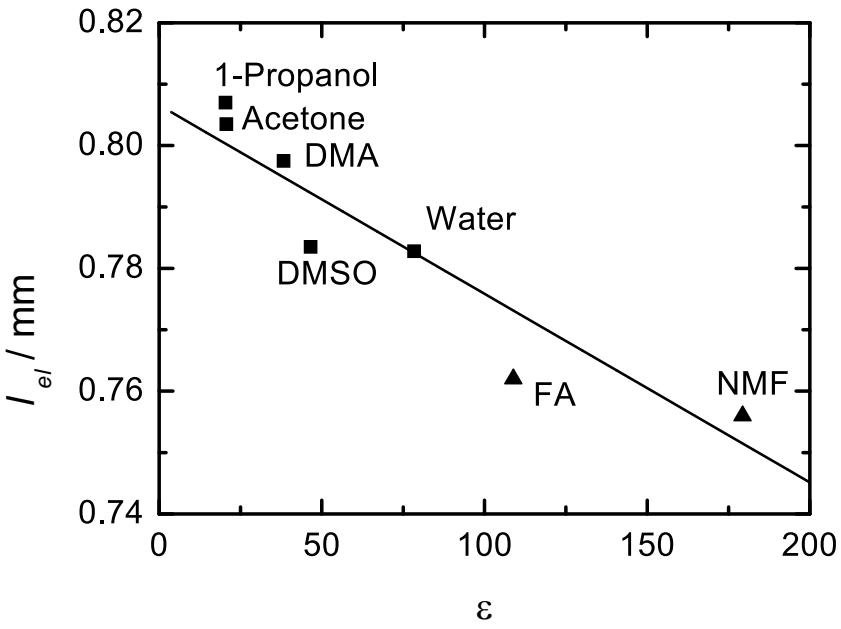

Figure 3.4: Diagram showing the values of the electrical pin length, l_{el}, of the T2 cell at 25 ^{o}C for different solvents characterized by their static permittivity, ε: ■ data from this work, ▲ data from [104].

Table 3.3: The parameters of the used cells mechanical and electrical pin length, l_{mech} and l_{el}, the ratio of the feeding line impedance to the impedance of the empty cell g, the starting point of the time window, t_0, of time increment Δt.

Cutoff cell	l_{mech}	l_{el}	g	t_0	Δt
T1	0.0	≈ 0.350	0.4416	82.0	1.0
T2	0.5	≈ 0.800	0.4416	82.0	1.0
T11	1.5	1.890	0.42855	89.1	1.0 or 2.0

units: l_{mech} and l_{el} in mm; t_0 and Δt in ns.

maximum measurable frequency is determined as $\nu_{\max} = 1/2\Delta t$. However, this value does not have practical relevance because of the smaller bandwidth of 20 GHz determined by the total instrument rise time. A small value of Δt is important for the determination of the starting point t_0 of the Laplace transformation corresponding to the arrival of the first signal at the detector (see table 3.3). The electrical pin length, l_{el}, different for each cell defines $t_{\max}$. $t_{\mathrm{start}} < t_0$ is chosen in such a way that a proper determination of the baseline is possible at the optimum value of the minimum accessible frequency $\nu_{\min} = 1/(t_{\mathrm{stop}} - t_0)$. The intensity of the signal reflected from the sample, $V_{rx}(t)$, is compared with $V_{rr}(t)$ representing the transient obtained from the cell filled with a reference (air or a solvent of known permittivity, $\hat{\eta}_r(\nu) = 1$). From the relative reflection coefficient, $\hat{\rho}(\omega)$, calculated with the eq.(3.15) the generalized complex permittivity, $\hat{\eta}_x(\nu)$, is obtained (see eq.(3.16) and eq.(3.17)). The transients are involved in data processing after the averaging over all the 256 single traces.

Chapter 4

Data analysis

4.1 Remarks to the data analysis

After the frequency dependent dielectric permittivity, $\hat{\varepsilon}$, was measured, the experimentally obtained values of ε' and ε'' were fitted by an appropriate relaxation model in terms typical for the description of dielectric relaxation spectra, as ε_i, τ_i, ε_∞ and eventually the corresponding empirical parameters. The possible band-shape models are described in detail in 2.3.

The choice of the relaxation model follows some basic rules. The obtained parameters must be physically reasonable and the variance of the fit, σ^2, (eq.(4.1)) should be small. Further, the number of the relaxation processes should be reasonable and the relaxation models should not change within one concentration or temperature series. It should be also possible to assign the resulting relaxation processes to some physical or chemical changes in the system.

It should be noted that the same system can be often described by various relaxation models with similar σ^2, since the application of the model is dependent on the measured frequency range and also the precision of the data and the empirical conductivity correction of the TDR apparatus. For the evaluation of the data the MWFIT program based on the method of Gauß and Marquardt [105] was used. It applies the chosen relaxation model to the experimentally obtained ε' and ε'' and the smaller the resulting variance (eq.(4.1)) the better the fit.

$$\sigma^2 = \frac{m}{2\,m - n} \sum_{i=1} \left[(\varepsilon'_i - \varepsilon'_{i,\mathrm{calc}})^2 + (\varepsilon''_i - \varepsilon''_{i,\mathrm{calc}})^2 \right] \tag{4.1}$$

In eq.(4.1) m represents the number of value triples, n the number of fit parameters, $\hat{\varepsilon}_i$ the experimental and $\hat{\varepsilon}_{i,\mathrm{calc}}$ the calculated dielectric permittivity.

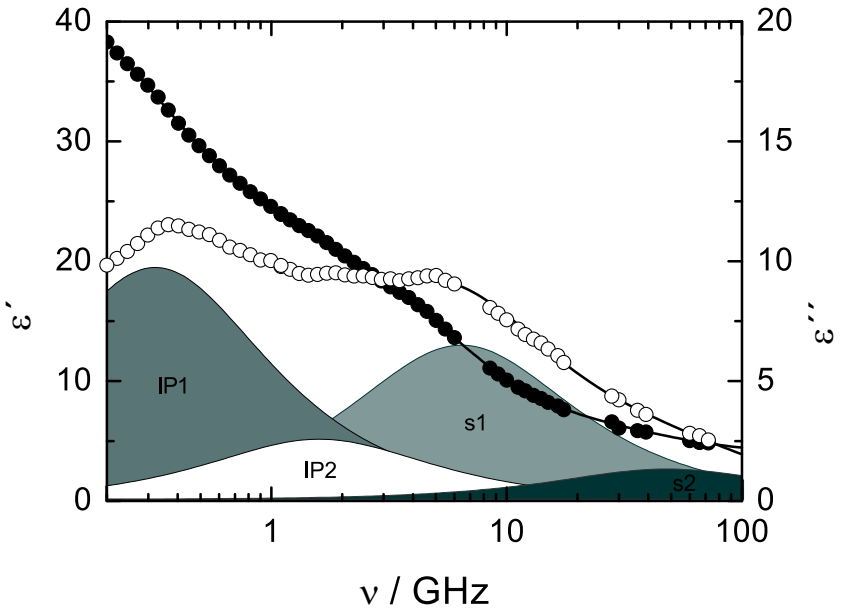

Figure 4.1: Example of a spectrum showing dielectric permittivity, ε', (•), and dielectric loss, ε'', (∘), of LiCl in DMA (c = 1.795 mol L^{-1}) at 298.15 K. The areas indicate the contribution of the solute (IP1,IP2) and solvent relaxation (s1, s2) to ε''.

4.2 Temperature dependent DRS measurements

4.2.1 Choice of the relaxation model

The LiCl/DMA system was measured by the DRS over the entire concentration range at five different temperatures in the temperature range -15 $\leq t/°C \leq$ 65. However, the measurements at the temperatures below 0 °C do not seem to be very reliable. The most probable reason for the bad quality of low-temperature data could be the penetration of moisture into the cells and eventually ice crystallization during or between the measurements. So the data at -15 °C are not shown here and will not be discussed further.

All possible relaxation models were applied to the experimental data and the best variation of the fit, σ^2, was reached by the superposition of four Debye processes (4D fit). The data obtained by the application of the 4D fit seemed to be physically reasonable and internally consistent over the corresponding concentration range. The low-frequency relaxation processes were ascribed to the presence of ion-pair species (IP1 and IP2 in fig. 4.1). Especially with increasing LiCl concentration the low-frequency relaxation processes became well pronounced (see fig. 4.1). The corresponding permittivities, ε_1, ε_2 and ε_3 (see fig. 4.2) and the resulting amplitudes, S_1 and S_2, seemed to be reasonable as well. The corresponding relaxation times, τ_1 and τ_2, were in the right order of magnitude typical for the tumbling motion of ionic species [14, 106, 107], even though their values did not show a clear concentration dependence (see section 4.4).

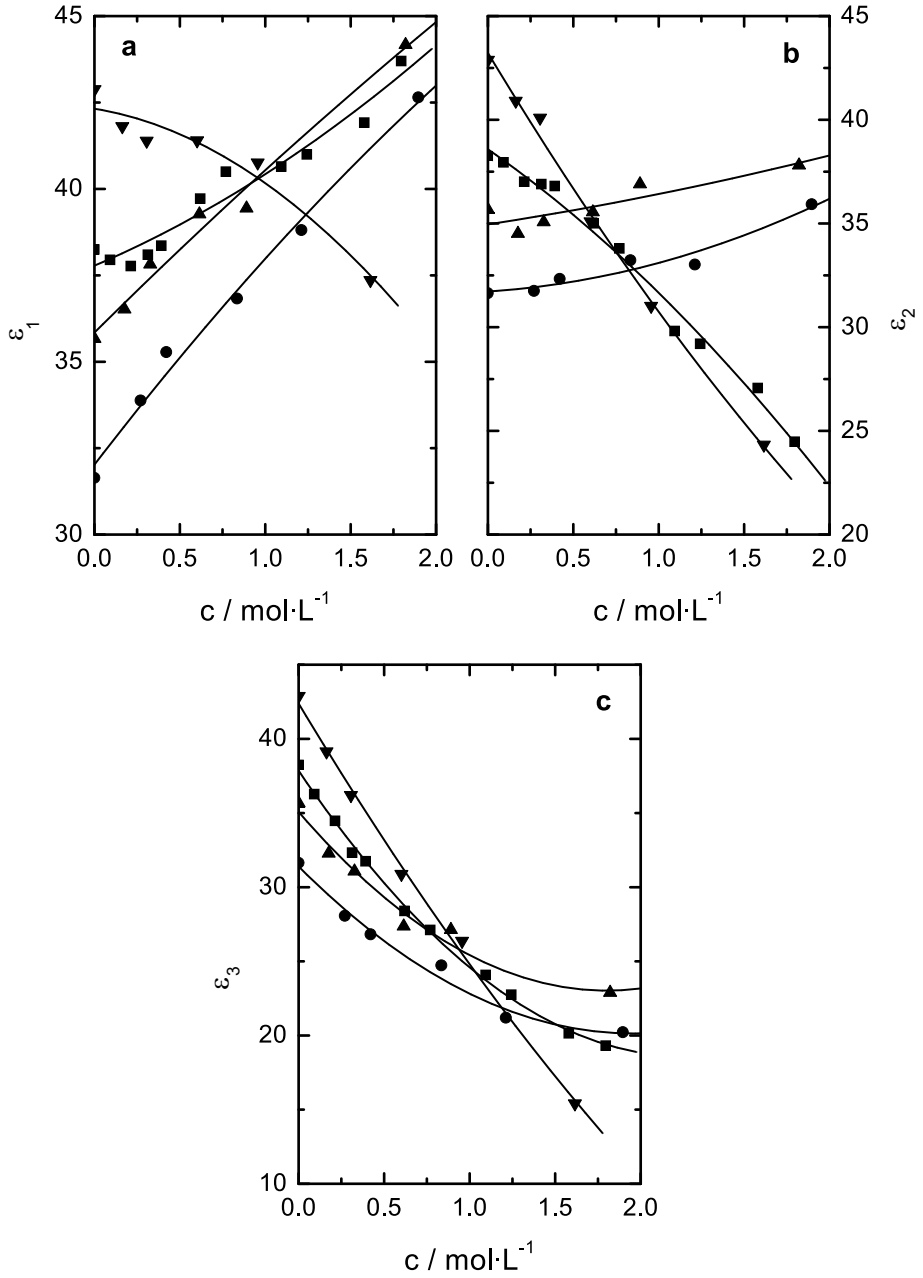

Figure 4.2: The comparison of the first three permittivities ε (a), ε_1 (b) and ε_2 (c) resulting from the 4D-fit at 278.15 K (▼), 298.15 K (■), 318.15 K (▲) and 338.15 K (●).

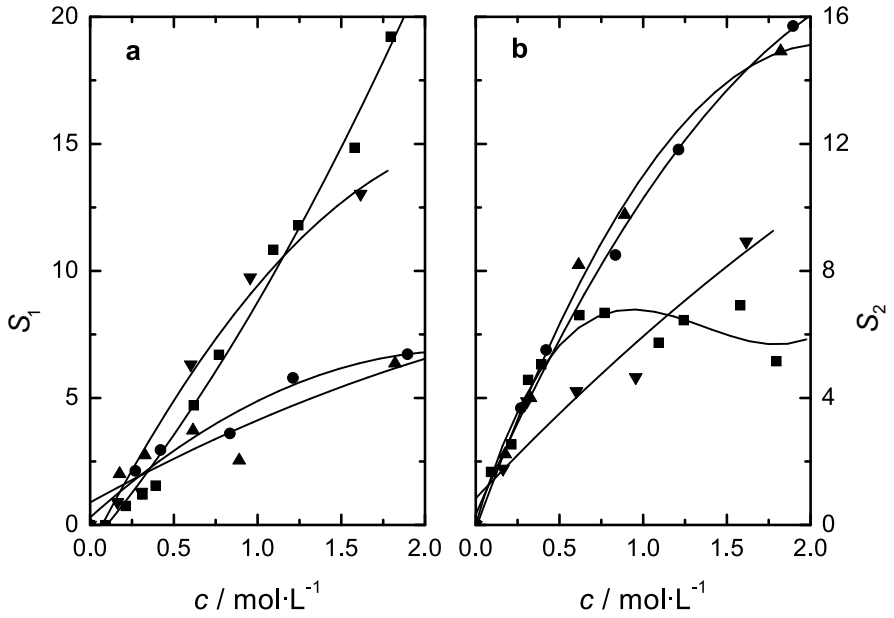

Figure 4.3: The comparison of the first two amplitudes S_1 (a) and S_2 (b) resulting from the 4D-fit at 278.15 K (▼), 298.15 K (■), 318.15 K (▲) and 338.15 K (●).

When the amplitudes at different temperatures were compared, the tendency of the curves was not the same for all temperatures (see fig. 4.3) and the behavior of the corresponding relaxation times did not show any clear tendency either (see fig. 4.4). The latter observation, combined with the fact that the relative ion-pair concentrations calculated from the corresponding amplitudes (S_1 and S_2 in fig. 4.3) behaved nearly independently from each other, which is not very typical for such systems, lead us to the conclusion that this was probably not the correct model for the description of this system. Therefore another model was proposed.

Table 4.1 shows a comparison of various relaxation models applied to the complex permittivity spectrum of a concentrated LiCl/DMA solution at 298 K. It can be seen that the 3D fit is not sufficient for the description of the spectrum. So the combination of two Debye and one Cole-Cole or Cole-Davidson has to be applied to the spectrum. The parameters α or β corresponding to the used model are for the lack of space listed behind the ε_∞. In comparison to the 4D fit the CC+D+D fit results in higher variance of the fit and higher static permittivity (ε(4D) = 41.92; ε(CC+D+D) = 48.01). The D+CC+D fit does not lead in this case to physically reasonable parameters. The CD+D+D fit yields only slightly higher static permittivity than the 4D fit at σ^2 comparable to the CC+D+D fit. However, the values of β are very low, and it could not be applied for all the measured spectra. The D+CD+D does not resolve the last solvent relaxation process, similar to the 3D fit.

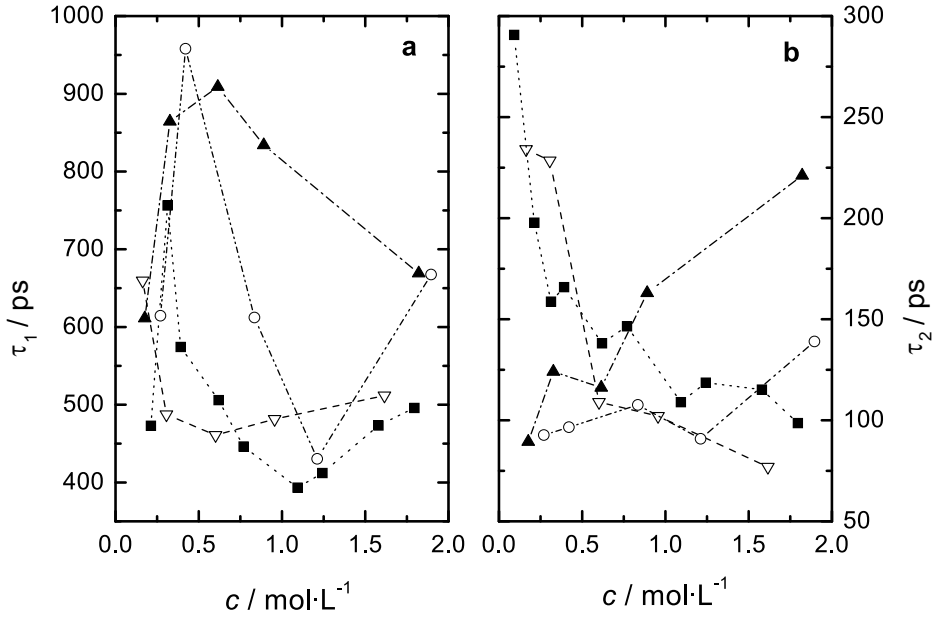

Figure 4.4: The comparison of the first two relaxation times τ_1 (a) and τ_2 (b) resulting from the 4D-fit at 278.15 K (▽), 298.15 K (■), 318.15 K (▲) and 338.15 K (○).

Table 4.1: Comparison of dielectric parameters (limiting permittivities $\varepsilon_{\mathrm{IP1}}$, $\varepsilon_{\mathrm{IP2}}$, $\varepsilon_{\mathrm{s1}}$, $\varepsilon_{\mathrm{s2}}$, ε_∞, relaxation times τ_{IP1}, τ_{IP2}, τ_{s1}, τ_{s2}, the corresponding relaxation time distribution parameter, α or β, and variance of the fit σ^2) resulting from the application of various models to the complex dielectric spectrum of a LiCl/DMA solution ($c = 1.5795$ mol L^{-1}) at 298 K.

Model	$\varepsilon_{\mathrm{IP1}}$	τ_{IP1}	$\varepsilon_{\mathrm{IP2}}$	τ_{IP2}	$\varepsilon_{\mathrm{s1}}$	τ_{s1}	$\varepsilon_{\mathrm{s2}}$	τ_{s2}	ε_∞	σ^2
3D	40.68	372	24.1	42.9	12.45	11.6			4.4	0.0414
4D	41.92	476	27.07	115	20.15	23.0	6.48	4.02	3.89	0.0083
CC+D+D [a]	48.01	419			18.28	23.5	6.01	4.20	3.81	0.0092
CD+D+D [b]	42.57	688			14.11	23.4	3.63	5.26	2.83	0.0095
D+CD+D [c]	42.50	545	29.55	249	12.41	22.2			2.14	0.0104

units: τ_i in 10^{-12} s; [a] $\alpha_{\mathrm{IP1}} = 0.259$; [b] $\beta_{\mathrm{IP1}} = 0.448$; [c] $\beta_{\mathrm{IP2}} = 0.369$

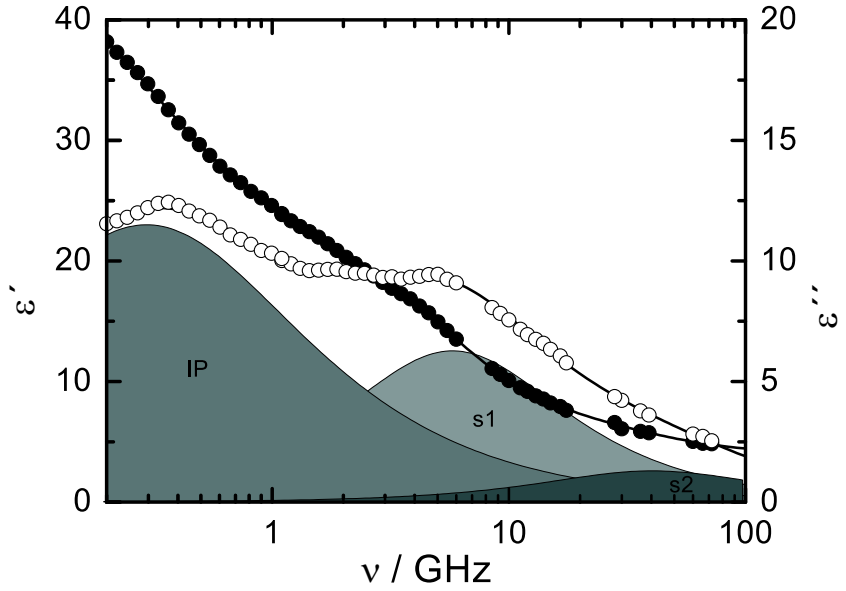

Figure 4.5: Example of a spectrum showing dielectric permittivity, ε', (•), and dielectric loss, ε'', (○), of LiCl in DMA (c = 1.795 mol L^{-1}) at 298.15 K. The shaded areas indicate the contribution of the solute (IP) and solvent relaxation (s1, s2) to ε''.

4.2.2 Applied relaxation model

The CC+D+D fit lead to physically reasonable results for all measured spectra with the smallest σ^2 next to the 4D fit. However, the large values of the parameter α (see tables 4.2, 4.3, 4.4 and 4.5) indicate the possibility of the existence of two or more relaxation processes which cannot be properly resolved. Example of a fitted complex permittivity spectrum is shown in fig. 4.5. In this case only one relaxation resulting from the ionic motion was observed (IP). The concentration-dependent behavior of the permittivities and amplitudes resulting from the new relaxation model is demonstrated in figs. 4.6 and 4.7. When the values of S_1 (fig. 4.7a) are compared with the corresponding values of the amplitudes S_1 and S_2 resulting from the 4D fit (fig. 4.3), it can be seen that the CC+D+D model leads to smoother dependence of the relaxation parameters on the temperature and LiCl concentration in comparison to the 4D model. The two first relaxation times, τ_1 (IP) and τ_2 (s1), are displayed in fig. 4.8. In this figure it can be seen that the use of this model results also here, in the case of relaxation times as function of temperature, in a more coherent picture of the system. The frequency-dependent spectra showing the dielectric permittivity, ε', and dielectric loss, ε'', at various LiCl concentrations are displayed for the following temperatures: 298 K (fig. 4.9), 278 K (fig. 4.10), 318 K (fig. 4.11) and 338 K (fig. 4.12). Although it is evident that the CC+D+D fit does not describe the system in its whole complexity, the results seem to be more appropriate for the description of the measured spectra than the parameters resulting from the 4D model. Thus, the further analysis of the data is based on the CC+D+D fit.

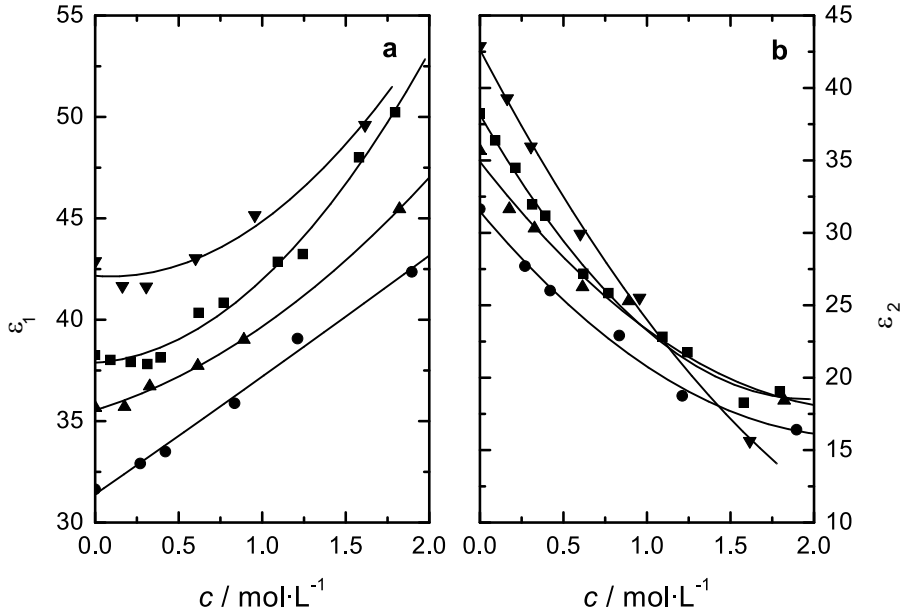

Figure 4.6: The first two permittivities ε (a) and ε_1 (b) resulting from the CC+D+D fit at different temperatures - 278.15 K (▼), 298.15 K (■), 318.15 K (▲) and 338.15 K (●).

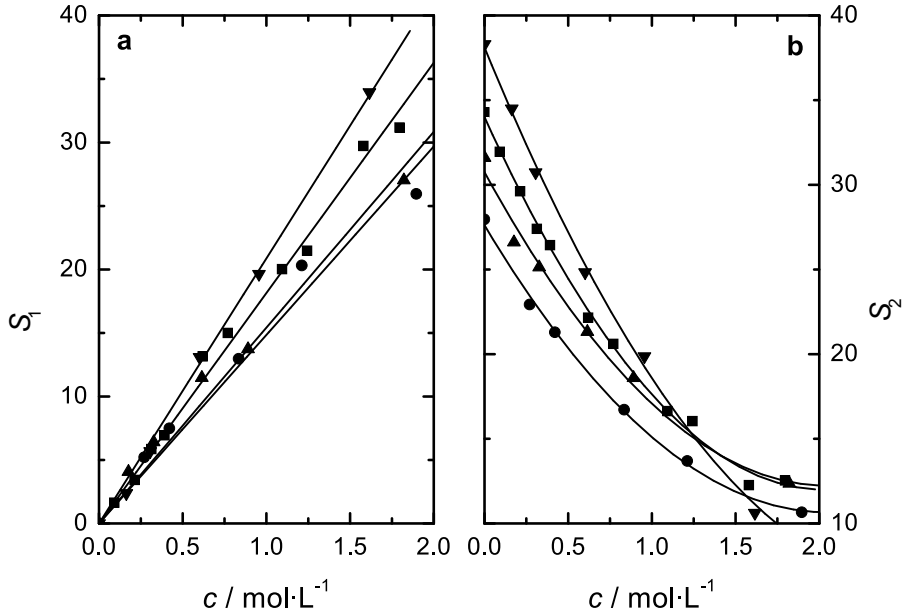

Figure 4.7: The amplitudes of the first and second relaxation process, S_1(a), and S_2(b) resulting from the CC+D+D fit at 278.15 K (▼), 298.15 K (■), 318.15 K (▲) and 338.15 K (●).

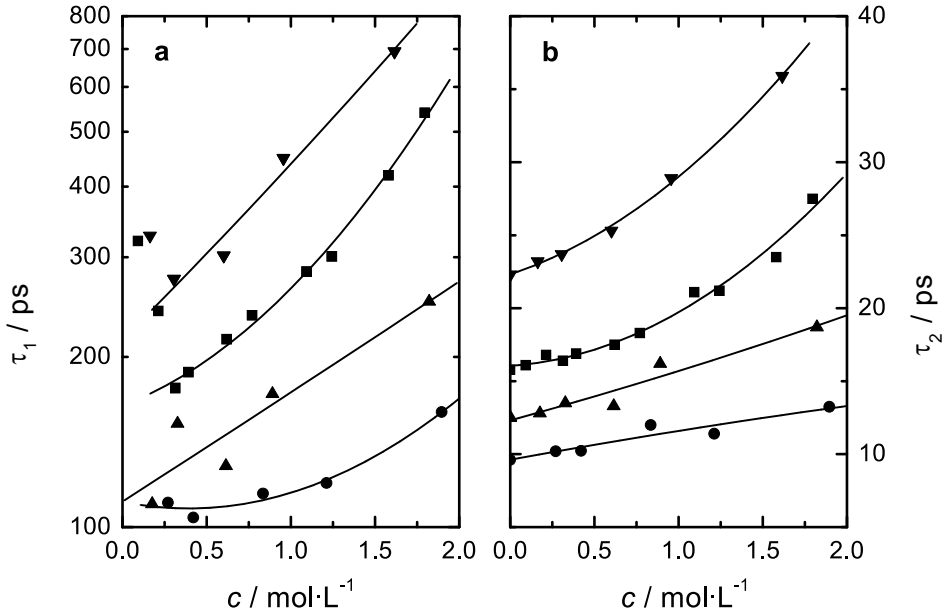

Figure 4.8: The relaxation time of the first and second relaxation process, τ_1(a) and τ_2(b) resulting from the CC+D+D fit at 278.15 K (▼), 298.15 K (■), 318.15 K (▲) and 338.15 K (●).

Table 4.2: Dielectric parameters (limiting permittivities ε_1, ε_2, ε_3, ε_∞, relaxation times τ_1, τ_2, τ_3, relaxation time distribution parameter, α, and variance of the fit σ^2) of the CC+D+D model fitted to the complex permittivity spectra of LiCl and in DMA at 298 K.

c	ε_1	τ_1	α	ε_2	τ_2	ε_3	τ_3	ε_∞	σ^2
0 [a]				38.25	15.8	3.97	0.95	2.98	0.021
0.0912	38.02	321	0.012	36.38	16.1	4.43	2.82	3.42	0.016
0.2124	37.92	241	0.066	34.49	16.8	4.87	2.72	3.31	0.010
0.3130	37.82	176	0.088	31.96	16.4	4.56	2.40	3.42	0.014
0.3911	38.14	188	0.076	31.19	16.9	4.75	1.17	2.48	0.010
0.6191	40.34	215	0.195	27.18	17.5	5.02	2.83	3.62	0.015
0.7693	40.84	237	0.172	25.84	18.3	5.23	1.82	3.07	0.013
1.0932	42.86	283	0.198	22.83	21.1	6.19	4.16	3.73	0.014
1.2427	43.24	301	0.182	21.76	21.2	5.71	2.81	3.65	0.016
1.5795	48.01	419	0.259	18.28	23.5	6.01	4.20	3.81	0.009
1.7953	50.23	540	0.191	19.05	27.5	6.51	3.84	3.93	0.014

units: c in mol L^{-1}; τ_1, τ_2, τ_3 in 10^{-12} s. [a] Ref. [14]

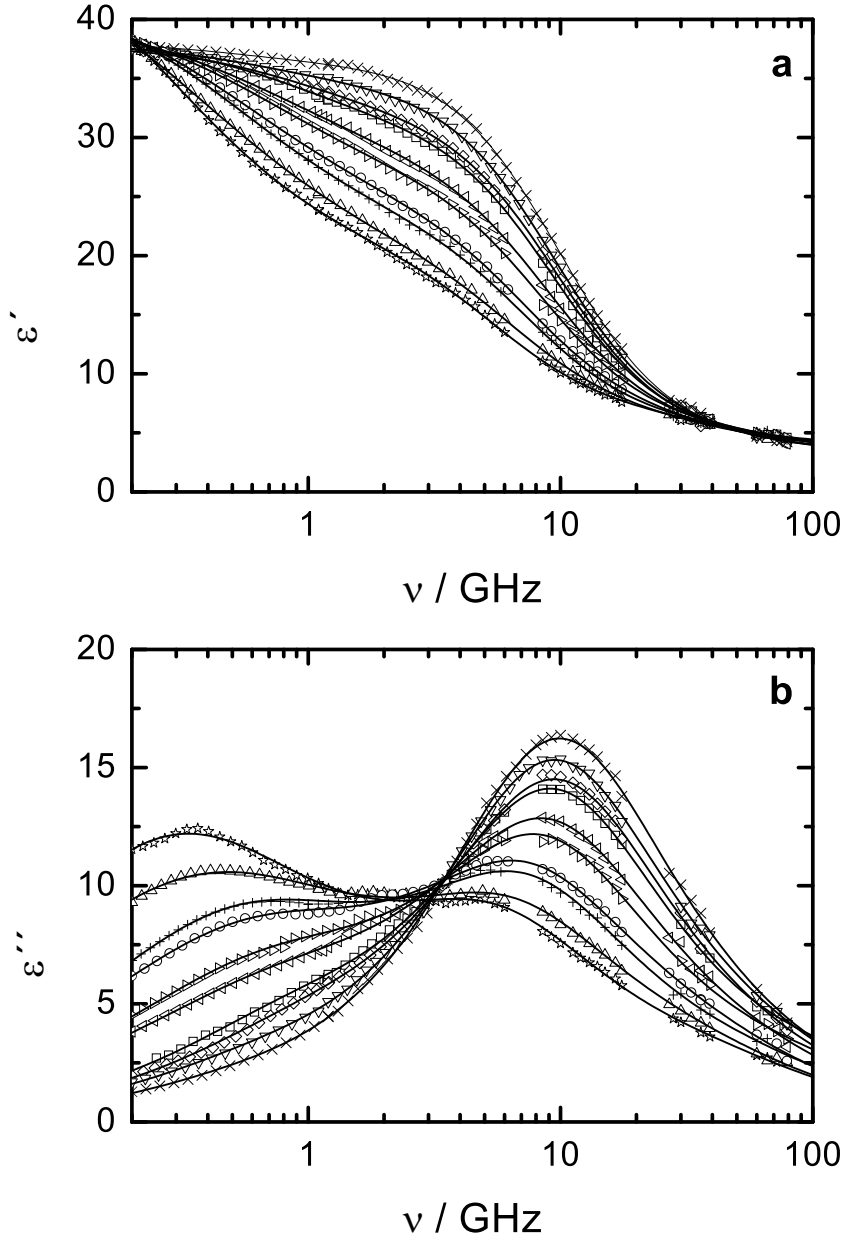

Figure 4.9: Diagram showing dielectric permittivity, ε', (a), and dielectric loss, ε'', (b), of LiCl in DMA at 298.15 K for different concentrations: c = 0.091 mol L^{-1} ($\times$); c = 0.212 mol L^{-1} ($\triangledown$); c = 0.313 mol L^{-1} ($\diamond$); c = 0.391 mol L^{-1} ($\square$); c = 0.619 mol L^{-1} ($\triangleleft$); c = 0.769 mol L^{-1} ($\triangleright$); c = 1.093 mol L^{-1} ($\circ$); c = 1.243 mol L^{-1} (+); c = 1.580 mol L^{-1}($\triangle$); c = 1.795 mol L^{-1} ($\star$). The lines represent the CC+D+D fit.

Table 4.3: Dielectric parameters (limiting permittivities ε_1, ε_2, ε_3, ε_∞, relaxation times τ_1, τ_2, τ_3, relaxation time distribution parameter, α, and variance of the fit σ^2) of the CC+D+D model fitted to the complex permittivity spectra of LiCl and in DMA at 278 K.

c	ε_1	τ_1	α	ε_2	τ_2	ε_3	τ_3	ε_∞	σ^2
0 [a]				42.88	22.3	4.58	2.10	3.23	0.049
0.1631	41.66	327	0.006	39.28	23.2	4.78	1.53	3.03	0.013
0.3059	41.63	275	0.074	35.95	23.7	5.22	2.37	3.47	0.011
0.6012	43.03	302	0.260	29.93	25.3	5.10	2.47	3.56	0.018
0.9561	45.15	449	0.273	25.51	28.9	5.64	4.13	3.93	0.012
1.6154	49.59	693	0.388	15.64	35.9	5.02	3.99	3.65	0.015

units: c in mol L^{-1}; τ_1, τ_2, τ_3 in 10^{-12} s. [a] Ref. [14]

Table 4.4: Dielectric parameters (limiting permittivities ε_1, ε_2, ε_3, ε_∞, relaxation times τ_1, τ_2, τ_3, relaxation time distribution parameter, α, and variance of the fit σ^2) of the CC+D+D model fitted to the complex permittivity spectra of LiCl and in DMA at 318 K.

c	ε_1	τ_1	α	ε_2	τ_2	ε_3	τ_3	ε_∞	σ^2
0 [a]				35.67	12.5	4.06	0.54	1.37	0.036
0.1759	35.71	110	0.160	31.64	12.8	5.03	3.08	3.37	0.019
0.3267	36.72	152	0.178	30.31	13.5	5.18	2.26	3.19	0.017
0.6144	37.73	128	0.114	26.26	13.3	4.94	1.55	2.98	0.024
0.8905	39.02	172	0.121	25.29	16.2	6.69	3.78	3.62	0.028
1.8211	45.46	251	0.179	18.43	18.7	6.07	3.18	3.78	0.028

units: c in mol L^{-1}; τ_1, τ_2, τ_3 in 10^{-12} s. [a] Ref. [14]

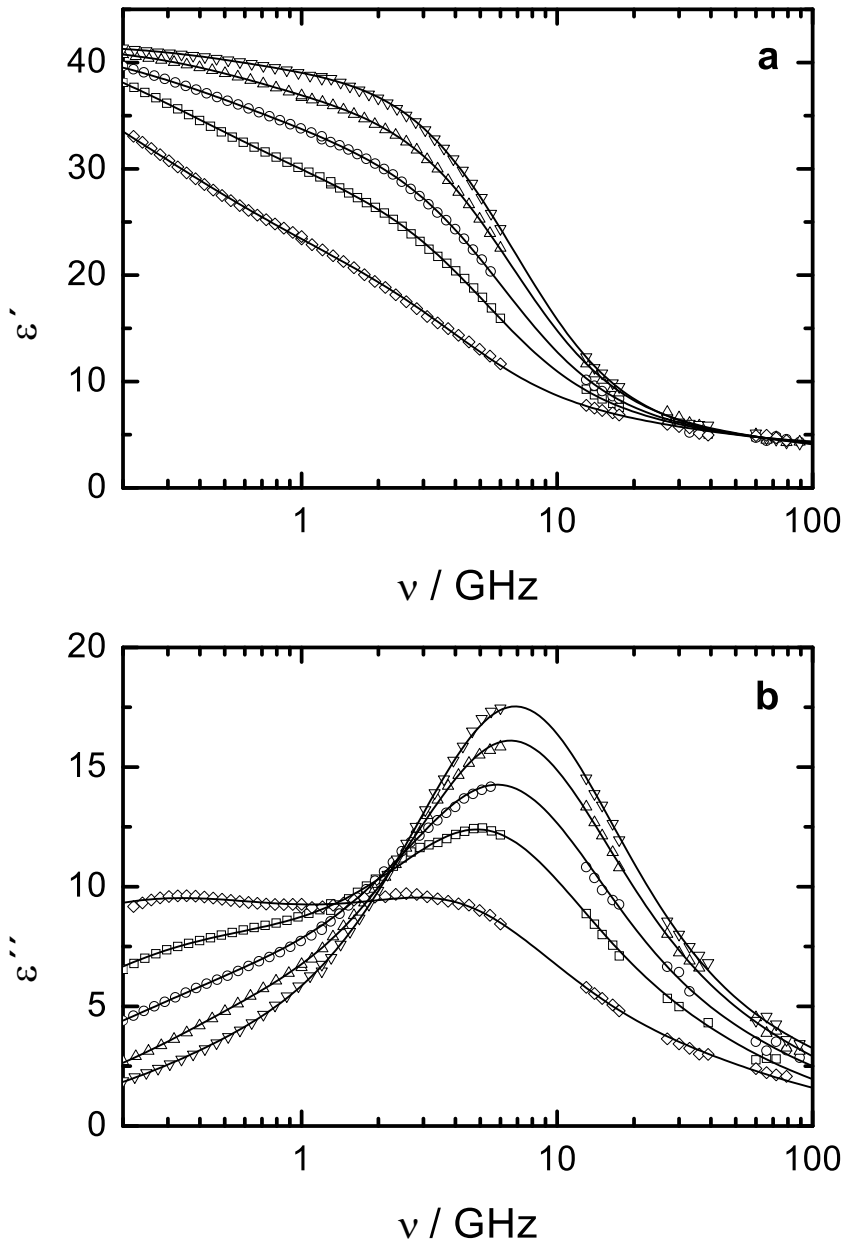

Figure 4.10: Diagram showing dielectric permittivity, ε', (a), and dielectric loss, ε'', (b), of LiCl in DMA at 278.15 K for different concentrations: c = 0.163 mol L^{-1} ($\triangledown$); c = 0.306 mol L^{-1} ($\triangle$); c = 0.601 mol L^{-1} ($\circ$); c = 0.956 mol L^{-1} ($\square$); c = 1.615 mol L^{-1} ($\diamond$). The lines represent the CC+D+D fit.

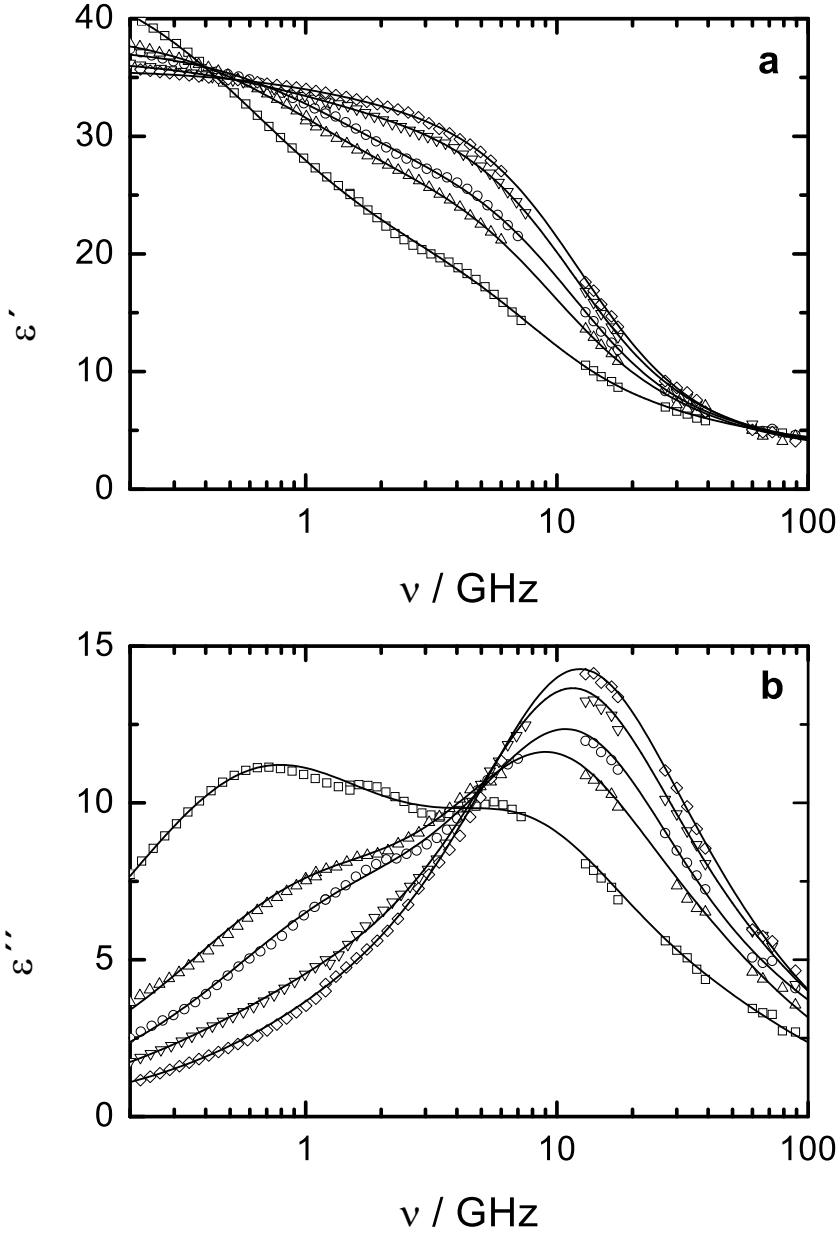

Figure 4.11: Diagram showing dielectric permittivity, ε', (a), and dielectric loss, ε'', (b), of LiCl in DMA at 318.15 K for different concentrations: c = 0.176 mol L^{-1} ($\diamond$); c = 0.327 mol L^{-1} ($\triangledown$); c = 0.614 mol L^{-1} ($\circ$); c = 0.891 mol L^{-1} ($\triangle$); c = 1.821 mol L^{-1} ($\square$). The lines represent the CC+D+D fit.

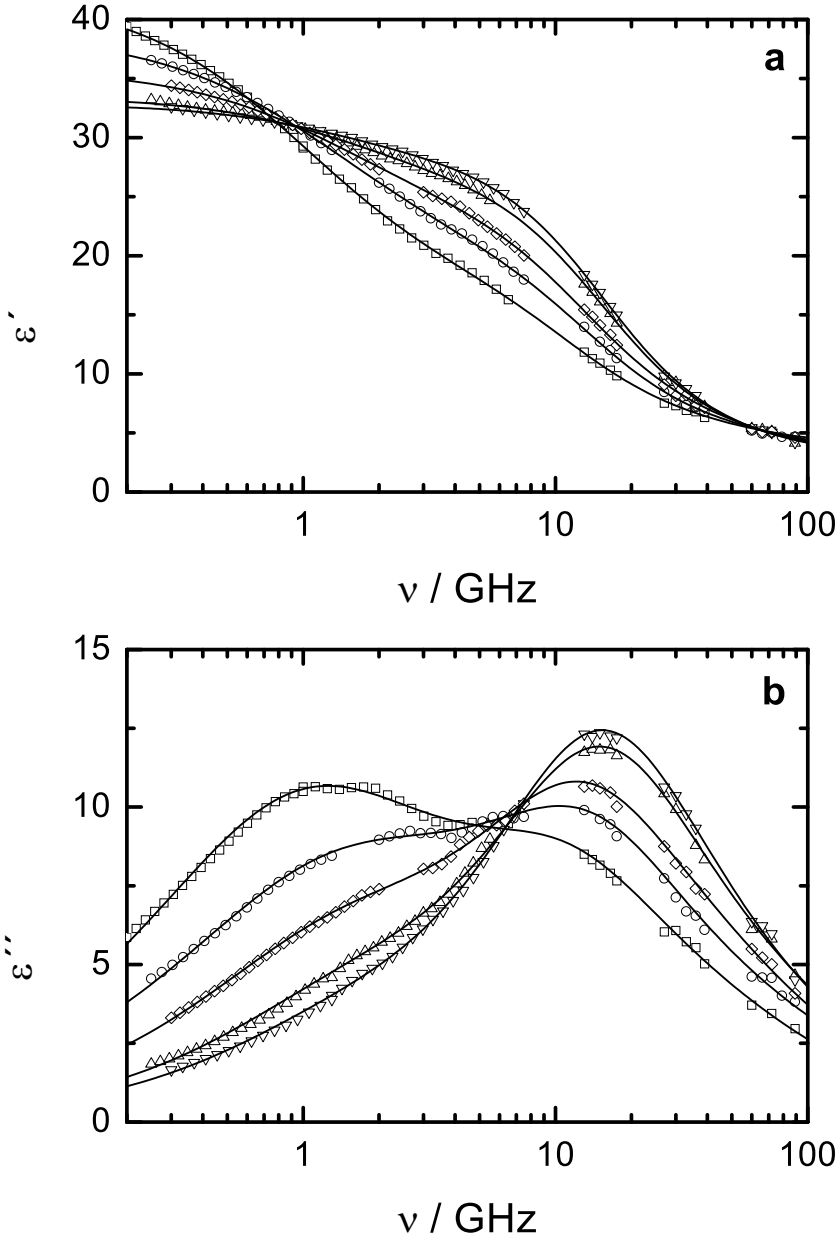

Figure 4.12: Diagram showing dielectric permittivity, ε', (a), and dielectric loss, ε'', (b), of LiCl in DMA at 338.15 K for different concentrations: c = 0.270 mol L^{-1} ($\triangledown$); c = 0.421 mol L^{-1} ($\triangle$); c = 0.835 mol L^{-1} ($\diamond$); c = 1.212 mol L^{-1} ($\circ$); c = 1.896 mol L^{-1} ($\square$). The lines represent the CC+D+D fit.

Table 4.5: Dielectric parameters (limiting permittivities ε_1, ε_2, ε_3, ε_∞, relaxation times τ_1, τ_2, τ_3, relaxation time distribution parameter, α, and variance of the fit σ^2) of the CC+D+D model fitted to the complex permittivity spectra of LiCl and in DMA at 338 K.

c	ε_1	τ_1	α	ε_2	τ_2	ε_3	τ_3	ε_∞	σ^2
0 [a]				31.64	9.61	3.68	0.55	1.62	0.030
0.2701	32.91	111	0.136	27.70	10.2	4.77	2.61	3.25	0.014
0.4205	33.50	104	0.142	26.01	10.2	4.72	1.97	2.88	0.014
0.8348	35.88	115	0.169	22.91	12.0	6.19	3.02	3.31	0.013
1.2115	39.07	120	0.208	18.75	11.4	5.06	2.01	3.24	0.017
1.8957	42.36	160	0.186	16.41	13.2	5.75	2.97	3.84	0.015

units: c in mol L^{-1}; τ_1, τ_2, τ_3 in 10^{-12} s. [a] Ref. [14]

4.3 DRS measurements of aqueous solutions

The aqueous LiCl solutions were measured at 298 K in a very small concentration range ($0.1 \lesssim c$ / mol $L^{-1} \lesssim 1$) as the conductivity of these solutions is very pronounced [108, 109] which makes the DRS-measurements at low frequencies difficult. Note that the saturation limit of aqueous LiCl solutions at 298 K is approx. 15 mol L^{-1} [110]. So all the experiments were performed in the dilute region. It should be remarked that this system was measured previously by Popp [111] and Wei et.al. [112]. The former author described his spectra (measured in the following frequency range $1.3 \leq \nu$/ GHz ≤ 17.5) by one Debye (D) model. Wei et.al. recorded the spectra between $0.045 \leq \nu$/ GHz ≤ 20 in a broad concentration range. The authors used the D model at lower concentrations ($c \leqq 5.11$ mol L^{-1}) and the CD equation at high concentrations ($c \geqq 7.2$ mol L^{-1}).

4.3.1 Relaxation model

In our case the best fits of the data were achieved by the application of a D+D fit in the measured concentration range. The use of the D, CC or CD model (one relaxation process) resulted in higher values of the variance of the fit, σ^2. At the lowest concentration the difference between the σ^2 of the D or CD and D+D fits was approximately 18 % whereas in the most concentrated solutions ($c \sim 1$ mol L^{-1}) even 230 %. The combinations of CD+D and CC+D did not lead to any physically reasonable results ($\beta > 1$ or $\alpha < 0$). Therefore the D+D fit was chosen for the description of the spectra. An example of a spectrum fitted by the D+D model is shown in figure 4.13. The measured spectra as frequency-dependent dielectric permittivity, ε', and dielectric loss, ε'', are presented for all concentrations in fig. 4.14. The obtained relaxation parameters are listed in table 4.6 and shown in figs. 4.15 and 4.16.

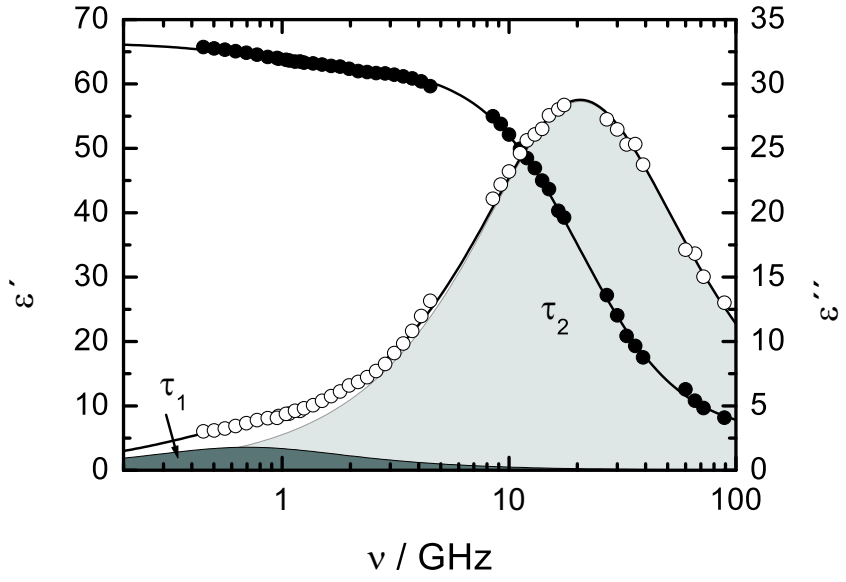

Figure 4.13: Example of a spectrum showing dielectric permittivity, ε' (•), and dielectric loss, ε'' (∘), of LiCl in water at 298.15 K at concentration c = 0.984 mol L^{-1}.

Table 4.6: Dielectric parameters (limiting permittivities ε_1, ε_2, ε_∞, relaxation times τ_1, τ_2, and variance of the fit σ^2) of the D+D model fitted to the complex permittivity spectra of LiCl and in water at 298 K.

c	ε_1	τ_1	ε_2	τ_2	ε_∞	σ^2
0^a	78.37			8.36	5.65	
0.0883	77.33	245	76.11	8.24	5.48	0.215
0.2171	75.56	161	73.82	8.18	5.43	0.185
0.4866	71.81	318	69.98	8.02	5.42	0.109
0.6686	70.41	334	67.46	7.87	5.78	0.083
0.9837	66.33	219	62.76	7.70	5.48	0.119

units: c in mol L^{-1}; τ_1, τ_2, τ_3 in 10^{-12} s. ^{a} data from ref. [115]

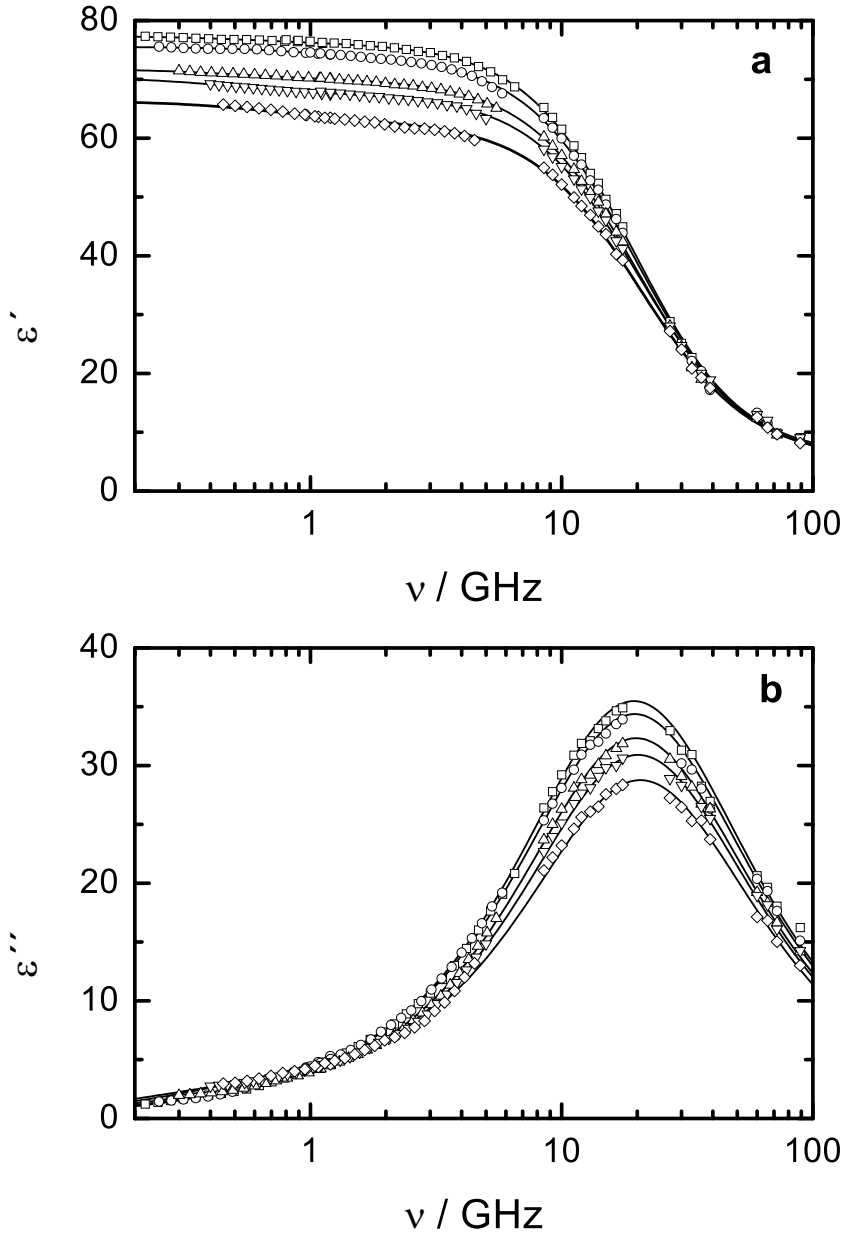

Figure 4.14: Absorption (a) and dispersion (b) spectra of aqueous LiCl solutions at 298 K for different concentrations: (□) c = 0.088 mol L^{-1} ; (○) c = 0.217 mol L^{-1}; (△) c = 0.487 mol L^{-1}; (▽) c = 0.669 mol L^{-1} and (◇) c = 0.984 mol L^{-1}. The lines represent the D+D fit.

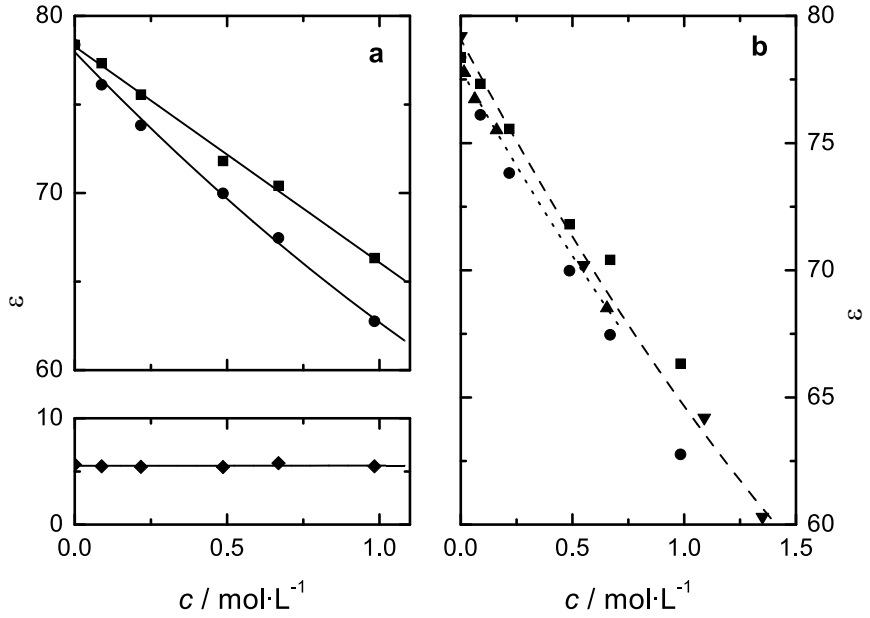

Figure 4.15: (a) Diagram showing the concentration dependence of the following relaxation parameters in aqueous LiCl solutions at 298 K: ε_1 (■), ε_2 (●) and ε_∞ (♦). The lines represent linear or polynomial fit of the data; (b) Comparison of ε_1 and ε_2 with the data from literature ([111](▲) and [112](▼)). The dotted line represents the fit of the literature data [111] and the dashed line the fit of the data from ref. [112].

It should be noted that our experiments did not detect any additional high-frequency process ($\tau \sim 1$ ps) resulting from the reorientation of mobile water molecules in the solutions observed in some previous studies [113, 114]. Fig. 4.15b compares the permittivity values from literature and our experiments whereas the relaxation time and the corresponding amplitude are compared in fig. 4.16. It can be seen that the values of the static permittivities are very similar in all three cases, however, due to the chosen model, the difference is growing with increasing LiCl concentration. The values of relaxation times and the amplitudes of the solvent process, τ_2 and S_2, are in good agreement with the data from Popp [111] whereas the data from Wei et.al. [112] are considerably different. However, the relaxation parameters presented by the working group of Wei were slightly higher also in other cases [114].
Conductivities and densities at 298 K necessary for the analysis of the data were extrapolated from the data in the following references: density [116], conductivity [108] and [109].

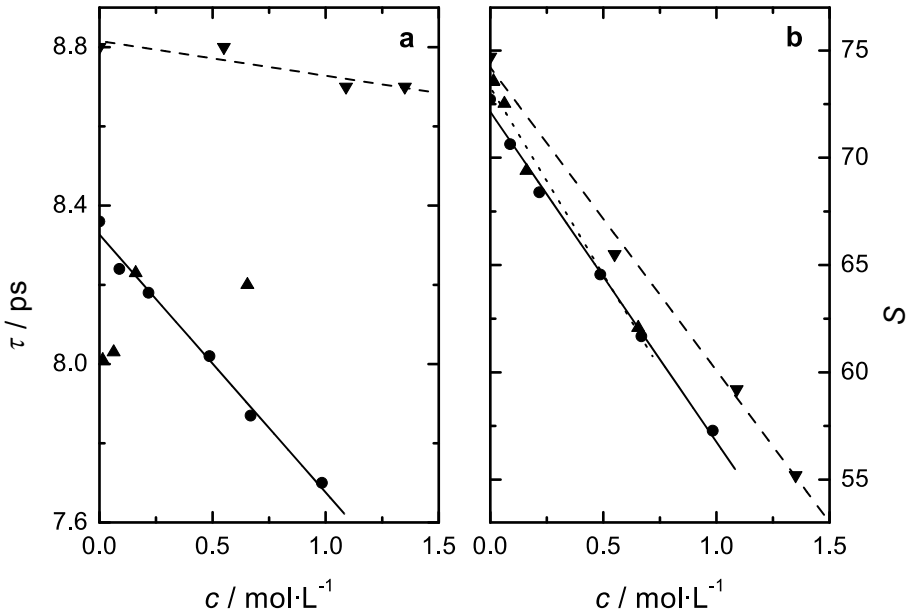

Figure 4.16: (a) Comparison of the relaxation time, τ_2, and (b) the amplitude of the second relaxation process, S_2 (•), with the corresponding literature data ([111](▲) and [112](▼)) at various concentrations of LiCl in water at 298 K. For the explanations of the lines see fig. 4.15.

4.4 DRS measurements in the mixed solvent system DMA/Water

As we showed that water plays a role of inhibitor in the solubilization of cellulose (see chapter 4.5.2) some information about the influence of water on the relaxation behavior of LiCl/DMA solutions seemed necessary. For this exploratory investigation a solution of LiCl in DMA of a high concentration (7.89 wt%) was diluted with water. This led to solutions with water content increasing from 3.5 up to 20.4 mol L^{-1} (for details see table 4.7). These solutions were measured at 298 K with the DRS. The measurements were aimed to demonstrate the changes of the relaxation behavior with growing content of water. Since the concentration of the starting water-free LiCl/DMA solution was close to a previously measured concentration (see table 4.2) the relaxation parameters were extrapolated from the data of table 4.2.

4.4.1 Choice of the relaxation model

For the description of the spectra various combinations of relaxation models were tested. The spectra could be fitted by the D+D+D+D+D (5D) model, however, the difference between σ^2(5D) and σ^2 (4D) fit was very small (2-4 %) and the relaxation parameters were not that smooth as in the case of 4D fit. So the latter was preferred for the interpretation of the spectra. When the CC+D+D fit was applied on the water containing system (note that the CC+D+D fit was used for the interpretation of the DRS spectra of LiCl/DMA solutions) σ^2 became worse (at low water concentration by 31 %; at high water concentration by 40 %). The parameters resulting from the CC+D+D model, however, did not exhibit the expected behavior and their values were rather scattered. This is demonstrated in fig. 4.17 where the relaxation times and amplitudes resulting from the CC+D+D fit are presented.
As the character of the amplitudes from the CC+D+D fit is rather strange, the 4D fit seems to represent a more reasonable interpretation of the data. The resulting relaxation parameters are shown in fig. 4.18 and can be compared to the parameters of the CC+D+D fit in fig. 4.17. The obtained relaxation parameters are summed up in table 4.8. The dispersion and absorption curves for different water contents are shown in fig. 4.19.
In fig. 4.17 the parameter values for $c_W = 0$ are shown for both the possible fits: the 4D fit (empty symbols) and the CC+D+D fit (filled symbols).

Table 4.7: The composition and properties of the LiCl/DMA/Water solutions used for the DRS measurements: the molar concentration of water, c_W, LiCl, c_{LiCl}, and DMA, c_{DMA}, the conductivity, κ, and density, ρ, and the molar ratios of water to LiCl, c_W/c_{LiCl}, and DMA to water, c_{DMA}/c_W.

c_W	c_{LiCl}	c_{DMA}	κ	ρ	c_W/c_{LiCl}	c_{DMA}/c_W
0	1.8666	10.603	0.4783	1.0028		
3.520	1.7624	10.042	0.3949	1.0129	2.00	2.85
6.690	1.6651	9.486	0.4341	1.0174	4.02	1.42
9.470	1.5786	8.989	0.5091	1.0205	6.00	0.95
15.672	1.3802	7.862	0.7422	1.0256	11.36	0.50
20.422	1.2232	6.968	0.9840	1.0265	16.70	0.34

units: all c in mol L^{-1}; κ in S m^{-1}; ρ in g cm^{-3}.

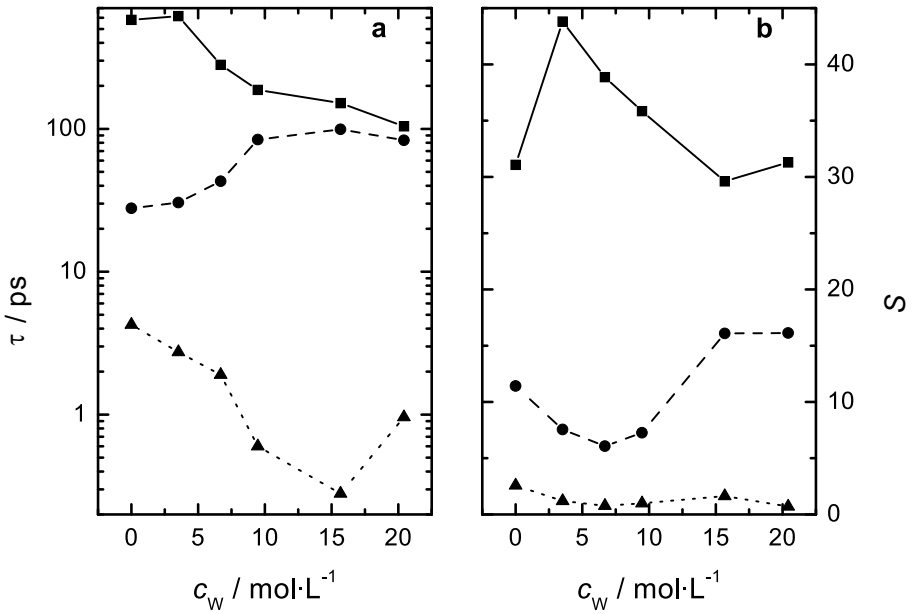

Figure 4.17: (a) The relaxation times τ_1 (■), τ_2 (•) and τ_3 (▲) resulting from the CC+D+D fit of the DRS spectra of LiCl/DMA/Water solutions; (b) the corresponding amplitudes, S_1 (■), S_2 (•) and S_3 (▲).

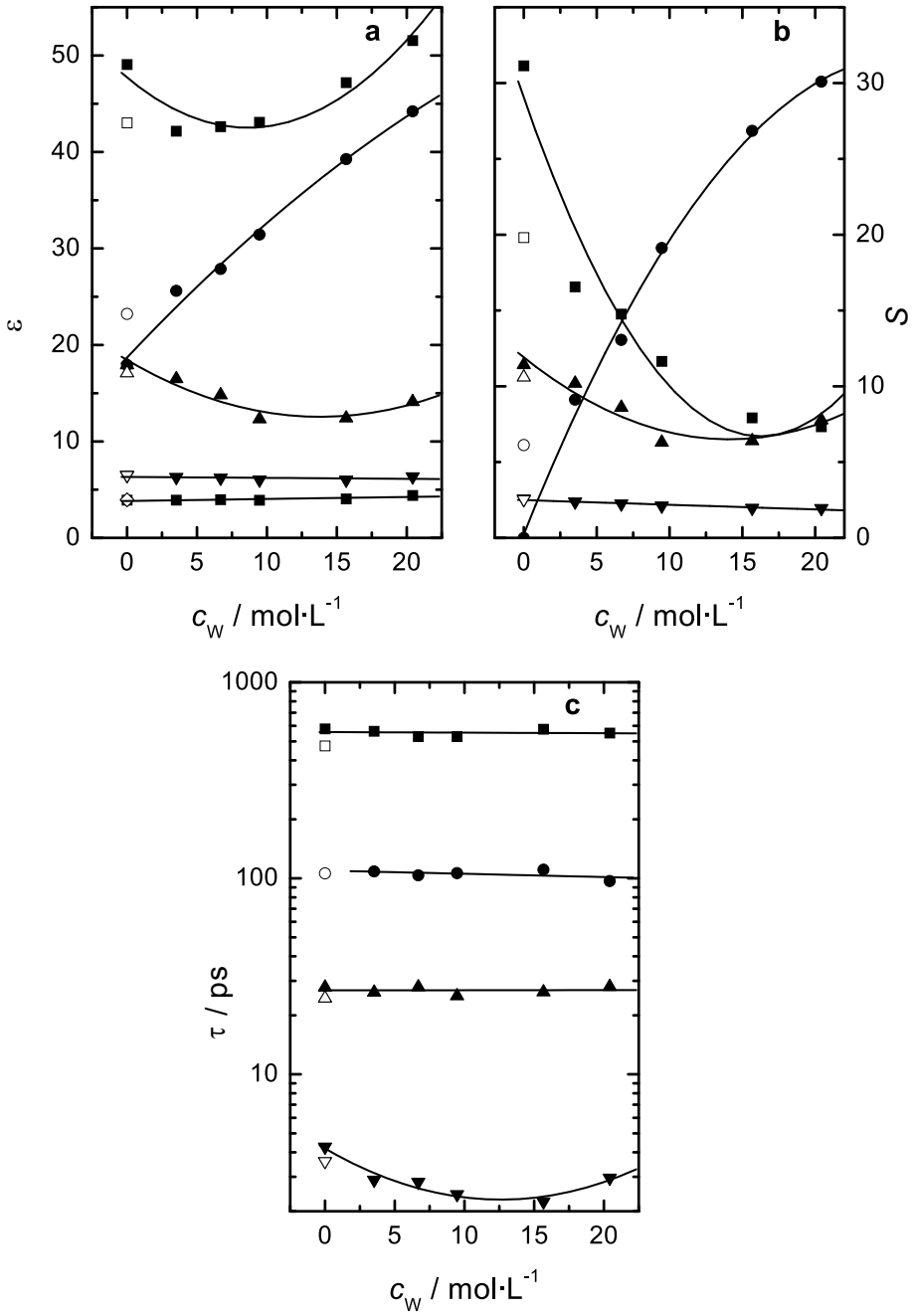

Figure 4.18: (a) The dielectric permittivities, ε_1 (■), ε_2 (●), ε_3 (▲), ε_4 (▼) and ε_∞ (♦), resulting from the 4D fit of the DRS spectra of LiCl/DMA/Water solutions ; (b) the corresponding amplitudes, S_1 (■), S_2 (●), S_3 (▲) and S_4 (▼); (c) the corresponding relaxation times τ_1 (■), τ_2 (●), τ_3 (▲) and τ_4 (▼). The open symbols represent in all graphs the 4D fit of the water-free solution. The lines symbolize the linear or polynomial fit of the data (starting from the CC+D+D fit of the water-free solution).

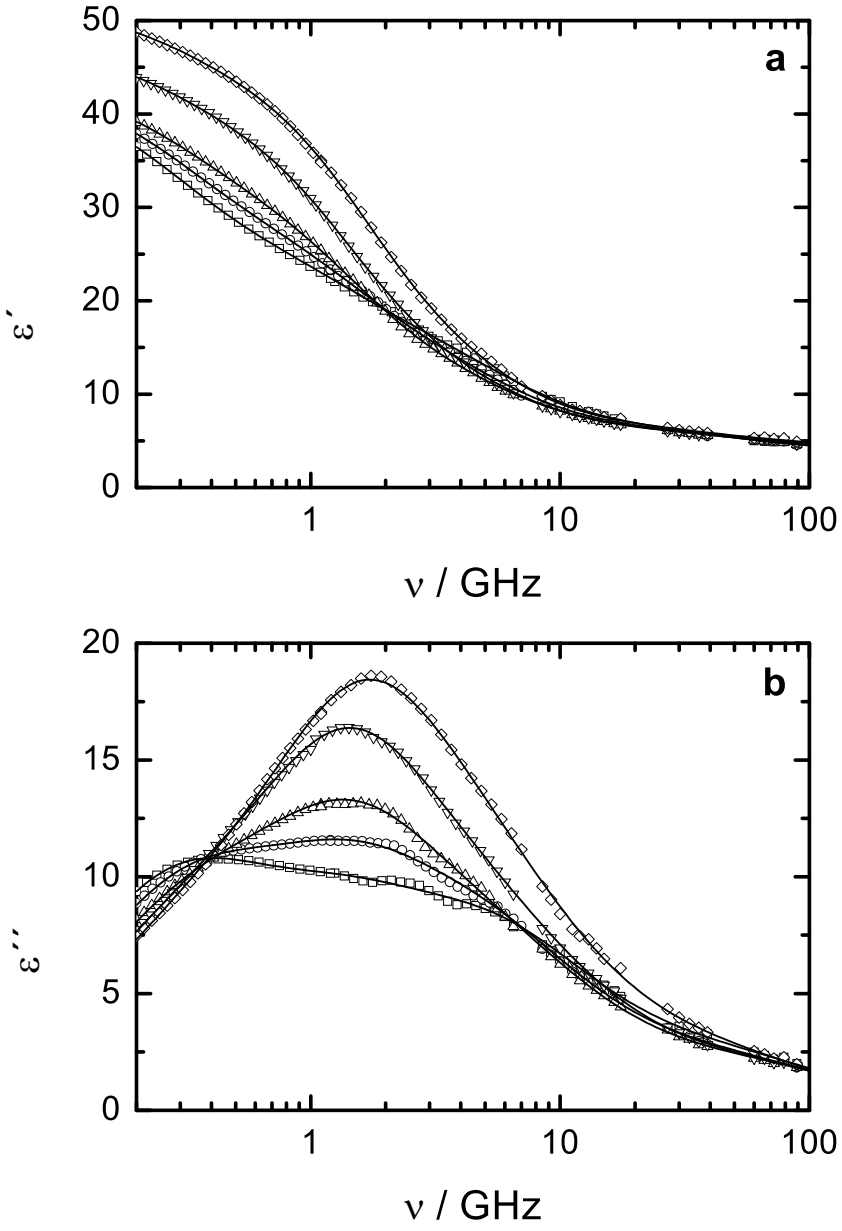

Figure 4.19: Diagram showing dielectric permittivity, ε', (a), and dielectric loss, ε'', (b), of LiCl/DMA/Water solutions at 298 K with different water concentrations: c = 3.520 mol L^{-1} (□); c = 6.690 mol L^{-1} (○); c = 9.470 mol L^{-1} (△); c = 15.672 mol L^{-1} (▽); c = 20.422 mol L^{-1} (◇). The lines represent the 4D fit.

Table 4.8: Dielectric parameters (limiting permittivities ε_1, ε_2, ε_3, ε_4, ε_∞, relaxation times τ_1, τ_2, τ_3, τ_4, and variance of the fit σ^2) of the 4D model fitted to the complex permittivity spectra of LiCl/DMA/water system at 298 K.

c_W	ε_1	τ_1	ε_2	τ_2	ε_3	τ_3	ε_4	τ_4	ε_∞	σ^2
0^a	49.06	579			17.92	27.8	6.50	4.26	3.92	-
0^b	43.02	474	23.21	105.9	17.09	24.4	6.49	3.60	3.95	-
3.520	42.16	563	25.60	108.4	16.48	26.2	6.29	2.89	3.91	0.0100
6.690	42.63	529	27.87	103.5	14.81	27.9	6.21	2.82	3.96	0.0095
9.470	43.08	528	31.44	106.2	12.32	25.1	6.02	2.44	3.90	0.0088
15.672	47.18	576	39.26	110.7	12.41	26.3	6.01	2.24	4.04	0.0066
20.422	51.54	551	44.21	96.8	14.12	28.0	6.35	2.96	4.40	0.0156

units: c in mol L^{-1}; all τ_x in 10^{-12} s; ^{a} extrapolated CC+D+D fit and ^{b} extrapolated 4D fit of the LiCl/DMA system at 298 K.

4.5 Studies on cellulose

4.5.1 Comments

The activated cellulose samples were provided by the coworkers of the Christian-Doppler laboratory in Vienna and we experienced some difficulties arising from the aging of the activated samples. For the phase diagrams cellulose samples with $M = 290000$ g mol^{-1} were used. For the DRS measurements samples with lower molecular weight ($M = 54000$ g mol^{-1}) had to be prepared because of the high viscosity of the normal samples (see table 4.9), which made it impossible to fill the samples in the cells.

4.5.2 Phase diagrams

Influence of the temperature

Preliminary experiments leading to two phase diagrams at different temperatures were performed in order to find the maximum cellulose solubility at a given temperature and LiCl concentration. The samples were observed after three days; results are presented in figs. 4.20a and 4.20b. The graphs revealed that, while at 25 °C already a 3 % LiCl/DMA solution dissolves some minimum amount of cellulose, at 5 °C solubilization could be achieved only with more than 4 % LiCl in DMA. On the other hand, at 5 °C more cellulose could be dissolved. The viscosity of the solutions was rather high (see table 4.9). Above approx. 3 % of cellulose in the mixture, the mixtures must be considered as gels, rather than solutions. At even higher cellulose concentrations the gels became so rigid that they reminded of

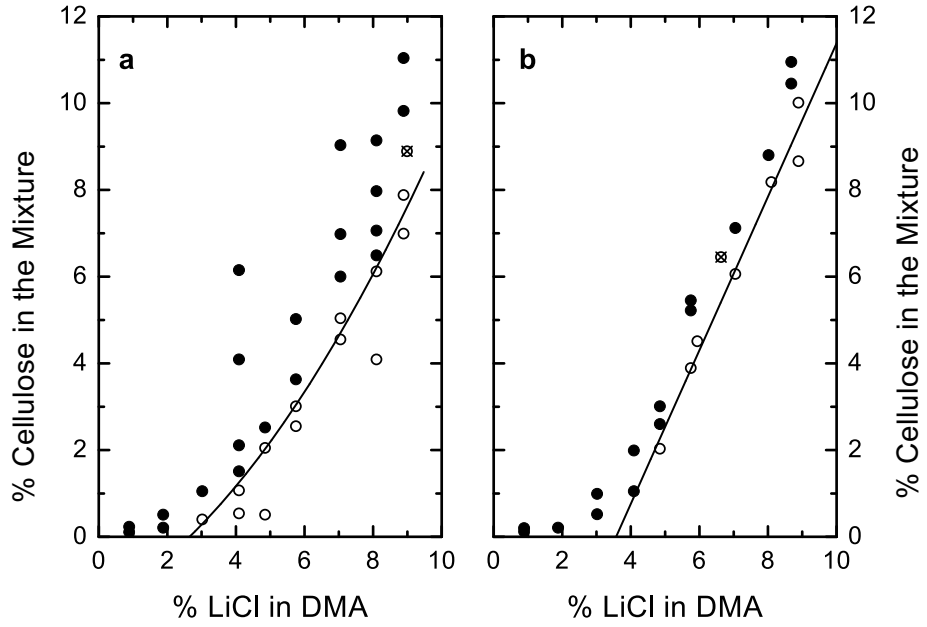

Figure 4.20: Phase diagram of the ternary system LiCl/DMA/Cellulose at (a) 25 °C and (b) 5 °C. In the diagrams the (○) symbolize the isotropic points, (⊗) transition samples and (●) stand for biphasic samples (either with liquid crystals or with non-dissolved cellulose).

some sort of jelly or transparent rubber; it was nearly impossible to remove them from narrow devices, such as tubes.

Influence of water

Three sets of samples with different cellulose content were prepared. The cellulose concentrations were 0.5, 1.0 and 2.0 %, respectively. The samples were stored at 5 °C for three days. The experiments were carried out some months later on the same preactivated cellulose samples, whose solubilization ability had already decreased by 10-20 %. For each set a separate phase diagram was recorded. The results are presented in figs. 4.21a-c. Surprisingly, the biphasic region had become quite large. Therefore, the samples were again measured after one month from their preparation (figs. 4.22a-c). The diagrams recorded one month later showed a disappearing biphasic region in favor of a growing isotropic phase. The phase boundary between the non-dissolved or liquid crystalline region remained nearly the same. This suggests a slow dynamics of the solubilization process. For analysis, only data from the second set of measurements were used. When comparing the two measurements, a remarkable difference was observed in the case of mixtures with 2 % of cellulose. Whereas after three days most of the probes appeared as biphasic in the diagram, the range of the isotropic region became larger as can be seen from the second measurement. In the case of 1 % cellulose solutions the biphasic region nearly completely disappeared. The maximum solubility seems to be well comparable with the boundary of the biphasic

Table 4.9: Cellulose content (%) in the LiCl/DMA solution (8.4 %), initial and infinite dynamic viscosity (η_0 and η_∞) and their errors (difference between two measurements divided by two).

Cellulose(wt%)	η_0	Error	η_∞	Error
0.5	55	4	29	6
1.1	383	12	164	3
1.5	1590	20	483	4
2.0	2020	20	519	2
2.5	35600	5600	13900	2800
3.0	71400	3800	26000	2700

units: η_0,η_∞ and their errors in mPa s.

region after three days. From figs. 4.21 and 4.22 it can be seen that the maximum additional water content tolerable in all of these samples was less than 3 %, even for the most concentrated LiCl/DMA solutions. This finding is in accordance with the common procedure of precipitating cellulose from the solutions by dilution with water.

4.5.3 Rheology

All of the examined solutions exhibited isotropic behavior. The dynamic viscosity increased with growing cellulose content as expected. Under the conditions used, the viscosity measurements were possible only up to 3 % of cellulose, at higher concentrations the solutions turned into gels. The sudden increase in the "stiffness" of the sample can be seen from the results in table 4.9 and fig. 4.23a. In the next experiments, an increasing LiCl content in DMA under constant cellulose concentrations (1 %) was studied. From table 4.10 it can be seen that the dynamic viscosity of the samples increased only very slightly with the growing LiCl content in the samples. This increase was so small that the changes can be considered as insignificant at given accuracy of the measurement and the dispersion of the data (see fig. 4.23b). The viscosity in these probes can be considered as constant.

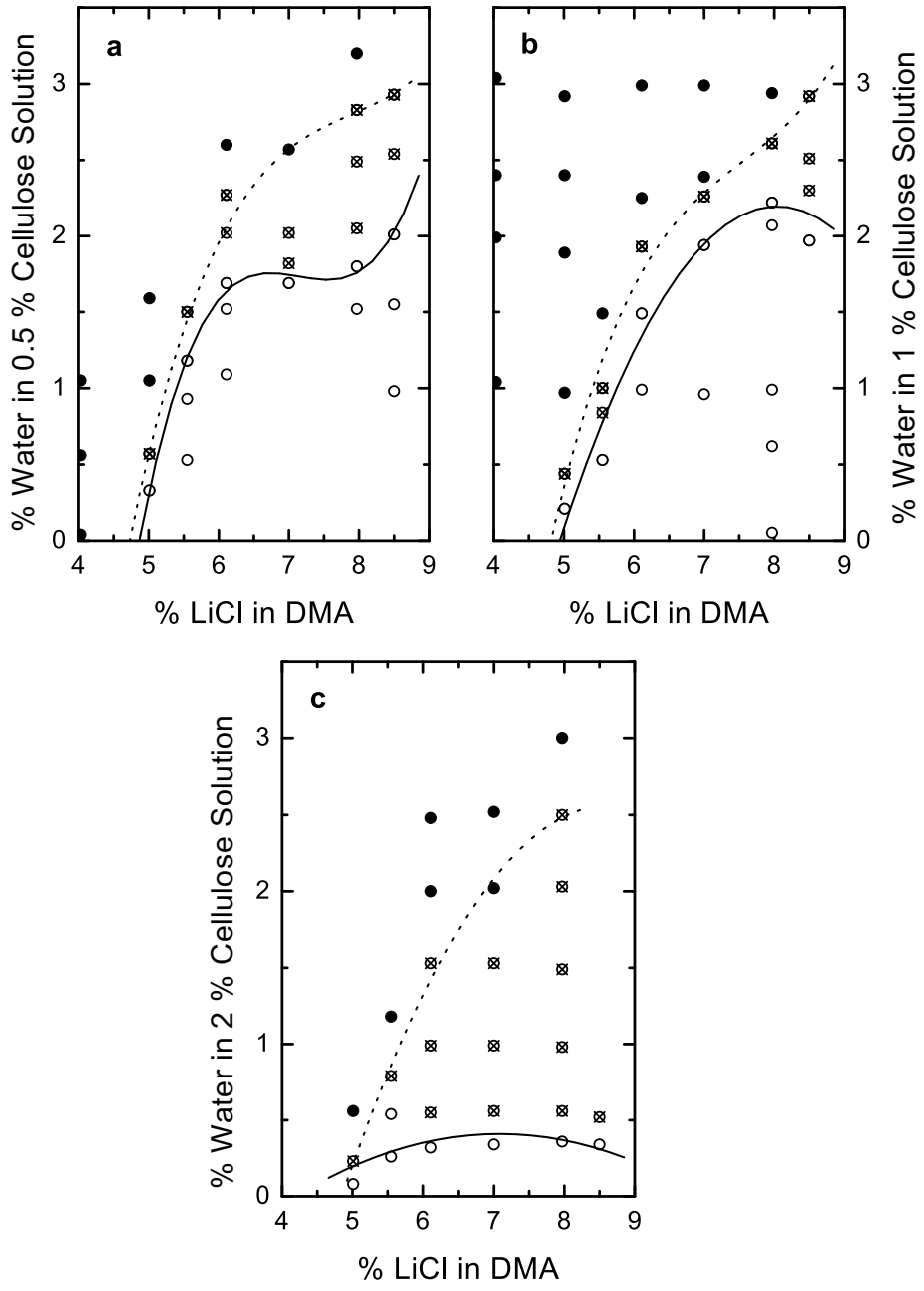

Figure 4.21: Phase diagram of the quaternary system LiCl/DMA/Water/Cellulose with (a) 0.5 %; (b) 1.0 % and (c) 2.0 % of cellulose in the mixtures measured after three days. The symbols have the same meaning as in fig. 4.20, the bold line represents the approximate boundary between the isotropic and transition region and the dotted line the interface between the transition and biphasic region.

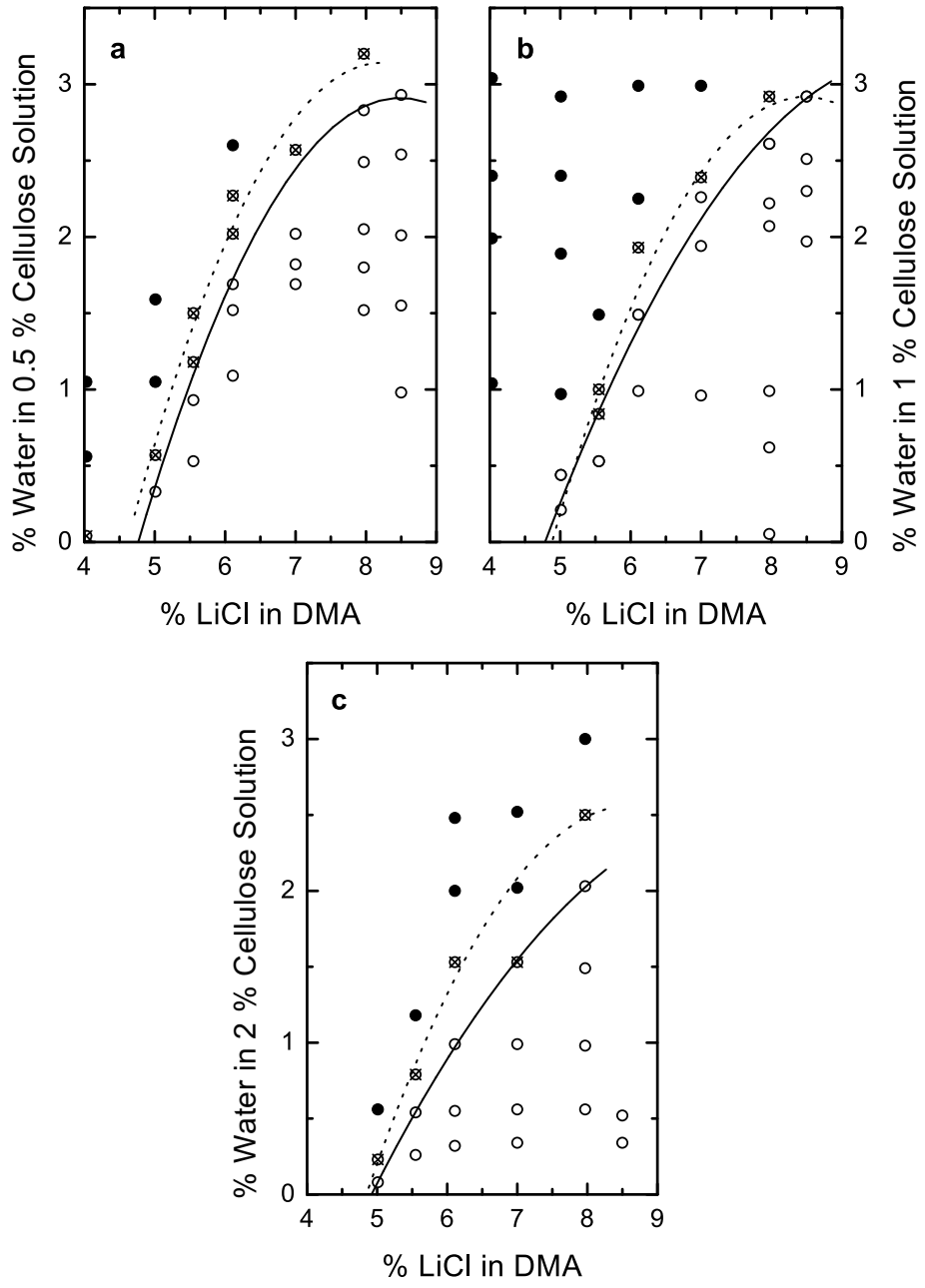

Figure 4.22: Phase diagram of the quaternary system LiCl/DMA/Water/Cellulose with (a) 0.5 %; (b) 1.0 % and (c) 2.0 % of cellulose in the mixtures measured after one month. For the explanation of the symbols and lines see figs. 4.20 and 4.21.

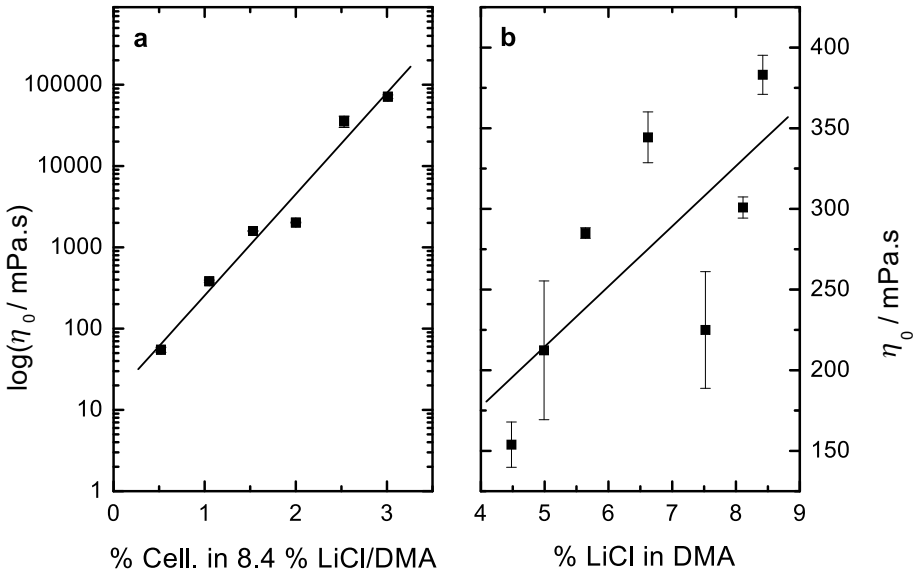

Figure 4.23: Rheological behavior (expressed as initial viscosity, η_0) of probes with increasing content of cellulose (a) and constant cellulose content with changing concentration of LiCl in DMA (b). The corresponding values of η_0 and η_∞ (infinite viscosity) are listed in tables 4.9 and 4.10.

Table 4.10: LiCl content (%) in DMA solutions with constant content of cellulose (1%), initial and infinite dynamic viscosity (η_0 and η_∞) and their errors (difference between two measurements divided by two).

Cellulose(wt%)	η_0	Error	η_∞	Error
4.5	154	14	72	1
5.0	210	40	86	14
5.6	285	3	114	1
6.6	344	16	135	3
7.5	230	40	89	12
8.1	301	7	121	2
8.4	383	12	164	3

units: η_0, η_∞ and their errors in mPa s.

Table 4.11: The relaxation parameters resulting from the CC+D fit of the TDR spectra (limiting permittivities ε_1, ε_2, ε_∞, relaxation times τ_1, τ_2, the relaxation distribution parameter α and variance of the fit σ^2) of three cellulose solutions in LiCl/DMA (8.05 % LiCl).

wt% Cell	ε_1	τ_1	α	ε_2	τ_2	ε_∞	σ^2
0	48.1	566	0.20	19.1	34.5	6.70	0.0267
1	46.5	559	0.13	20.3	35.6	7.31	0.0208
2	45.6	616	0.16	19.8	38.0	7.51	0.0198
3	46.1	744	0.17	20.8	35.6	7.94	0.0207

units: all τ_x in 10^{-12} s.

4.5.4 TDR measurements

Only a very small set of samples was measured by the TDR-technique. Measurements on larger scale were not possible because of the construction of the cells which prevents the usage of very viscous materials. The other problem we faced during the experiments was the high conductivity of some samples which made the correct use of the T11-cell impossible. The starting LiCl/DMA solution contained 8.05 % LiCl. The prepared samples contained between 1-3 % of the activated cellulose ($M = 54000\ \mathrm{g\,mol^{-1}}$). The results presented in the table 4.11 should not be over interpreted as only the frequency range $0.1 \leq \nu/\mathrm{GHz} \leq 6.5$ at 25 °C was covered.

The spectra were fitted by the CC+D model as the high-frequency data were not available (see fig. 4.24). The quality of the data set was rather low either. This makes the quantitative interpretation of the spectra difficult.

From table 4.11 it can be seen that the amplitude of the first process, S_1, decreases from *ca.* 29 for the cellulose-free solution to 25.3 for solution containing 3 % of cellulose. The corresponding relaxation time, τ_1, increases in the same range only slightly - from 570 to 740 ps. This difference is considerably small.

From the obtained results only the conclusion can be drawn that at these concentrations the rotational relaxation of the present $[Li(DMA)_x]Cl$ ion-pair remains nearly the same as in cellulose-free solutions.

It should be noted that we worked here at mole ratios (LiCl/AGU) much larger than 2:1 which seems to be required for the solubilization [47]. So it can be assumed that there are still too many 'free' $[Li(DMA)_x]Cl$ ion pairs which can be then observed.

For the understanding of the system more measurements near to the maximal solubilization should be performed.

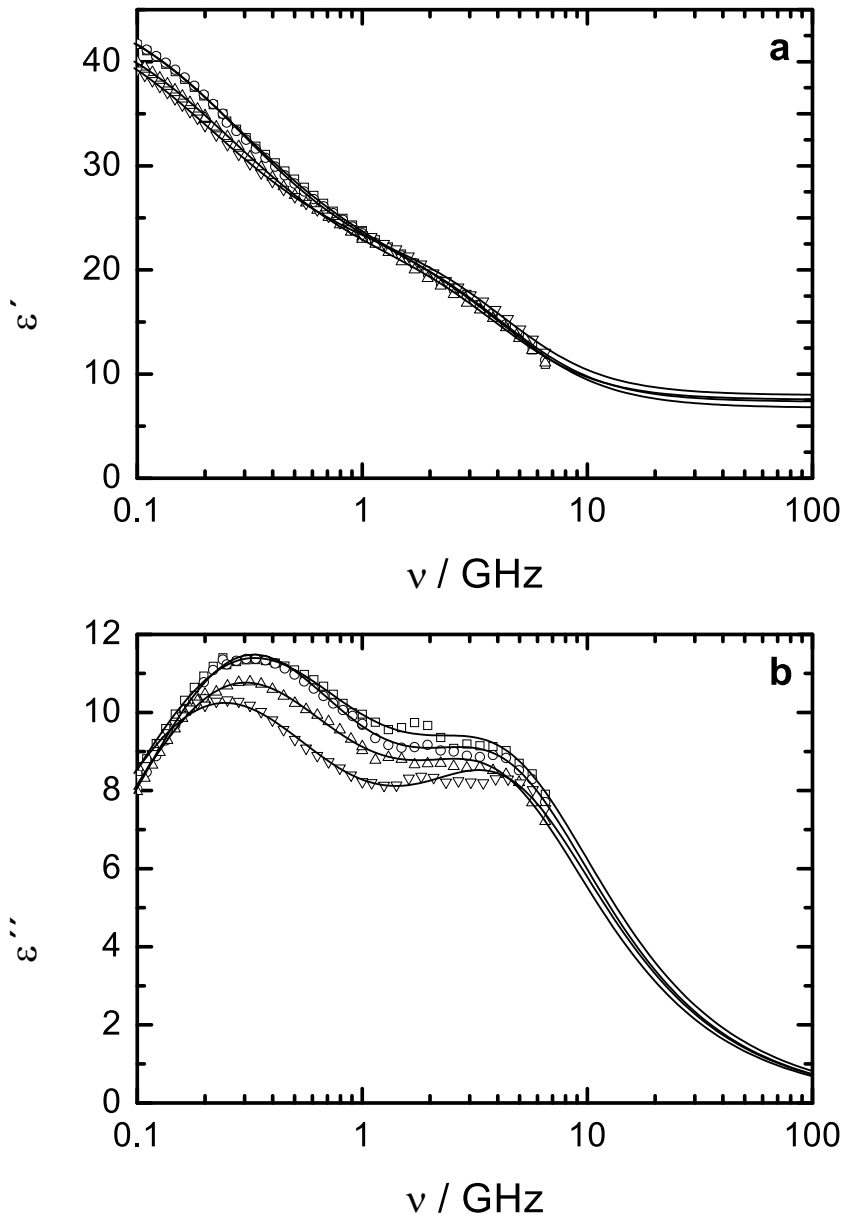

Figure 4.24: Diagram showing dielectric permittivity, ε', (a), and dielectric loss, ε'', (b), of LiCl/DMA/Cellulose solutions at 298 K with different cellulose content: 0 wt% (□); 1 wt% (○); 2 wt% (△); 3 wt% (▽). The lines represent the CC+D fit.

Chapter 5

Discussion

5.1 LiCl/DMA solutions

In general, the interaction of alkali metal cations with various amides is supposed to be very strong [117–119] and was studied by many different techniques. Quite a lot of information is provided on the Li^+/amide system in general but only few studies report on LiCl/DMA itself [54, 117, 120, 121, 133, 134, 138, 145, 154, 156, 157]. Many authors used $LiClO_4$ as an example for the behavior of lithium salts [15, 119–122, 133, 143, 160, 162]. However, it was shown that Cl^- exhibits much stronger interaction with the $[Li(DMA)_x]^+$ complex than the perchlorate anion [120, 121]. Considering the choice of amide most of the studies report on some primary [122] and secondary amides [117–119, 122–124, 137]. However, the properties of tertiary amides differ strongly because no hydrogen bonding between the amide molecules is possible. IR studies suggest that the interaction between LiCl and amides decreases in the order tertiary amide > secondary amide > primary amide [118]. Even the studies with DMF as solvent [117–119, 122, 124, 137, 160] are not directly comparable due to the acidic hydrogen atom of DMF. The interaction of DMA with cations is stronger as can be demonstrated e.g. by the higher donor number [123, 124] and the Gibbs free energy of transfer for Li^+ from acetonitrile to amide, ΔG_t^0, which is -47 $kJ\,mol^{-1}$ for DMA and -39 $kJ\,mol^{-1}$ for DMF [119]. The difference between DMF and DMA in the interaction with alkali metals or alkali metal salts is shown in many experimental [14, 117, 122] and theoretical studies [123–125]. Also concerning cellulose dissolution it should be mentioned that whereas LiCl/DMA solutions represent a powerful solvent for cellulose (see section 1.2.3), the solubilization strength of LiCl/DMF solutions is limited [40].

5.1.1 Solvent relaxation

As mentioned in the general introduction the DRS represents a well-established technique for the investigation of solvent-solvent, ion-solvent or ion-ion effects in electrolyte solutions. With the help of this method the structure and dynamics of the solvation shell can be investigated [96].

In section 4.2 it was shown that the relaxation behavior of LiCl solutions in DMA can be described by a single low-frequency relaxation resulting from the ion pair formation and two high-frequency processes resulting from the solvent relaxation, characterized by the amplitudes, S_{s1} and S_{s2}. The data of pure DMA measured by Wurm [126] and presented in ref.[14] showed that a formal description of both solvent relaxations with a single equation (by the conventionally used band-shape functions) is not possible. The interpretation of the high-frequency process, S_{s2}, led to the assumption that this contribution is not an independent mode and that it probably results from inertial contributions to the diffusive solvent relaxation [14]. This implies that for the correct interpretation of the DRS-spectra of LiCl solutions in DMA, it is necessary to analyze both solvent contributions together. Thus, the total solvent dispersion, $S_s = S_{s1} + S_{s2} = \varepsilon_s - \varepsilon_\infty$, was used in the further quantitative analysis.
In order to obtain some information about the solvation shell of LiCl in the solutions the following procedure was applied. The apparent solvent (DMA) concentration in the solution, c_s^{ap}, was calculated by means of the total equilibrium dispersion solvent amplitude, S_s^{eq}, using the modified *Cavell* equation [127] normalized to the pure solvent

$$c_s^{ap}(c) = c_s^\circ F_{Cav} \frac{2\varepsilon(c)+1}{\varepsilon(c)} S_s^{eq}(c) \tag{5.1}$$

where c_s° is the analytical concentration of pure DMA, and $\varepsilon(c)$ the static permittivity. The Cavell factor, F_{Cav}, is defined as follows

$$F_{Cav} = \frac{\varepsilon(0)}{[2\varepsilon(0)+1]S_s(0)} \tag{5.2}$$

The calculation of S_s^{eq} involves correction of the observed dispersion amplitude, S_s, for kinetic depolarization (kd) associated with the movement of the solvated ions in the applied field

$$S_s^{eq}(c) = S_s(c) + \Delta_{kd}\varepsilon(c) \tag{5.3}$$

as described in section 2.5. Assuming that the Kirkwood factor for the solvent, g_K, is independent of the solute concentration [15] then the number of 'irrotationally bound' solvent molecules Z_{ib}, can be obtained from the following expression

$$Z_{ib} = (c_s - c_s^{ap})/c \tag{5.4}$$

where c represents the electrolyte concentration, c_s the corresponding analytical concentration of DMA in the solutions, and c_s^{ap} the number of 'rotationally free' solvent molecules in the solution. In the calculations all boundary conditions for the transport of the ions were assumed (see table 5.1). According to previous findings [15, 115, 128] the most probable values should be the results for *slip* boundary conditions.
Figure 5.1a shows the development of the solvation shell at 298 K with increasing LiCl concentration. At c $\rightarrow$ 0 about 6 molecules of DMA are irrotationally bound. With increasing LiCl concentration Z_{ib} linearly drops to approximately 3 DMA molecules in

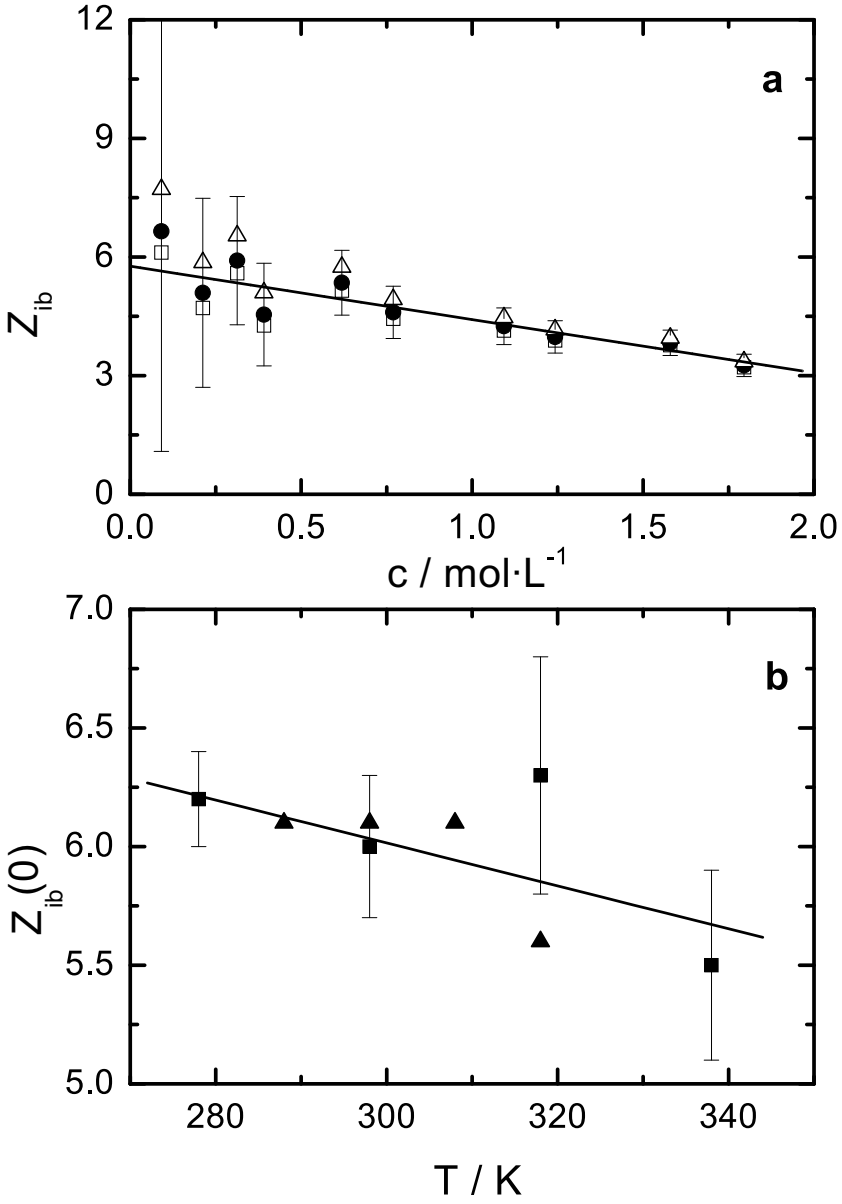

Figure 5.1: (a) Effective solvation numbers, Z_{ib}, as a function of electrolyte concentration, c, at 25 ^{o}C for *stick*(□), *slip* (•) and *negligible*(△) kinetic depolarization conditions (error bars only for *slip* conditions). (b) Comparison of the limiting effective solvation numbers, $Z_{\mathrm{ib}}(0)$, at all temperatures under *slip* conditions (■) with results from IR measurements in ref. [129] (▲).

Table 5.1: Limiting effective solvation numbers, $Z_{\mathrm{ib}}(0)$, in LiCl/DMA solutions at different temperatures calculated from the solvent dispersion, S_{s}, resulting from the application of the Cavell equation assuming different boundary conditions for ion transport.

T	Z_{ib}^{stick}	Z_{ib}^{slip}	Z_{ib}^{neg}
278.15	5.8 ± 0.2	6.2 ± 0.2	6.8 ± 0.2
298.15	5.6 ± 0.3	6.0 ± 0.3	6.8 ± 0.3
318.15	6.0 ± 0.5	6.3 ± 0.5	7.0 ± 0.6
338.15	5.2 ± 0.3	5.5 ± 0.4	6.0 ± 0.4

units: T in K .

high-concentrated solutions. This would suggest a direct contact between cation and anion at high electrolyte concentrations. This corresponds well to the traditionally proposed coordination number 3 or 4 at least for various solid lithium complexes, see [130, 131]. Fewer complexes have been prepared with coordination number 5, whereas more lithium-complexes coordinated with six ligand molecules are known [130]. For a number of solid complexes with mainly organic ligands the lithium coordination number of 7 or 8 was obtained [131]. However, the direct comparison between the coordination number of solid complexes and of structures in solutions is not always possible.

From table 5.1 and fig. 5.1b can be seen that the development of the solvation shell with temperature is not very pronounced. At $c \to 0$ the values of the limiting effective solvation numbers vary in the range $5.5 \leq Z_{\mathrm{ib}} \leq 6.3$ and they seem to decrease only slightly with increasing temperature. Figure 5.1b also shows the comparison with the data from IR measurements of the $LiClO_4$/DMA [129]. All the DRS-values of $Z_{\mathrm{ib}}(0)$ coincide well with the IR-results. Only the value at 318 K seems to be too large. Previous DRS-measurements on $LiClO_4$/DMA system resulted at 298 K in $Z_{\mathrm{ib}} = 6.6 \pm 0.2$ [15], whereas the corresponding value for LiCl/DMA in this study is $Z_{\mathrm{ib}} = 6.0 \pm 0.3$. However, as mentioned in the introduction to this chapter, the behavior of $LiClO_4$ in aprotic systems seems to be different in comparison to LiCl.

Now the question for the assignment of the obtained effective solvation numbers should be tackled. In aprotic solvents Cl^- is supposed to be very weekly solvated [132]. This was shown in various conductance studies [133, 134]. In ref. [133] the solvation number of Cl^- in the solutions was estimated to 0.89. According to ref. [134] the limiting ionic conductivity of a set of different lithium salts in DMA decreases with increasing size of anions which implies that these anions remain unsolvated in this solvent. The ionic Stokes' radii for the anions were always smaller than the crystallographic radius, r_{s} (Cl^-) = 1.37 10^{-10} m [134] (compare to the value for Cl^- in table 5.2). So the observed solvation numbers can be assigned to the cation as in the case of the perchlorate solutions [15].

Generally for amide-lithium complexes the literature data usually suggest the coordination number 4 (mainly IR-studies). The LiO_4 tetrahedra exhibits specific vibration in the range of 500-400 cm^{-1} whereas LiO_6 octahedra is located at approximately 300 cm^{-1} [135]. This seems to be the case for inorganic [136] and some organic systems (amides, ethers, ketones) as well. In the spectra of amide complexes with lithium cation only the presence of a 400 cm^{-1} band was observed [118, 135, 137]. In another IR-study performed on concentrated solutions of LiCl in DMA the presence of a new peak in the spectra was observed which was ascribed to a formation of a complex between LiCl and three molecules of DMA [138]. From transference numbers the following solvation numbers for Li^+ in various amides were determined - 5.5 in N-methylformamide [139], 5.2 in N,N-dimethylformamide [139] and 5.1 in N-methylacetamide [140]. In DMF/$LiClO_4$ system the solvation with four molecules of DMF was observed in the ^{1}H-NMR spectra [141]. X-ray measurements suggested for the same system some sort of network structure with the unit LiCl·DMF·1/2 H_2O[142]. A similar study on DMA/$LiClO_4$ system claimed the presence of the following complex $Li[(DMA)(H_2O)_2]ClO_4$ [143]. Crystallographic studies of other systems favored more the presence of four amide molecules around lithium [144]. A solid LiCl/DMA complex with a well-defined melting point was prepared in ref. [145]. However, no nearer explanation of its structure was provided. By using the Robinson-Stokes equation the solvation number of 4.13 was obtained [133]. Recent X-ray studies on the liquid system LiCl/DMA revealed that lithium is surrounded be five DMA molecules in less concentrated solutions and with four molecules at high LiCl concentrations. Here the formation of chain-like structures was invoked [146].

So far only the dispersion amplitude of the solvent was evaluated. Thus the relaxation times of the dispersion can also yield interesting information. The relaxation time of the first solvent process, τ_{s1}, associated with the tumbling motion of DMA molecules in the bulk increases with concentration of the electrolyte and decreases with temperature. This behavior can be described by the application of the Arrhenius equation eq. (2.93) which yields the corresponding activation energy, E_a, of the rotational motion in DMA. In fig. 5.2 a comparison between the temperature dependence of ln τ_{s1} and ln η (data from ref. [50, 147]) is shown. The similarity of the slopes in both diagrams indicates that the increase of the activation energy with concentration is connected with the increase of the viscosity with growing LiCl concentration. The value for pure DMA obtained from the relaxation time is 10.8 kJ mol^{-1} [14], whereas the value obtained from viscosity data is 8.8 kJ mol^{-1}. So the viscosity contribution to the rotational barrier is about 80%. However, for LiCl/DMA solutions the situation at high LiCl concentrations is reversed. The value of E_a at the highest concentration measured by Shoshina at al. $E_a(c$ =1.22 mol $L^{-1})$ is 18.5 kJ mol^{-1}, whereas the corresponding value of $E_a(\tau_{s1})$ = 12.2 kJ mol^{-1}. For a 2 molar solution the $E_a(\tau_{s1})$ = 14.4 kJ mol^{-1}. This implies that the rotational motion of the bulk solvent molecules is less affected by the dissolved electrolyte than shear motion involved in the viscous flow. Similar result was observed for other electrolyte solutions in DMA or DMF [15].

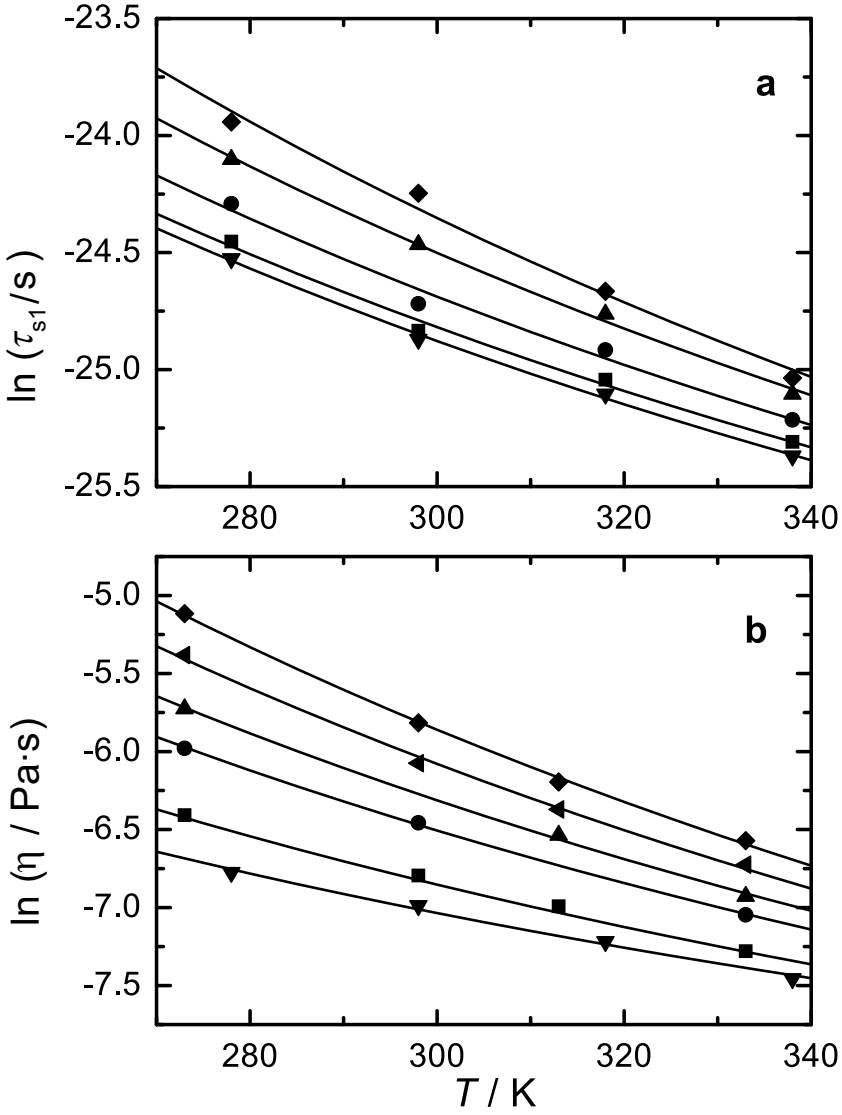

Figure 5.2: (a) Temperature dependence of ln τ_{s1} in DMA (▼) and LiCl/DMA solutions of c =0.3 mol·L^{-1} (■), c =0.8 mol·L^{-1} (●), c =1.5 mol·L^{-1} (▲) and c =2.0 mol·L^{-1} (♦). Figure (b) describes the temperature dependence of ln η for DMA (▼) and LiCl/DMA solutions of c =0.1 mol·L^{-1} (■), c =0.5 mol·L^{-1} (●), c =0.73 mol·L^{-1} (▲), c =1.0 mol·L^{-1} (◄) and c =1.22 mol·L^{-1} (♦).

5.1.2 Solute relaxation

As described in the experimental part (4.2) the temperature dependent DRS-spectra of LiCl in DMA solutions were in the end fitted by the following combination: CC+D+D. The two high-frequency processes analyzed in the previous section were assigned to the solvent, whereas the low-frequency process was attributed to the solute. Its relaxation time, τ_{IP}, is in the magnitude typical for tumbling motion of ion-pair species [83] and it significantly increases with growing temperature or LiCl concentration in the solutions. However, unlike to the previously examined perchlorate solutions in DMA [15], the relaxation time in this case shows a broad distribution with α reaching 0.3 at high LiCl concentrations. Although the attempt to describe the complex permittivity spectra by four Debye processes resulted in reasonable values for all temperatures, the comparison of the obtained dielectric parameters was not consistent. The relaxation times of the first and second ion-pair process did not show any clear temperature dependence and the shapes of the amplitudes of these processes corresponded well with each other only for 278 and 298 K or 318 and 338 K respectively (for details see section 4.2). So both processes were fitted as one relaxation with dispersion amplitude, S_{IP}, and relaxation time, τ_{IP}.
From the amplitude of the process, S_{IP}, the concentrations, c_j, of the individual ionic species j can be determined with the help of the generalized *Cavell* equation as shown in eq.(2.72)- eq.(2.75) in the theoretical section. In order to interpret the data quantitatively, the geometry of the possible ionic species has to be assumed. The dissolution of electrolytes in an appropriate solvent generally leads to the formation of free solvated cations and anions. This step can be followed by the formation of associates - solvated ion-pairs.

$$\mathrm{Li^+}n\mathrm{DMA} + \mathrm{Cl^-}m\mathrm{DMA} \rightleftharpoons \mathrm{Li^+(DMADMA)Cl^-} + (n+m-2)\mathrm{DMA} \qquad \text{(I)}$$

In this case the ions retain their primary solvation shells and solvent-separated ion pairs (2SIP) are formed. This can further lead to the formation of solvent-shared ion-pair (SIP) or to the formation of contact ion-pairs (CIP)

$$\mathrm{Li^+(DMADMA)Cl^-} \rightleftharpoons \mathrm{Li^+(DMA)Cl^-} + \mathrm{DMA} \qquad \text{(II)}$$

$$\mathrm{Li(DMA)Cl^-} \rightleftharpoons \mathrm{Li^+Cl^-} + \mathrm{DMA} \qquad \text{(III)}$$

If the associates are sufficiently stable, the equilibria can be described by an association constant, K_{A}.
K_{A} can be obtained from the dispersion amplitude, S_{IP}, and compared to the results from other measurements. At first the geometry of the probable ion-pairs has to be defined. For the calculation it is generally assumed that the ion-pair can be approximated by a spheroid or a prolate ellipsoid of semiprincipal axes $a > b = c$,

$$a = r_+ + r_- + n \cdot r_s \qquad (5.5)$$

where r_j is the radius of the individual species (see table 5.2) and n describes the number of solvent molecules dividing the ion pair (in this case $n = 0$, 1 or 2). The other axis,

Table 5.2: Radius, r, polarizability, α of the ions, DMA and water, dipole moment of the solvents, μ, water and DMA respectively.

species	r	α	μ
Li^+	0.78 [148]	0.0284 [149]	
Cl^-	1.81 [127]	3.013 [149]	
DMA	3.24 [14]	9.65 [150]	3.81 [150]
water	1.425 [151]	1.444 [152]	1.834 [152]

units: r in 10^{-10} m, α in $4\pi\varepsilon_0\ 10^{-30}$ m^{-3} and
μ in D (1D = $3.336 \cdot 10^{-30}$ C m).

$b = c$, is defined as the largest radius of the present cation, anion or solvent. When the charge is considered to be located in the center of the ions, the charge distance, d, between the ions can be calculated as follows

$$d = r_+ + r_- + 2nr_s \tag{5.6}$$

The ion-pair dipole moment for symmetric (1:1) electrolytes, μ_j, can be then obtained from the following expressions

$$\mu_j = \mu_0 - \mu_{\text{ind}} - n\mu_s \tag{5.7}$$

where

$$\mu_0 = e_0 d \tag{5.8}$$

with e_0 representing the elementary charge.
In eq.(5.7) μ_s represents the dipole moment of the solvent and μ_{ind} the induced dipole moment due to the polarizability of the ions [153]

$$\mu_{\text{ind}} = \frac{(4\pi\varepsilon_0)d^4 e_0(\alpha_+ + \alpha_-) + 4e_0 d\alpha_+\alpha_-}{4\pi\varepsilon_0 d^3)^2 - 4\alpha_+\alpha_-} \tag{5.9}$$

where α_+ represents the polarizability of the cation, α_- the polarizability of the anion.
The polarizability, α_j, of the corresponding species can be obtained as

$$\alpha_j = \alpha_+ + \alpha_- + n\alpha_s \tag{5.10}$$

with α_s representing the polarizability of the solvent. The parameters necessary for the calculations are summed up in table 5.2.
With the possible ion-pair models we faced some difficulties as it proved to be necessary to involve the solvent shell in the calculation to some extent. The problems can be well demonstrated on the case of CIP. By the application of the usually accepted model which

Table 5.3: All possible ion-pair species and their semi-principal axes, a and b, the charge distance d, their dipole moments, μ_{IP} and polarizability, α.

IP	a	b	d	μ_{IP}	α
CIP1	2.59	1.81	2.59	10.25	3.04
CIP2	4.02	4.02	2.59	14.06	12.69
$PSIP_4$	4.02	3.24	5.28^a	15.27^a	12.69
SIP	5.83	3.24	9.07	39.60	12.69
2SIP	9.07	3.24	15.55	67.00	22.34

units: a, b, d in 10^{-10} m; μ_{IP} in D ($1\,\mathrm{D} = 3.33564 \cdot 10^{-30}\,\mathrm{C\,m^{-1}}$); α in $4\,\pi\varepsilon_o 10^{-30}\ m^3$, ^{a} from MOPAC calculations.

involves only the cation and anion according to the eq.(5.5), no physically reasonable results were obtained (values of $I < 0$). This model is is presented in table 5.3 under the name CIP1. As it is known that LiCl tends to form ion-pairs in DMA [54, 120, 138, 154] further models for CIP were proposed involving also the solvent shell around the cation in the calculation. However, only the application of the parameters described in table 5.3 led to reasonable values in this case. As it can be seen this species, CIP2, can be hardly understood as a 'true' contact ion-pair as the properties are determined more by the solvent ($a = b = c = r_+ + r_s$). Considering the common use of the cavity field theory CIP1 and CIP2 models can be understood as limiting species. In figure 5.3 the dashed-dotted ellipsoids characterize the models applied in the calculation of the dipole moments necessary for the use of the Cavell equation.

The dashed line in the scheme of CIP shows the shape of CIP1. As the application of the classical models resulted in c_j larger than the analytical concentration of the solute, the existence of some sort of penetrating solvent-shared ion pair (PSIP) was supposed. This penetrating species should be viewed as a model describing some species of certain geometry and certain dipole moment. Two possible geometries with 4 or 6 DMA molecules respectively are shown in fig. 5.4. For the calculations we assumed this PSIP as a spheroid with parameters shown in table 5.3. According to the performed MOPAC-calculations the existence of such species is possible (at least in the gas phase). For the other ion-pairs the usual approximations as ellipsoidals could be used. Note that for the calculation of the rotational volumes of the so proposed species the solvation sphere around lithium was considered as a part of the model.

The MOPAC calculations were performed using the PM3 method with the molecular mechanics correction term (MMOK) [155], in order to get some insight into the structure and relative stability of $Li(DMA)_xCl$ complexes ($0 \leq x \leq 6$). The results are summarized in table 5.4. It should be remarked that the same system was studied with the MNDO

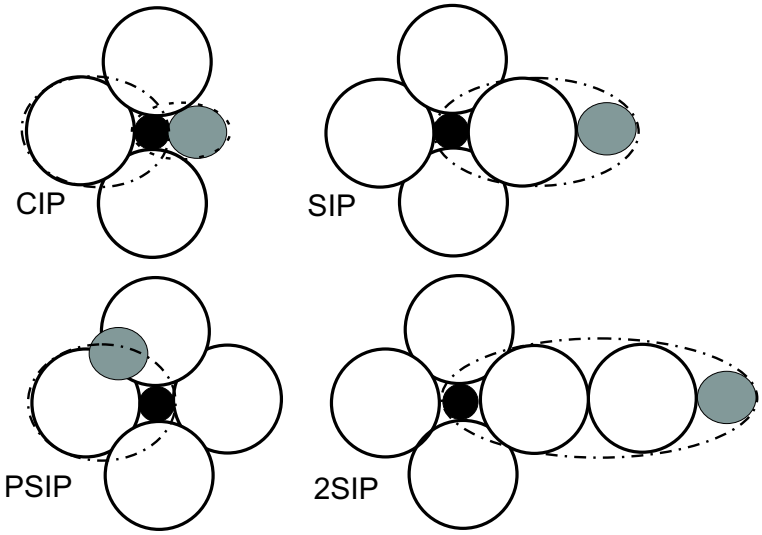

Figure 5.3: Models of the possible ion pairs which were used for the calculation of the parameters (nearer explanation see text). Used symbols for the cation, anion and solvent considered as spheres: Li^+ (black), Cl^- (grey) and DMA(white).

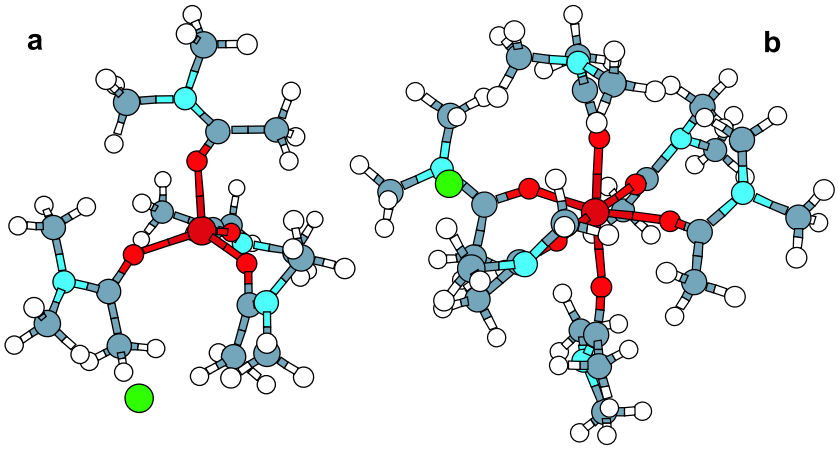

Figure 5.4: Structures of the penetrating solvent-shared ion pairs containing different number of DMA molecules: (a) $[Li(DMA)_4]Cl$ and (b) $[Li(DMA)_6]Cl$ suggested by the semi-empirical PM3 method (dark red: lithium, red: oxygen, light blue: nitrogen, dark blue: carbon, white: hydrogen, green: chlorine).

method [156, 157]. However, the authors studied only complexes up to three molecules of DMA and concentrated their attention mainly on the first complex, Li(DMA)Cl.
The reaction enthalpy of the stepwise complex formation, ΔH_{r1}, corresponds to the following reaction

$$\mathrm{Li(DMA)_{x-1}Cl} + \mathrm{DMA} \longrightarrow \mathrm{Li(DMA)_xCl} \tag{IV}$$

and ΔH_{r2} represents the enthalpy of the formation of the complexes from their components

$$\mathrm{LiCl} + x\,\mathrm{DMA} \longrightarrow \mathrm{Li(DMA)_xCl} \tag{V}$$

As can be seen from table 5.4, ΔH_{r1} becomes positive for all complexes with $\mathrm{x} \geq 3$. The situation is different for ΔH_{r2}, which is negative for all the investigated complexes up to six DMA molecules, which means that for $1 \leq \mathrm{x} \leq 6$ added solvent DMA molecules all complexes are stable relative to the elements. The enthalpy gain per added solvent molecule, $-\Delta_{\mathrm{r2}}H/\mathrm{x}$ (not tabulated), decreases linearly with increasing x and crosses zero at $\mathrm{x} \sim 6.8$. Thus, all complexes with x> 6 are unstable with respect to $[\mathrm{Li(DMA)_6}]\mathrm{Cl}$. So at least in the gas phase the contact ion pair $[\mathrm{Li(DMA)_3}]\mathrm{Cl}$ with tetrahedral coordination of $\mathrm{Li^+}$ is the most stable species, corroborating the results of Tsygankova et.al. [157]. For the solutions this does not seem to be the case as it will be discussed below. In agreement with the literature Li–O bonding proved to be more favorable than Li–N [117, 123–125]. Our data show also the influence of growing number of DMA molecules in the complex on the following interatomic distances, Li-Cl and Li-O and the charge redistribution in the system. The partial charge on oxygen is slightly increasing to more positive values whereas the charge on chlorine becomes strongly negative (very remarkable in the case of the complex with six DMA molecules -0.91). This strong basicity of chlorine in DMA is considered as one of the possible reason for the dissolution of cellulose in LiCl/DMA solutions [7, 54].
Further with the help of S_{IP} and the ionic concentrations, c_j, the stability constants

$$\beta = c_j/(c - c_j)^2 \tag{5.11}$$

were evaluated for all the possible ion-pair models. From β the association constants, K_{A}, could be obtained with the Guggenheim-type eq.

$$\log \beta = \log K_{\mathrm{A}} - 2A_{\mathrm{DH}}\,|z_+ z_-|\,\sqrt{I} + b_\beta I \tag{5.12}$$

where A_{DH} is the *Debye-Hückel* parameter of the solvent [158], b_β represents an empirical parameter and I the ionic strength of 1:1 electrolytes, $I = c - c_j$. It should be remarked that this equation was originally developed for diluted solutions. However, in the past it was successfully applied to different electrolyte solutions studied by the DRS, see [15, 128]. So far no better theoretical description of the system properties has been found.
Comparison with K_{A} from conductivity measurements (fig. 5.5) shows that none of the ionic species by itself can describe the relaxation behavior of the whole system. The values of K_{A} for CIP2 (and PSIP) are larger than the comparable data from literature [147, 159] whereas the K_{A} of SIP and 2SIP species are far too low. In the case of 2SIP this is not

Table 5.4: Some properties of various gas-phase $[Li(DMA)_x]Cl$ ($0 \leq x \leq 6$) complexes calculated by MOPAC with the PM3 method: the number of DMA molecules in the complex, x; interatomic distances, d; atomic charges, q, on the atoms Li, Cl and O; standard enthalpies of formation, $\Delta_f H$, and reaction according to scheme (IV) , $\Delta_{r1} H$, and (V), $\Delta_{r2} H$; dipole moment, μ.

Complex	x	d		Atomic	charges		$\Delta_f H$	$\Delta_{r1} H$	$\Delta_{r2} H$	μ
		$Li..Cl$	$Li..O$	$q(Li)$	$q(Cl)$	$q(O)$				
LiCl		1.88		0.57	-0.57		-201			6.54
DMA						-0.36	-219			3.03
	1	1.91	1.91	0.27	-0.54	-0.30	-494		-74	11.32
	2	2.02	1.93	0.17	-0.61	-0.28	-758	-45	-119	6.63
	3	2.11	1.96	0.03	-0.66	-0.25	-1013	-36	-155	4.20
	4	2.19	2.02	-0.02	-0.68	-0.23	-1216	16	-139	5.76
	5	2.22	2.08	-0.09	-0.67	-0.20	-1412	23	-116	7.02
$PSIP_6$	6	4.28	2.06	-0.06	-0.91	-0.20	-1574	57	-59	14.35
$PSIP_4$	4	5.28	1.92	0.05	-0.77	-0.25	-1164	68	-87	15.27

units: d in Å; charges in e^{-1}; ΔH_f and ΔH_r in $k\mathrm{J\,mol^{-1}}$ and μ in D.

Table 5.5: Association constants, K_A, for different ion-pair models and their comparison with data from literature.

T	K_A^{CIP}	K_A^{PSIP}	K_A^{SIP}	K_A^{2SIP}	T	K_A^a	K_A^b
278.15	85 ± 25	49 ± 10	6.6 ± 1.2	2.6 ± 0.4	273.15	31.2	63.6
298.15	160 ± 20	83 ± 8	9.7 ± 0.7	3.8 ± 0.3	298.15	56.1	77.9
318.15	220 ± 50	146 ± 37	12.9 ± 0.6	5.0 ± 0.2	313.15	60.3	79.6
338.15	320 ± 70	142 ± 15	16 ± 2	6.4 ± 0.8	333.15	64.1	70.6

units: T in K; K_A in L $\mathrm{mol^{-1}}$. [a] ref. [147]; [b] ref. [159].

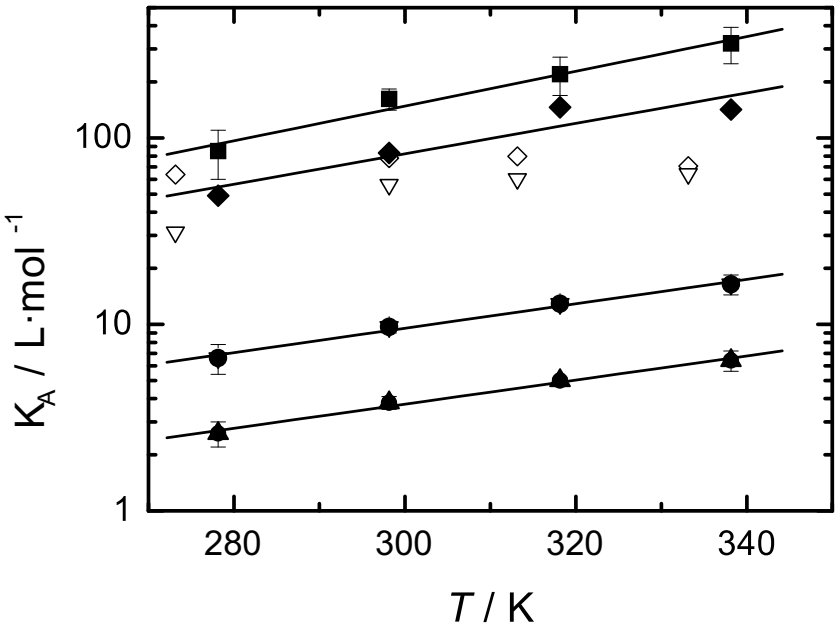

Figure 5.5: Association constants, K_A, as a function of temperature compared to some literature data. (■) K_A^{CIP}; (♦) K_A^{PSIP}; (●) K_A^{SIP}, (▲) K_A^{2SIP}; (▽) ref. [147]; (◊) ref. [159], K_A^{PSIP} without error bars.

surprising as the Cl^- is supposed to remain unsolvated in DMA and so the formation of solvent-separated ion pairs can be excluded.

The corresponding values of K_A at 298 K for LiCl obtained from other conductivity studies of different Li^+ salts in DMA are 45.8 for LiCl, 33.1 for LiBr, and 30.1 L mol^{-1} for LiI [134]. From the DRS-measurements on the $LiClO_4$/DMA system the value of (3.6 ± 1.1) L mol^{-1} for the SIP model was obtained [15]. Interesting is also the temperature dependence of the DRS results: K_A values considerably increase with increasing temperature in contrast to K_A obtained from the conductivity measurements.

The obtained results can be interpreted in two different ways. Our measurements proved that the LiCl in DMA forms associates. This association seems to be stronger in DMA than in aqueous solutions (see next chapter), however, it is not possible to attribute the relaxation process to a single species. Multi-step IP equilibria have not yet been observed for electrolytes in DMA but are common e.g. in aqueous solutions [115]. Such equilibria should also be detectable for DMA solutions with DRS. Provided that all the species were stable enough and existed in the whole concentration range, it should be possible to separate them into various relaxation processes. However, this is not the case as mentioned at the beginning. In combination with the previously presented results of effective solvation numbers it implies that the ion-pair equilibrium involves a continuous distribution of species that is temperature and concentration dependent. So the distribution of the species present changes with concentration of LiCl. A similar situation was revealed in the

Table 5.6: Rotational parameters of the species, a and b, and calculated volumes of rotation for *slip*, V_{r}^{slip}, and *stick* hydrodynamic boundary conditions, V_{r}^{stick}, of the tested ion-pair models (ref. [161]).

IP	a	b	V_{r}^{slip}	V_{r}^{stick}
CIP2	7.26	7.26	~ 0	1600
PSIP	7.26	7.26	~ 0	1600
SIP	9.07	7.26	100	2100
2SIP	12.31	7.26	580	3600

units: a, b in 10^{-10} m; $V_{\mathrm{r}}^{\mathrm{slip}}$, $V_{\mathrm{r}}^{\mathrm{stick}}$ in 10^{-30} m^3.

$LiClO_4$/DMF solutions examined by various spectroscopic techniques [160]. In contrast to the LiCl/DMA system, the ion association was observed only in concentrated solutions and it was interpreted by the presence of two ion-pair equilibria between free ion pairs, SIP and CIP. The measured association constants were rather small.
Also the analysis of the relaxation times and corresponding viscosities indicates the presence of more than one species in the solutions. The viscosity values, η, from ref. [50] and [147] were used for the calculation of the rotational correlation times, τ_j^{or}, and of the effective volume by using the modified Stokes-Debye-Einstein equation eq.(2.88). In the calculation it was assumed that the ion-pair volume can be approximated by a spheroid or a prolate ellipsoid of semi principal axes as described before, however, including the solvent into the calculation of the theoretical volume.
The corresponding value of the effective volume, $190{\cdot}10^{-30}$ m^3, obtained from τ_{IP} was rather constant at all temperatures. Unfortunately, the determination of the volumes of rotation does not show a clear difference between the possibly present species. Assuming *slip* conditions only the presence of 2SIP can be excluded as the calculated theoretical value of V^{slip}(2SIP) exceeds the determined V_{eff}. The distinction between the SIP, CIP or PSIP forms is not possible as the determined value of V_{eff} could correspond to all the proposed geometries. Table 5.6 summarizes the corresponding parameters resulting from different models and values of volumes of rotation for the different hydrodynamic conditions under the involvement of the solvent shell.
Assuming the existence of a single step equilibrium the rate constants of the ion pair formation, k_{12}, could be obtained according to [127]

$$Y = (V_{\mathrm{r}}^{\mathrm{e}})^{-1} + k_{12}X = \frac{3\eta}{k_B T \tau_{IP}} \tag{5.13}$$

with

$$X = \frac{3\eta}{k_B T} \cdot (K_{\mathrm{A}}^{-1} + 2I) \tag{5.14}$$

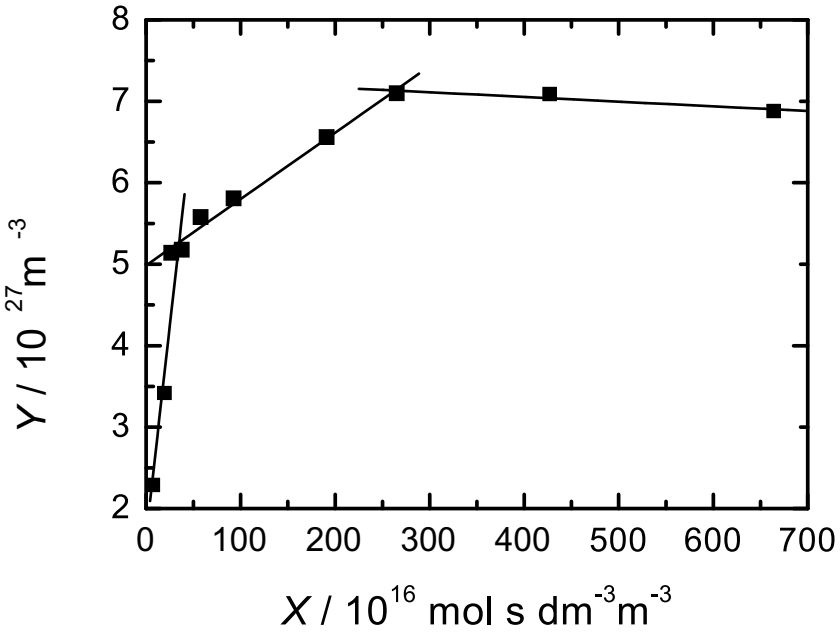

Figure 5.6: Example of the analysis of the kinetic behavior in LiCl/DMA solutions at 298 K. In the figure three different regions can be distinguished which indicates the presence of various species in the system.

The k_{21} was obtained from the relation $K_{\mathrm{A}} = k_{12}/k_{21}$, where K_{A} is the association constant (see eq. 5.12). The so calculated values were for PSIP in the range from $k_{12} = 3.7 \cdot 10^8$ L (mol s)$^{-1}$ at 278 K to $k_{12} = 12.3 \cdot 10^8$ L (mol s)$^{-1}$ at 338 K and for SIP in the range from $k_{12} = 1.76 \cdot 10^8$ L (mol s)$^{-1}$ at 278 K to $k_{12} = 7.8 \cdot 10^8$ L (mol s)$^{-1}$ at 338 K respectively. The rate constants of the decay were 3.5 to 6 times larger for PSIP than in the case of SIP. However, these observations have to be interpreted carefully as the calculation involves K_{A} whose values were determined only for the proposed models. Furthermore, from figure 5.6 showing the kinetic behavior of the LiCl/DMA solutions at 298 K, it can be seen that the kinetic behavior of the system is not unambiguous. It seems that the diagram can be divided into two or three regions. This also supports our hypothesis about a broad distribution of species dependent on the concentration of LiCl in the solutions.
The relaxation time, τ_{IP}, was also evaluated by the help of the Arrhenius equation (eq. 2.93). The temperature dependence of ln τ_{IP} is shown in figure 5.7a and the correlation between the concentration dependent values of activation energies, E_a, obtained from τ_{IP} and the viscosities, η, in the LiCl/DMA system. It is obvious that the increase of E_a for τ_{IP} is caused mainly by the increase in the viscosity with growing LiCl concentration. The values of E_a are in the range $10 < E_a/\mathrm{kJ\,mol^{-1}} < 24$. This is of course more than in the case of the rotational barrier of the solvent (see fig. 5.2). The values of activation energy obtained at higher temperatures for $LiClO_4$/DMA system in an ^{1}H-NMR study were *ca.* 80 kJ mol^{-1} [162].

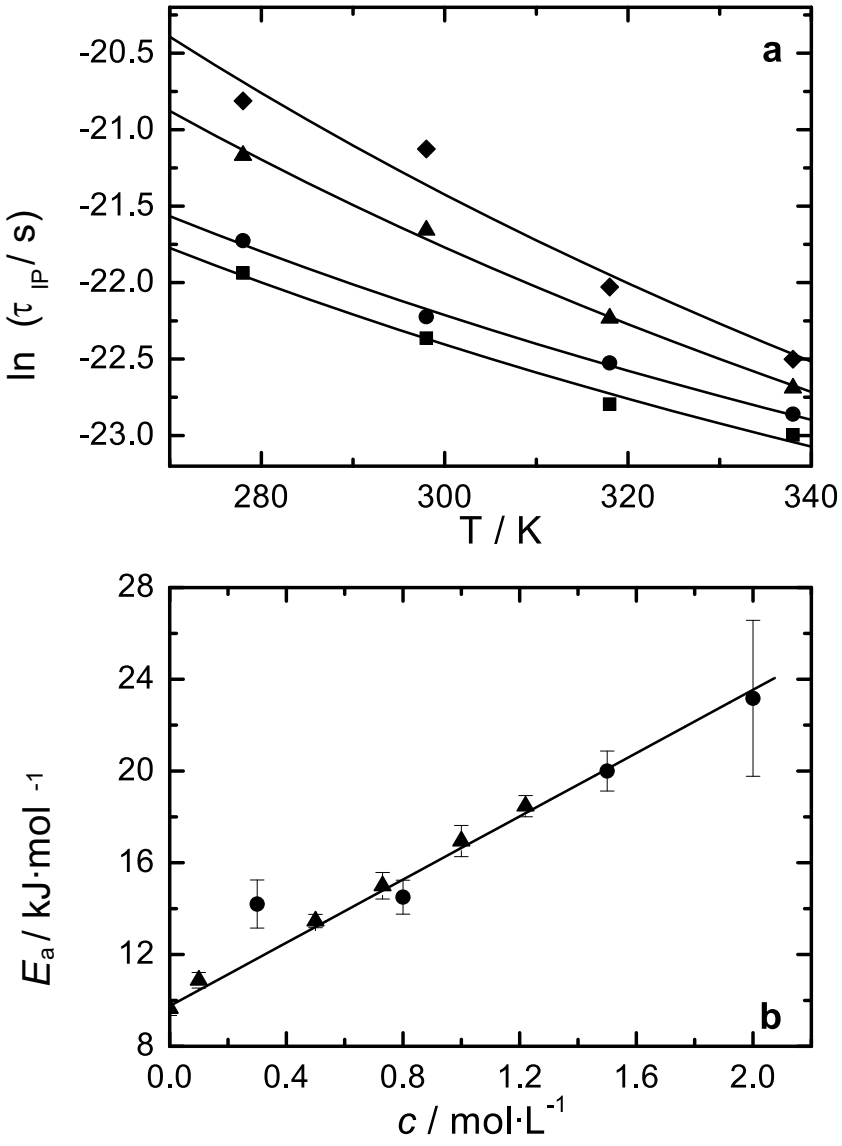

Figure 5.7: (a) Temperature dependence of ln τ_{IP} in LiCl/DMA solutions of $c = 0.3$ mol·L^{-1} (■), $c = 0.8$ mol·L^{-1} (•), $c = 1.5$ mol·L^{-1} (▲) and $c = 2.0$ mol·L^{-1} (♦). In figure (b) the dependence of activation energy values of the ion pair process in LiCl/DMA solutions obtained from DRS data (•) are compared with values obtained from viscosity data from ref. [147] (▲).

Finally as a conclusion from the presented results an association mechanism for LiCl/DMA solutions can be proposed:

$$Li^+(DMA)_x + Cl^- \rightleftharpoons IP + DMA \tag{VI}$$

$$Li^+(DMA)_{x-1}Cl^- \rightleftharpoons PSIP \rightleftharpoons (Li^+Cl^-)DMA_{x-2} + DMA \tag{VII}$$

In low concentrated LiCl/DMA solutions Li^+ seems to be considerably solvated (or complexed) in DMA, whereas Cl^- ion remains unsolvated. The 'free' Cl^- interacts further with the $Li^+(DMA)_x$ associate which leads to the formation of some ion pair (IP). Our DRS results indicate that this IP is represented by the solvent-shared ion pair (SIP) of a general form $[Li(DMA)_{x-1}]Cl$. At higher LiCl concentrations Cl^- seems to penetrate into the solvation shell of the present $[Li^+(DMA)_{x-1}]$ complex which results in the formation of some sort of penetrating ion pair (PSIP) with probably 6-4 molecules of DMA involved. At the highest LiCl concentration the formation of contact ion pair (CIP) containing about 3-4 DMA molecules $[Li(DMA)_{x-2}]Cl$ can be expected. The proposed mechanism, however, can be valid only provided that the equilibria for the proposed species are established fast enough that the resulting species are stable enough to be observed by the DRS.
Nevertheless the proposed mechanism seems to be in a good agreement with the fact that the investigated system is able to dissolve cellulose samples only in a certain concentration range (see section 1.2.3). This was shown also in the phase diagrams with cellulose performed as a part of this work [47]. In some studies the authors found another structural feature of LiCl/DMA solutions. They assumed some chain-like complex formation in LiCl/DMA solutions [146, 154]. However, in order to observe such structures in the DRS spectra, those polymer-like chains would have to be non-symmetrical and have some permanent dipole moment. In the case of symmetrical structures no contribution to the relaxation mode can be expected.

5.2 Aqueous LiCl solutions

Because of their interesting and relatively simple composition of one structure making, Li^+, and structure breaking ion, Cl^-, aqueous LiCl solutions have been subject of many studies. Both the ions exhibit strong interaction with water. The extent of hydration strongly depends on the concentration of the electrolyte in the solutions. This is well demonstrated in some reviews dealing with the solvation or hydration of ions, see [140, 163, 164].
The complex permittivity spectra of diluted aqueous LiCl solutions were fitted by the D+D model (see section 4.3). In our case only one water relaxation was observed (τ_2 ∼8 ps), and no high-frequency water process was revealed as in the DRS-measurements of some other aqueous electrolyte solutions [127]. Additionally one relaxation ascribed to a weak ion-pair formation characterized by a single Debye equation ($\tau_1 \sim 230$ ps) was found. Other aqueous Cl^- solutions of alkali metals studied by the DRS, see [114, 128], could be characterized by a single CC equation. Only in the case of dilute CsCl aqueous solutions similar behavior was observed [114], however, the authors expressed doubts on the real existence of this relaxation resulting from the ion-pair formation. Other DRS studies on aqueous LiCl solutions used only one relaxation process [111, 112] for the description of the spectra.
The low-frequency relaxation process with the dispersion amplitude S_1 was evaluated in terms of ion-pair formation, and the high-frequency solvent relaxation with the amplitude S_2 was ascribed to the cooperative relaxation of bulk water, modified by the addition of LiCl.

5.2.1 Solvent relaxation

Before we present our results, some comments on the available literature data concerning hydration numbers of lithium and chlorine should be made. For aqueous solutions of lithium salts X-ray or neutron-scattering (NS) measurements usually yielded hydration number of 4 [163, 165]. However, many studies also demonstrated the strong concentration dependence of the hydration numbers of both ions reaching from 5.5 (for molal concentration, $m = 3.6$ mol kg^{-1}) to 2.3 ($m = 27.8$ mol kg^{-1}) for Li^+ and from 6 ($m = 3.6$ mol kg^{-1}) to 4.4 ($m = 14.9$ mol kg^{-1}) for Cl^- respectively [166]. NS measurements also provided some evidence for the existence of a further shell of weakly coordinated molecules around Li^+ [167] which was not observed for Cl^-. NMR measurements generally resulted in comparatively low lithium hydration number of 3 [168, 169]. There are also a lot of computational studies dealing with this subject. MD and MC simulations led to a lot of different results depending on the chosen method distributed over the range of 3-7 (for details see overview in ref. [163, 165]). For dilute solutions lithium hydration with six water molecules of octahedral symmetry was suggested [170–172]. The tetrahedral coordination of four water molecules was assumed to provide the best description for concentrated Li^+ solutions and a formation of a stable second coordination sphere containing about twelve water molecules was proposed [165]. Some authors suggested the presence of two or even three hydration shells with up to 30 water molecules [173]. According to recent ab-inito

Table 5.7: Effective hydration numbers, Z_{ib} of LiCl in dilute aqueous solutions at certain LiCl concentration, c, for different kinetic depolarization conditions.

c	Z_{ib}^{stick}	Z_{ib}^{slip}	Z_{ib}^{neg}
0.0883	10.4 ± 6.4	12.6 ± 6.4	17.1 ± 6.5
0.2171	7.8 ± 2.6	9.9 ± 2.6	14.1 ± 2.6
0.4866	6.1 ± 1.2	7.9 ± 1.2	11.6 ± 1.2
0.6686	6.2 ± 0.8	7.9 ± 0.8	11.4 ± 0.9
0.9837	5.9 ± 0.6	7.5 ± 0.6	10.8 ± 0.6

units: c in mol L^{-1}.

calculations the tetrahedral complex should be in general more stable than the octahedral symmetry [174, 175].

For the evaluation of the dispersion amplitude of water, S_2, the same procedure was applied as described in the section (5.1.1). From the amplitude S_2 the apparent solvent (water) concentrations, c_{s}^{ap}, could be calculated using the Cavell equation eq.(5.1) normalized for the pure solvent under different kinetic depolarization (kd) conditions. Eq.(5.4) led then to the effective hydration numbers, Z_{ib}. As different studies showed, the residence time of chloride in the hydration sphere is comparable with the relaxation time of water exchange [176, 177] and so the observed effective hydration numbers, Z_{ib}, can be ascribed to the hydration of the cation, in this case to Li^+ [72, 114, 128]. This approach proved to be consistent for different aqueous solutions. The resulting values of Z_{ib} for the measured LiCl solutions are listed in table 5.7 and their concentration dependence is shown also in figure 5.8.

When we take a look at figure 5.8, we see that a polynomial fit of the data (the solid curve) leads to the value of Z_{ib} (0) = 14.1 ± 0.8. So in our case the hydration number of Li^+ at infinite dilution should be 14. This value, however, is quite large and would imply that in dilute LiCl/water solutions, Li^+ is surrounded by two hydration shells containing up to 14 water molecules. As the residence time of water molecules in the second hydration shell should be comparable to the one of the water-exchange, it should not be observable in the spectra. From a closer look at the values of Z_{ib} at c→0 listed in table 5.7 it can be seen that those at low concentrations are connected with large error bars. For this reason they should not be taken into account. So only the data at $c \geq 0.3$ mol L^{-1} were used for the calculation of the corresponding $Z_{\mathrm{ib}}^{kd}(0)$. The linear fit of $Z_{\mathrm{ib}}(c)$ (see lines fig. 5.8) resulted in the following values of Z_{ib} (0): $Z_{\mathrm{ib}}^{stick}(0) = 6.4 \pm 0.3$, $Z_{\mathrm{ib}}^{slip}(0) = 8.4 \pm 0.3$ and $Z_{\mathrm{ib}}^{neg}(0) = 12.5 \pm 0.2$. As the kd conditions should not be negligible, the hydration shell of Li^+ at low concentrations seems to be composed of 6 or 8 irrotationally bound water molecules. Similar values were obtained from DRS measurements in aqueous LiCl solutions by other authors [111, 112]. Wei et.al. obtained for the dilute region the following values of

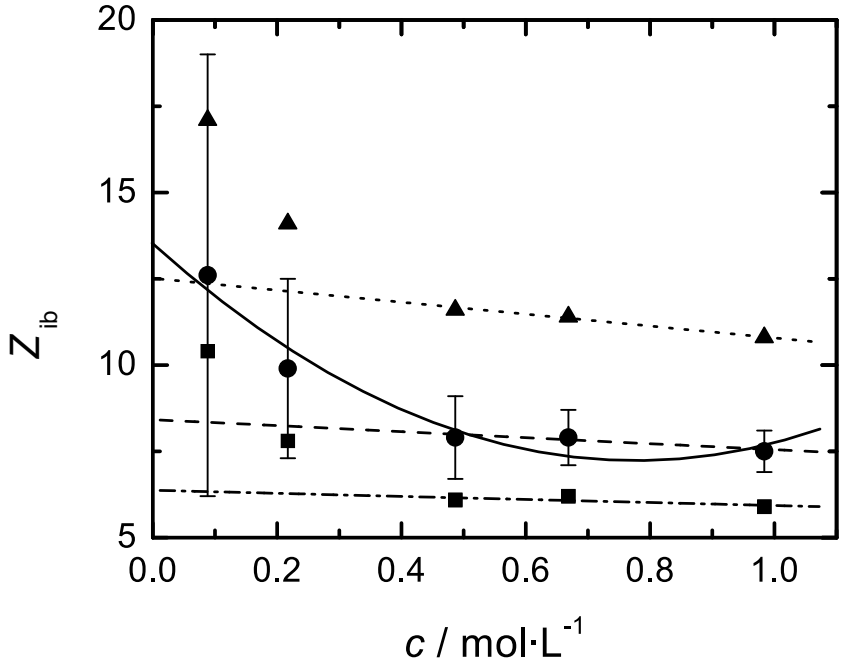

Figure 5.8: Effective solvation numbers, Z_{ib}, as a function of LiCl concentration, c, in aqueous LiCl solutions at 298 K for *stick* (■), *slip* (•) and *negligible* (▲) kinetic depolarization conditions (error bars only for *slip* conditions). The polynomial fit of Z_{ib}^{slip} (solid line), and linear fits of all Z_{ib} without the two first values (dashed and dotted lines).

hydration numbers: 7.6 ($c = 0.55$ mol L^{-1}) and 6.5 ($c = 1.09$ mol L^{-1}) [112]. Popp applied the Hubbard-Onsager theory for *slip* and *stick* conditions which yielded the following values for the comparable concentrations (only *slip* conditions): 8.6 ($c = 0.16$ mol L^{-1}) and 6.8 ($c = 0.65$ mol L^{-1}) [111]. Our values at the corresponding concentrations are higher due to the different fit of the spectra and the difference in the applied calculation procedure. One of the 'pioneer' studies dealing with the dielectric properties of water and ionic solutions [178] resulted in the observation of 6 ($\pm$ 1) irrotationally bound water molecules in dilute LiCl solutions. The hydration with 6 water molecules in dilute solutions is in a good agreement with the data from the literature as discussed at the beginning of this section.

5.2.2 Solute relaxation

The first relaxation process with rather small but increasing amplitude, S_1, and relaxation time, τ_1, was ascribed to ion-pair formation. The values of the relaxation time ($160 \leq \tau_1$ / ps ≤ 330) are fairly large for aqueous solutions. Usually the residence time of water molecules in the hydration sphere of Li^+ is estimated to *ca.* 10 ps, see [167]. Inelastic NS data propose that the residence time of water molecules in the primary solvation shell of Li^+ is about 25 ps in a 2M LiCl solution [179]. However, there are several MD studies

Table 5.8: The semi principal axes, a and b, dipole moments, μ_{IP}, polarizability, α, and the association constants, K_{A} for all possible ion-pairs in LiCl/water solutions .

IP	a	b	μ_{IP}	α	K_{A}
CIP	2.59	1.81	10.25	3.041	140 ± 180
SIP	4.02	1.81	23.8	4.485	4.2 ± 2.0
2SIP	5.44	1.81	35.9	5.929	1.8 ± 1.0

units: a, b in 10^{-10} m; μ_{IP} in D ($1\,\mathrm{D} = 3.33564 \cdot 10^{-30}\,\mathrm{C\,m^{-1}}$); α in 4 $\pi\varepsilon_o 10^{-30}$ m^3; K_{A} in L mol^{-1}.

predicting that Li^+ exhibits a strong interaction with water resulting in a pronounced primary solvation shell, where the water molecules are kept for about 33 ps (at 278 K) [176], 41 ps [180] or 190 ps [170], respectively. Though it should be noted that the reliability of such calculations is strongly dependent on the used model. The authors of the last named publication obtained for the same system by the change of the applied model a value of *ca.* 400 ps [171].

The amplitude of this relaxation process, S_1, was analyzed in the same way as described in section 5.1.2 with the help of the Cavell equation eq.(2.72)- eq.(2.75) in terms of present ionic species. The necessary input values were calculated from parameters listed in table 5.2. The corresponding geometrical parameters of the probable ionic species are shown together with the resulting association constants, K_{A}, in table 5.8. It can be seen that for CIP the error of K_{A} is larger than the K_{A} itself. This is not very surprising as the number of measured points is rather small. On the other hand, since the ions are supposed to be fully hydrated at these concentrations, the formation of CIP is very improbable anyhow. The corresponding literature values of K_{A} obtained from the measurements of electric conductance in dilute aqueous LiCl solutions are: 0.81 L mol^{-1} [181] and 2.75 L mol^{-1} [182], respectively. Thus the association takes place via the formation of either SIP or 2SIP.

From $\tau_1(0) = 231$ ps, the corresponding microscopic relaxation time, $\tau_{1\mathrm{s}} = 160$ ps, was obtained with the help of eq.(2.84). The Stokes-Debye-Einstein equation (2.88) yielded then the value of effective volume of the rotation at 298 K, $V_{eff} = 246\ 10^{-30}\mathrm{m}^{-3}$. The viscosity of water at 298 K was used from ref. [132]. The value of V_{eff} is too large to belong to any ionic species presented in table 5.8 as long as the solvation sphere of the cation is omitted. This demonstrates again the necessity to include the whole solvation shell in the calculation of the theoretical volume of the considered species. So a similar model as in the case of LiCl/DMA solutions was proposed and the resulting parameters are presented in table 5.9. The parameters a and b characterize in this case the shape and size of the hydration shells of the corresponding ion-pair assuming full hydration shell around Li^+. So the values differ from the semi principal axes, a and b, (table 5.8) of the IP ellipsoids

Table 5.9: All possible ion-pair species and their semi principal axes, a and b, shape factor, $f_\perp$, and the corresponding volumes of rotation for stick, V_r^{stick}, and slip, V_r^{slip}, boundary conditions.

IP	a	b	$f_\perp$	V_r^{stick}	V_r^{slip}
CIP	4.02	3.63	1.03	230	~ 0
SIP	5.44	3.63	1.19	360	33
2SIP	6.87	3.63	1.43	590	80

units: a, b in 10^{-10} m; V^{kd} in 10^{-30} m^3.

necessary for the calculation of the dipole moment.
Albeit the values presented in table 5.9 do not allow us to decide which of the species is really present, we can conclude that the weak association observed in the aqueous LiCl solutions is to be assigned to the formation of solvent-shared ion pairs. Since the residence time of Cl^- in the hydration sphere is comparable with the relaxation time of water exchange, the formation of a solvent-separated ion pair should not be observable in the DRS spectra. Thus the most probable ionic species present is a solvent-shared ion pair. The solvation shell of Li^+ seems to be composed of 6-8 water molecules at infinite dilution.

5.3 LiCl/DMA/Water system

As reported in the introductive part (section 1.2.3) and proven in our phase diagrams (section 4.5.2) the ability of LiCl/DMA solutions to dissolve cellulose is strongly influenced by the water content in the solvent system and the polymer itself. We showed that even small amounts of water in the starting LiCl/DMA solutions led to a strong decrease of the solubilization power of this system (section 5.4.2). Water is also often used as a precipitating agent for cellulose. This implies that the addition of water causes strong changes either in the accessibility of the present cellulose hydroxy groups or, what is more probable, that the properties of the LiCl/DMA complex (its geometry and the resulting donor/acceptor or acidity/basicity properties) dramatically change in the presence of water. Assuming that the changes in the solubilization are related to the structure of the solvent system at a certain concentration and temperature, the following hypotheses can be proposed:

i. LiCl is preferentially solvated by water which leads to the formation of an associate composed only of LiCl and water.

ii. LiCl is preferentially solvated by DMA even in the presence of water.

iii. Some mixed complex of a general formula $[Li(DMA)_x(H_2O)_y]Cl$ is formed.

iv. Whereas the Li^+ solvation shell remains composed of DMA molecules, Cl^- undergoes interaction with water protons.

v. Water interacts with DMA directly and a formation of some solvate between the two solvents takes place.

In order to discuss all the mentioned points, some basic facts known from the literature should be presented.

5.3.1 Comments on literature data

The Gutmann donor numbers (DN) for water are 138 $kJ\,mol^{-1}$ [132], 75 $kJ\,mol^{-1}$ [123] and 92 $kJ\,mol^{-1}$ [183], respectively depending on the way they are determined. The last named value seems to be the most probable. The corresponding DN(DMA) = 116 $kJ\,mol^{-1}$ [123]. The comparison of acceptor numbers (AN) leads to the logical conclusion that DMA represents a stronger donor than acceptor, AN(DMA) = 13.6 and AN(Water) = 54.8 (both values from [132]). The solvatochromic parameter describing the polarizability of the solvent, π^*, is 1.09 for water and 0.88 for DMA (both values from [132]). The binding energies of Li^+ to water and to DMA are 170 and 232 $kJ\,mol^{-1}$ respectively [123]. The values of hydration enthalpy are 515 [184] or 531 $kJ\,mol^{-1}$ [185], whereas for the solvation enthalpy of Li^+ in DMA the value of 490 $kJ\,mol^{-1}$ was obtained [186]. The hydration enthalpy of Cl^- is 369 $kJ\,mol^{-1}$ [184] and can be compared to the solvation value in DMA which is 395 $kJ\,mol^{-1}$ [186].

The solvation of various lithium salts in the mixed solvent system has already been investigated by IR and Raman spectroscopy, NMR and other techniques. However, the conclusions drawn are often rather contradictory.
^{13}C-NMR study performed both on pure DMA/water mixtures and on DMA/LiCl(aq) or $LiClO_4$(aq) solutions [121] revealed only small changes in the spectra. Those were interpreted as a result of the formation of a mixed solvent complex. Li^+ was supposed to be solvated by three molecules of water whereas DMA was involved in the second shell interacting with water hydrogen atoms. This explanation does not appear correct as the presence of Cl^- is not properly involved in the interaction. There are other NMR studies concerning the LiCl/DMA/water system [117, 154]. In both of them the authors found a direct interaction between Li^+ and the carbonyl group of DMA and proposed a formation of a mixed solvation shell in the presence of water. Another NMR study, though on LiCl/DMF/water, concluded that the solvation of Li^+ changed with the composition of the bulk. In this case no indication for some preferential solvation in the one or the other solvent was found [187]. In ultrasonic studies [120] the authors observed a relaxation upon the addition of DMA to aqueous LiCl solutions (in the case of $LiClO_4$ no relaxation was observed) reaching its maximum at the DMA:water mole ratio of 2:1. Li^+ was supposed to be preferentially solvated by water, whereas the interaction of the cation with DMA proceeded only through the water molecules. In polarographic studies no reduction took place in $LiClO_4$/DMA solutions under anhydrous conditions. Only after water was added a reduction wave was observable [188]. A similar investigation on $LiClO_4$/DMA/water solutions led to the conclusion that an increasing water content in the solutions resulted in the replacement of DMA in the solvation sphere of Li^+ and in the decrease of the size of the shell [189]. Conductivity and viscosity studies on solutions of LiCl in the mixed solvent suggested the formation of a mixed solvation shell composed of both solvents [147]. A solid complex of the composition $Li[(DMA)(H_2O)_2]ClO_4$ was characterized with the help of crystallography [143]. Solubilization study of LiCl in dry and wet DMA [50] indicated that both solvents contributed to the solvation of Li^+. At high water concentration the interaction between water and DMA seemed to be the dominant feature determining the properties of the system.
Concerning the interaction between the two solvents several studies were published. A DRS study on supercooled binary mixtures of water and DMA was performed [190]. The relaxation behavior could be described by a model of ideally associated solution involving a monohydrate and trihydrate of DMA. In another temperature-dependent TDR study of DMA/water solutions [191] the spectra were fitted by a Cole-Davidson fit. At all the recorded temperatures a break in the static permittivity and relaxation time of the investigated solutions appeared in the composition range of 60-70 V% DMA. In viscosity and density measurements the largest deviations from the ideal behavior of the mixed solvent system occurred at the water:DMA mole ratio of 2.7:1 [192]. This seems to be a general feature of N,N-disubstituted amide/water solutions with the maximum located at water:amide mole ratio of approx. 2.5:1 [193]. More extensive density measurements at 298 K [194] and 303 and 308 K [195] respectively, were utilized for the calculation of excess molar volumes of different amide/water mixtures. In both studies a minimum of the curve

at the following mole fraction, $x_{DMA} = 0.4$, was observed. The situation was similar also for other investigated amides, nevertheless DMA seemed to exhibit the strongest interaction with water protons among the investigated amide compounds [195]. In an IR study on the hydrogen-binding capability of N,N-disubstituted amides, DMA showed a pronounced interaction with water protons compared to DMF or other investigated amides [196]. Water/DMA mixtures were also examined by CNDO/2 calculations and ^{13}C-NMR [121]. The authors predicted the presence of various DMA/water complexes and equilibria, however, did not show many proofs for their assumption. In another study [197], involving ^{1}H-NMR, viscosity and surface tension measurements, Kinart et.al. proved that the deviations from the ideal behavior reached all its maximum value in solutions with approximatively 33 mol % of DMA. The changes were interpreted as the result of the formation of a stable complex of DMA with two water molecules. The most recent study on this binary system applied different experimental techniques (overtone FT-IR, MS, X-ray diffraction) [198]. The preformed measurements revealed that depending on the composition (x_{DMA}) of the system different interpretations had to be considered. The whole concentration range was divided into four regions where certain structures or behavior was dominant. In the water rich region, $x_{DMA} \leq 0.1$, only water influence was observed. With increasing concentration of DMA, $0.1 < x_{DMA} \leq 0.3$, the presence of water clusters still dominated the spectra but their importance decreased. Spectra recorded in mixtures with $0.6 < x_{DMA}$ showed features typical for pure DMA. Finally a transition region was defined, $0.3 < x_{DMA} \leq 0.6$, where influences of both solvents were difficult to separate.
Returning back to the hypotheses (i.-v.) proposed at the beginning of this section, the following conclusions can be drawn. On the basis of the data known from the literature it is not possible to decide in which solvent LiCl should be preferentially solvated. Thus for the formation of solvation shells composed from either only water (i.) or DMA molecules (ii.) there is not enough scientific evidence. In this connection the immense importance of the composition of the mixed solvent should be noticed. The formation of a mixed solvation shell (iii.) seems to be the most probable case at least for Li^+. Cl^- is supposed not be solvated in aprotic solvents like DMA [134], whereas it proved to exhibit strong interaction with water hydrogens. Although the situation should not be so pronounced as proposed in point (iv.), the basicity of Cl^- should be strongly decreased in the presence of water. Considering the fifth point (v.) the literature survey showed that a formation of DMA hydrates of different composition depending on the mole ratios of both solvents is probable. The influence of the salt on the formation of these associates, however, is not clear.

5.3.2 Discussion of the DRS data

Before we take a closer look at the obtained results we should be aware of the fact that due to the small number of measured samples no quantitative interpretation of the data is possible. Thus only some qualitative statements can be made. The samples were prepared so that the mole ratio DMA:LiCl was kept constant at 5.7:1. The DRS spectra were fitted by a D+D+D+D fit. The low-frequency processes were attributed to the existence of two

ionic species relatively stable in the whole investigated concentration range and two high-frequency relaxation processes related to the solvent. The obtained dielectric parameters are listed in table 4.8 and shown in figure 4.18. At the DMA:water mole ratio of 2.85:1 the conductivity data measured for the system exhibited a shallow minimum.
The addition of water into the stock solution causes of course dilution of the samples. Furthermore, it may also result in specific interactions of water with the components of the system. According to our literature study, the addition of water should lead to the formation of a mixed solvation shell composed of both solvents. The previous analysis of the anhydrous LiCl/DMA solutions revealed a concentration dependent formation of different ionic species (see section 5.1.2). As the LiCl concentration in the starting LiCl/DMA solution corresponded nearly to the saturation limit at 298 K, the presence of CIP or PSIP in the solutions could be expected. The amplitude of the first solute relaxation process, S_1, ascribed in our previous analysis to the presence of ion-pair species in LiCl/DMA solutions, strongly decreases with the increasing water concentration (see fig. 4.18). In contrast to the amplitude the corresponding relaxation time, τ_1, remains nearly constant ($\sim$ 540 ps) as in water-free solutions. Additionally, a new process with the amplitude S_2 strongly connected to the water concentration appears. Its relaxation time, τ_2, is nearly constant in the whole investigated region ($\sim$ 100 ps).
If we omit the fact that the LiCl and DMA concentration decreases with increasing water concentration we may conclude that two stable ion-pairs are formed and their solvation shells do not change very much with the composition, only their concentrations. The imagination of an equilibrium as presented in the following scheme

$$\mathrm{Li(DMA)_xCl} + \mathrm{H_2O} \longrightarrow \mathrm{Li(DMA)_{x-1}(H_2O)Cl} + \mathrm{DMA} \qquad \text{(VIII)}$$

as proposed in polarographic studies [189] is possible. However, with the number of experiments provided we cannot verify its correctness. Due to the complexity of the subject any further statement about the structure of the present species would not be based on scientific facts.
In the case of the two solvent relaxation processes the situation is not simple either. The amplitude of the first solvent relaxation process, S_3, related in the anhydrous solutions to the relaxation of pure DMA exhibits an minimum at the water:DMA mole ratio $\sim$ 1:1. Between the water:DMA mole ratios 1:1 and 2:1 S_3 remains practically constant. The other solvent amplitude, S_4, which was considered as the second relaxation process of DMA decreases monotonously with increasing water content. The corresponding relaxation times, τ_3 and τ_4, do not change considerably with the increasing water concentration in the system. Only a small 'minimum' can be observed in the τ_4 between water:DMA mole ratios 1:1 and 2:1. However, this 'extreme' in the curve shape is not very pronounced. In the spectra no relaxation process resulting from pure water dispersion process ($\tau \sim 8$ ps) was detected.
As mentioned in the first part of this section dealing with the literature concerning DMA/water interaction the two known DRS-studies [190, 191] assumed the formation of various associates. The presence of mono- or trihydrates of DMA was proposed in the first study

[190], whereas the other assumed DMA-water-DMA structures turning into DMA-water forms [191]. In our case the correct explanation for the decrease of the solvent dispersion amplitudes S_3 and S_4 seems to be the decrease of the DMA concentration in the system. Unfortunately it is very difficult to separate the influence of the decreasing electrolyte and DMA concentration from the new effect resulting from the addition of water.

5.4 Analysis of the performed phase diagrams

5.4.1 Temperature influence

When figures 4.20a and 4.20b are compared it becomes evident that the curve corresponding to 25 °C starts at approximately 2.7 % LiCl with a rather small slope, whereas at 5 °C the curve is a straight line starting at 3.8 % LiCl with a larger slope. Thus, for high concentrations of LiCl, the solubilization potential of DMA/LiCl solutions is larger at 5 °C than at 25 °C. At lower temperatures more LiCl (approx. 1 %) is necessary in order to dissolve some minimum amount of cellulose. As only one kind of pulp was investigated no general conclusion could be drawn from this study. It is also difficult to compare our results to the results of other groups as the activation procedure and measurement conditions were different. It should be remarked that in contrast to other authors [42, 52, 53] we specified the phases only as either isotropic or non-dissolved. In many cases the presence of liquid crystals was observed (in the non-dissolved region). However, due to the viscosity of the samples, it was not possible to differentiate well between non-dissolved sample and isotropic samples with liquid crystals or fibers.
Considering the choice of temperature it is clear that the solubility at the used conditions is enhanced by keeping the samples at 5 °C in comparison to 25 °C. This was also revealed by other authors e.g. [45, 51]. The maximum solubility in the solutions with the highest LiCl concentrations was about 8% at 25 °C and 10 % at 5 °C. The stability of the solutions was not proved by any other technique as the degradation in the LiCl/DMA/Cellulose system at these temperatures should be minimal [6]. In the mentioned study of Terbochevich et.al. [52] the authors used celluloses with lower molecular weight and report diluting the solutions in the tube in the case of viscosimetric measurements. This would not be possible in the case of most of our samples containing more than 3 % of cellulose. As reported in the section 4.5.2 at these concentrations the samples formed a gel that would not 'go into solution' even after considerable amount of additional solvent was added. This difference in the appearance of the samples might be explained by the different activation method and also the larger DP of the samples used here (about 1790 in comparison to the max. 760 presented in [52, 53]).

5.4.2 Water influence

The comparison of figs. 4.21a-c and 4.22a-c demonstrates that after three days the dissolution has not yet been completed. In this case we may talk about some kinetic phase diagrams because the equilibrium state is reached after long time. It should be noted that there is no distinct difference between the first two sample sets (0.5 % and 1 % of cellulose), whereas the most concentrated solutions behave very differently. The samples with 2 % of cellulose are already very sensitive to the water content, which suggests that this is near the limiting concentration where competition for LiCl between cellulose hydroxyl groups and water becomes very pronounced, and even small amounts of water exert a strong influence on the system.

Table 5.10: Parameters a and b resulting from the linear fit $y = a + b\,x$ describing the boundary between soluble and non-soluble samples in figs.5.9a-c.

% Cellulose	a	b
0.5	3.2	0.46
1.0	3.25	0.51
2.0	3.3	0.62

units: a in mmol.

With these results at hand we searched for ratios of the concentrations of the different components and the border lines in the phase diagrams which could help us to interpret the diagrams. The only relation found is between the mole numbers of water and the mole numbers of LiCl. The results are shown in figs. 5.9 a-c (on the x-axis the mole number of water is indicated, y-axis represents the mole number of LiCl). In these diagrams, the data points indicating dissolved and non-dissolved or transition samples fall into two regions, which are located on both sides of a separation line within the error limits. This line represents the linear fit of the data for the most water concentrated, but still isotropic samples at a given cellulose concentration in the mixture. The values of the parameters a and b corresponding to the different concentrations are given in table 5.10.

It becomes evident that the type of the separation lines is equal for all the measured samples, giving approximately straight lines with similar slopes. The presented 'parameters' do not account for the whole cellulose concentration range as the number of measured samples is small. However, the results can serve as a tool for estimating the maximal still tolerable water content at a certain LiCl concentration, so that dissolution of the required cellulose amount occurs. This is important as complete removal of water is not always possible. The size of parameter b suggests that when the water concentration in the solutions is so high that the ratio between LiCl and water is 1:2 the solubilization of cellulose does not take place any more. It seems that the present LiCl/DMA ion-pair or complex is destroyed or its capability to involve the hydroxyl groups strongly influenced by the presence of water.

As the question of preferential solvation of LiCl in water and DMA is not yet sufficiently cleared we can just suppose that a formation of a mixed complex of the general form $Li[(DMA)_x(H_2O)_y]Cl$ as discussed in previous section considering the DRS data of the LiCl/DMA/water system is responsible for the changes in the system. The formation of an aqueous $Li[(H_2O)_2]Cl$ complex does not seem very probable in this case. This complex should be formed at this temperature, however, at very high LiCl concentrations as shown in solubility studies of LiCl in water [199, 200]. The solid state should have the same composition. The conditions in our system do not correspond well to this situation.

In order to demonstrate the influence of water on the solubilization process the following interpretation was chosen. In figure 5.10 the minimum amount of LiCl necessary to dis-

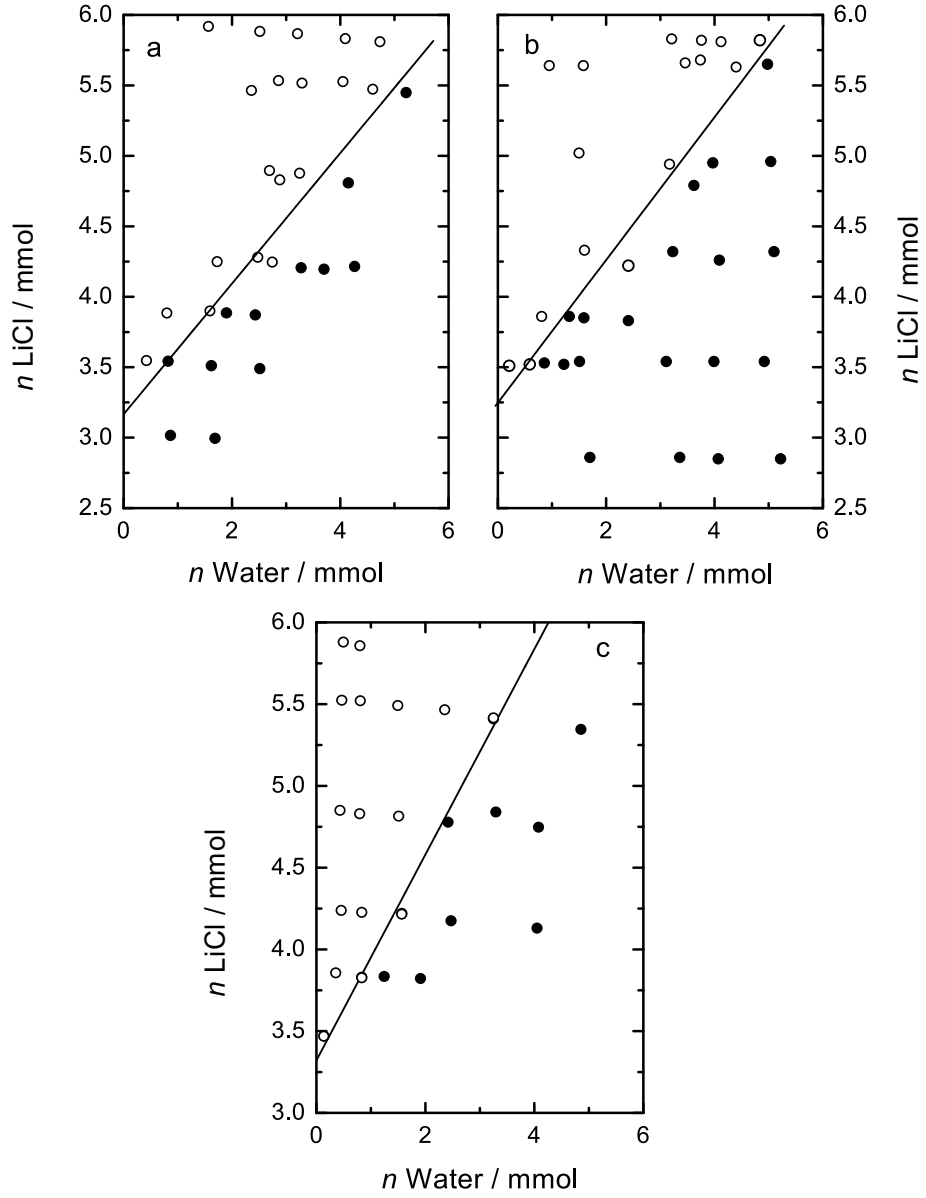

Figure 5.9: LiCl/Water molar ratio for samples of the system LiCl/DMA/Cellulose/Water with (a) 0.5 %, (b) 1.0 % and (c) 2.0 % cellulose. (○) symbolize the isotropic samples and (●) all others. The lines represent a boundary between the two regions in the graph.

Table 5.11: Parameters A and B resulting from the linear fit $y = A + Bx$ describing the boundary between soluble and non-soluble samples in fig. 5.10.

% Water	A	B
0.0	0.9	2.0
0.4	1.1	1.3
1.0	1.2	1.5
2.0	1.5	2.4

units: A in $\mathrm{mmol\,g^{-1}}$.

solve cellulose is indicated for various water contents. In the diagram isotropic samples with the highest water concentration are displayed with respect to the concentration of anhydroglucose and of LiCl in the mixtures. The concentration is expressed in mole numbers normalized to the weight of the sample. The amount of samples is small because only few samples with the same water content (tolerance 0.1%) were measured. It can be seen that the higher the water content the higher is the necessary LiCl concentration. This just justifies the previous observations. Similar to figs. 5.9a-c, the lines in fig. 5.10 represent linear fits according to $y = A + B\,x$. The values provide a qualitative overview of the characteristics of the system and are listed in table 5.11. Unfortunately no clear connection between the LiCl/DMA solvate and the present water content was found. This can be explained by the difficulties in defining the molecular weight of this complex and so its mole number. However, the importance of the presence of DMA should not be neglected.

Parameter A refers to the minimum amount of LiCl in the mixture necessary so that any dissolution takes place, $A \sim n(\mathrm{LiCl})_{\mathrm{min}}$. As expected it considerably increases with the growing water content in the samples. Even more interesting is the interpretation of parameter B that describes the ratio between LiCl and anhydroglucose unit (AGU), $B = n(\mathrm{LiCl})/n(\mathrm{anhydroglucose})$, necessary for the dissolution. Unfortunately the scatter of these values in the mixtures containing water is so pronounced that no quantitative conclusions can be drawn. In contrast, for the solutions prepared in anhydrous LiCl/DMA the number of points is sufficient to allow some interpretation. The corresponding value of parameter B is 2, which implies that twice as much LiCl is needed per AGU in order to dissolve the sample. This ratio is a little surprising as usually only one LiCl (or LiCl/DMA complex) is supposed to react with the accessible hydroxyl groups of cellulose. This was shown in studies with model substances, see [154]. In this case it would imply that two hydroxyl groups from each AGU are involved in the interaction.

As pointed out in the introduction section regarding cellulose properties and its dissolution in LiCl/DMA the dissolution mechanism in this solvent is not yet clear. As a non-degrading or non-derivatizing solvent for polysaccharides it is supposed to break down only the intermolecular and not the intramolecular hydrogen bonds in cellulose. The morphological

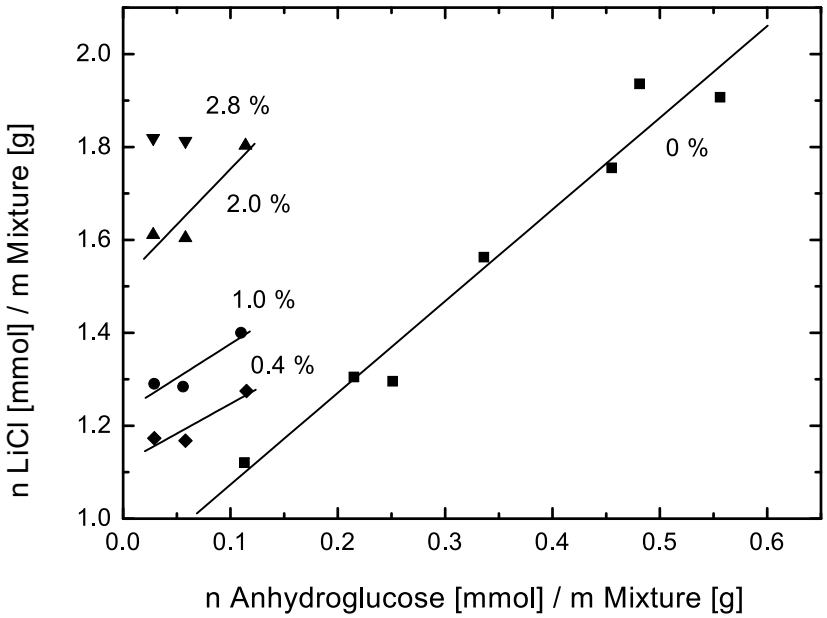

Figure 5.10: The molar ratio between LiCl and the anhydroglucose at different water concentrations which leads to the minimum concentration of LiCl necessary for the dissolution of cellulose.

structure should not be affected in this solvent either. So if two LiCl/DMA complexes react with the AGU this should result from the presence of two intermolecular hydrogen bonds. However, the crystalline modification of native cellulose (cellulose I) is usually described by the presence of two intra- and one intermolecular hydrogen bond, see [19]. In our case, nevertheless, it seems that at least some part of the intramolecular structure is influenced by the solvent system or that the hydrogen-bond structure in the solution is different from the crystalline state.

Chapter 6

Conclusions

The present study dealt with the investigation of the structure and dynamics of LiCl solutions in N,N-dimethylacetamide (DMA) by dielectric relaxation spectroscopy (DRS). Some rather exploratory DRS measurements were provided also on aqueous solutions of LiCl and mixtures of LiCl in water and DMA. Since the studied system is frequently utilized as a non-degrading solvent system for cellulose and other polysaccharides, several phase diagrams of cellulose in LiCl/DMA system were performed here as well. The results obtained from the analysis of the dielectric properties can be summed up as follows.

LiCl in anhydrous DMA

Solutions of LiCl in DMA were examined over the entire concentration range by DRS in the frequency range $0.2 \leq \nu/\text{GHz} \leq 89$ at 278, 298, 318 and 338 K. The obtained spectra were fitted at first by a superposition of four Debye processes. This interpretation, however, proved not to be consistent at all temperatures and therefore the combination of a Cole-Cole (CC) and two Debye (D) processes was chosen. The two high-frequency Debye processes were assigned to the solvent, whereas the low-frequency relaxation process could be attributed to the formation of solvated LiCl ion pairs.
The effective solvation numbers, representing the number of irrotationally bound DMA molecules, were obtained from the sum of the solvent amplitudes by the application of the modified Cavell equation. They were ascribed to Li^+ as Cl^- is supposed to remain unsolvated in DMA. The solvation shell of the cation undergoes considerable changes with increasing LiCl concentration in the system. The obtained effective solvation numbers decrease from *ca.* 6 at the infinite dilution to the value of 3 near the saturation limit. This indicates the presence of a direct interaction between Li^+ and Cl^- in concentrated solutions.
The CC process describing the low-frequency region exhibits a very broad relaxation time distribution. This seems to be a special feature of LiCl/DMA solutions. From the resulting dispersion amplitude of the solute relaxation process the ion-pair concentration was deduced. In the calculations ionic species of different geometries were assumed. The corresponding association constants were then obtained from the overall stability constants and

compared to the literature data. Additionally, the structures of possibly occurring complexes were calculated by the help of the semi-empirical PM3 method as $[Li(DMA)_x]Cl$, where $1 \leq x \leq 6$. The calculations predicted the complex $[Li(DMA)_3]Cl$ as the most stable species. The obtained association constants combined with the other features of this system led to the conclusion that LiCl/DMA solutions exhibited a broad concentration and temperature dependent distribution of ionic species. This observation seems to elucidate the fact that the dissolution of cellulose in LiCl/DMA solutions takes place only in a certain concentration range as demonstrated in our phase diagrams.

The analysis of the relaxation time and association constants showed that the presence of solvent separated ion pairs could be excluded. Thus at low concentrations the formation of solvent-shared ion pairs (SIP) takes place, whereas at high LiCl concentrations these are replaced by the contact ion pairs (CIP). Additionally a new species, the so called penetrating solvent-shared ion pair (PSIP), was introduced. PSIP was obtained from MOPAC calculations and described the dielectric properties of the system in the best way. It could be interpreted as an 'intermediate form' between SIP and CIP species.

LiCl in water

DRS spectra of aqueous LiCl solutions were measured at 298 K in the concentration range $0.1 \lesssim c \ / \ \mathrm{mol\,L^{-1}} \lesssim 1$. The spectra were interpreted by the D+D fit. The low-frequency process could be attributed to a weak association resulting from the formation of a solvent-shared ion pair yielding a very small association constant. The high-frequency relaxation process was ascribed to the cooperative relaxation of bulk water. Its dispersion amplitude was evaluated in the form of effective hydration numbers. Since the residence time of Cl^- in the hydration shell is comparable to the residence time of water molecules in the bulk, the resulting hydration numbers were ascribed to the cation. The values suggested the presence of *ca.* 6 to 8 water molecules in the solvation shell of lithium in the dilute region.

LiCl in the mixed solvent system DMA/water

The measurements on the LiCl/DMA/water system were performed as an exploratory study for a concentrated LiCl/DMA solution diluted by different amounts of water. The spectra were fitted by D+D+D+D model that resulted in the appearance of a new relaxation process with a dispersion amplitude strongly dependent on the water content in the solutions.

The amplitudes resulting from the two solvent relaxation processes decrease with increasing water concentration. However, this seems to result from the decreasing concentration of DMA in the system on the whole. The amplitude of the first ion-pair relaxation process decreases also significantly but this can be caused by the dilution of water leading to lower LiCl concentration. The new relaxation process appearing in the spectra is probably related to the formation of a mixed solvation complex with LiCl of a general form $[Li(DMA)_x(H_2O)_y]Cl$.

Cellulose studies

In the present work five phase diagrams of cellulose in the solvent system LiCl/DMA were established dealing with the influence of water and temperature on the dissolution. The first study proved that under the activation and dissolution conditions used, the lower temperature (278 K) was preferable in order to reach higher maximum solubility. At 278 K 10 wt% of cellulose could be dissolved at the highest possible LiCl concentration, in contrast to 8 wt% at 298 K. Nevertheless, the minimum amount of LiCl necessary for the dissolution increased with decreasing temperature. At the lower temperature it was possible to dissolve some cellulose only at c(LiCl) $\gtrsim$ 4 wt%, whereas at 298 K already 3 wt% were sufficient to dissolve some minimum amount of cellulose. This is in a good agreement with the DRS-results that suggest a different species distribution at low and high LiCl concentrations.
In the case of water-containing samples, the maximum water content in the samples that did not lead to precipitation or liquid crystal formation was always below 3 wt%. The minimum necessary concentration of LiCl in DMA increased strongly with increasing water concentration. Thus the relation between the concentration of water and LiCl in the samples seems to be the most important factor for the dissolution in this case. The maximum mole ratio between water and LiCl in the measured samples at which solubilization still occurred was 2:1. This implies that as soon as more than two water molecules per LiCl molecule are present the concentration of the salt is not sufficient for the complete dissolution of cellulose. This fact results probably from the formation of a mixed solvent complex as proposed in the DRS-studies or the decreased availability and basicity of Cl^- due to its solvation by water.
A relation between LiCl concentration and anhydroglucose unit (AGU) in cellulose was established as well. For samples in anhydrous LiCl/DMA solutions this ratio was 2:1. This suggests that the interaction of two LiCl with one AGU is required. This should result from the break down of two hydrogen bonds in the cellulose samples.

Prospects for future

In the next future several phase diagrams with different cellulose samples and water contents should be performed. These experiments would allow to draw some general quantitative conclusions concerning the ratio between LiCl and water or LiCl and AGU, respectively. This should help us to get a more precise description of the dissolution mechanism of cellulose in this solvent.
Furthermore, the samples in anhydrous LiCl/DMA solutions with low viscosity should be examined by means of TDR. Since this method reflects sensitively the dipole moment structural changes, the investigation of probes with composition near to the phase boundaries should determine if Cl^- was involved in the interaction with cellulose hydroxyl groups. The analysis of the relaxation pattern should also lead to a better understanding of the role of DMA in the dissolution process.

Bibliography

[1] D. Klemm, B. Philipp, T. Heinze, U. Heinze and W. Wagenknecht, *Comprehensive Cellulose Chemistry*, VCH, Weinheim, Germany, 1998.

[2] H. A. Kraessig, *Cellulose. Structure, Accesibility and Reactivity.*, Gordon Breach Science Publishers Yverdon, 1993.

[3] *Ullmann's Encyclopedia of Industrial Chemistry*, 5^{th} Ed., Vol. A5, VCH Weinheim, 1986.

[4] C. L. McCormick and D. K. Lichatowich, *J. Polymer Sci., Polymer Lett.*, 1979, **17**, 479-484.

[5] A. M. Striegel, *Carbohyd. Polym.*, 1997, **34**, 267-274.

[6] T.R. Dawsey and C.L. McCormick, *J. Macrom. Sci. Rev. Macrom. Chem. Phys.*, 1990, **C30**, 405-440.

[7] B. Morgenstern and H. W. Kammer, *Trends Polym. Sci.*, 1996, **4**, 87-92.

[8] A. Potthast, T. Rosenau, J. Sartori, H. Sixta and P. Kosma, *Polymer*, 2003, **44**, 7-17.

[9] J. P. Runt and J.J. Fitzgerald (ed.), *Dielectric Spectroscopy of Polymeric Materials: Fundamentals and Applications*, ACS, Washington, DC, 1997.

[10] D. Q. M. Craig, *Dielectric Analysis of Pharmacetical Systems*, Taylor and Francis, 1995.

[11] G. Smith, A. Duffy, J. Shen and C.J. Olliff, *J. Pharm. Sci.*, 1995, **84**, 1029-1044.

[12] K. Asami, *Prog. Polym. Sci.*, 2002, **27**, 1617-1659.

[13] J. Barthel and R. Buchner, *Chem. Soc. Rev.* , 1992, **21**, 263-270.

[14] J. Barthel, R. Buchner, and B. Wurm, *J. Mol. Liq.*, 2002, **98-99**, 51-69.

[15] B. Wurm, M. Münsterer, J. Richardi, R. Buchner and J. Barthel, *J. Mol. Liq.*, in press.

[16] T. P. Nevell and S. H. Zeronian (ed.), *Cellulose Chemistry and Its Applications*, Ellis Horwood Limited, England, 1985.

[17] O. Ellefsen, B. A. Tonnesen, in N. M. Bikales, L. Segal (eds.), *Cellulose and Cellulose Derivatives*, Wiley-Interscience, New York London Toronto, Part IV, 1971, 151-180.

[18] A.J. Mitchell and H.G. Higgins, *Tetrahedron*, 1965, **21**, 1109-1120.

[19] K.H. Gardner and J. Blackwell, *Biopolym.*, 1974, **13**, 1975-2001.

[20] F.J. Kolpak and J. Blackwell, *Macromol.*, 1976, **9**, 273-278.

[21] P. Zugenmaier, *Papier, Bingen*, 1989, **43**, 658-664.

[22] W. Berger, M. Keck and B. Philipp, *Cellulose Chem. Technolog.*, 1988, **22**, 387-397.

[23] J. W. S. Hearle, *J. Polymer Sci.*, 1958, **28**, 432-435.

[24] H. -P. Fink and E. Walenta, *Papier(Darmstadt)*, 1994, **48**, 739-748.

[25] a) H. Mark and K. H. Meyer, *Z. Phys. Chem.*, 1929, **B2**, 115-145; b) K. H. Meyer and L. Misch, *Helv. Chim. Acta*, 1937, **20**, 232-244.

[26] K. R. Andress, *Z. Phys. Chem.*, 1929, **34**, 190-206.

[27] A. Sarko and R. Muggli, *Macromolecules*, 1974, **7**, 486-494.

[28] H. Yamamoto and F. Horii, *Macromolecules*, 1993, **26**, 1313-1317.

[29] F. J. Kolpak, M. Weih and J. Blackwell, *Polymer*, 1978, **19**, 123-131.

[30] A. N. J. Heyn, *Cell. Biol.*, 1966, **29**, 181-197.

[31] H. -P. Fink, D. Hofmann and H. J. Purz, *Acta Polym.*, 1990, **41**, 131-137.

[32] A. F. Turbak, R. B. Hammer, E. R. Davies and H. L. Hegert, *Chem. Tech.*, 1980, **10**, 51-57.

[33] B. Philipp, H. Schleicher and H. Wagenknecht, *Cellul. Chem. Technol.*, 1978, **12**, 529-552.

[34] W. Berger, V. Kabrelian, M. Keck, J. Kressler, K. Herzog, D. Mun Sang and B. Philipp, *Acta Polym.*, 1990, **41**, 25-31.

[35] H. Leipner, S. Fischer, E. Brendler and K. Fischer, *Macromol. Chem. Phys.*, 2000, **201**, 2041-2049.

[36] R. P. Swatloski, S. K. Spear, J. D. Holbrey and R. D. Rogers, *J. Am. Chem. Soc.*, 2002, **124**, 4974-4975.

[37] H. Herlinger and M. Hengstberger, *Lenzinger Ber.*, 1985, **59**, 96-104.

[38] A. F. Turbak, A. Sakthivel, *CHEMTECH*, 1990, **20**, 444-446.

[39] A. F. Turbak, *Tappi J.*, 1984, **67**, 94-96.

[40] B. Morgenstern and W. Berger, *Acta. Polymer.*, 1993, **44**, 100-102.

[41] C. L. McCormick and P. A. Callais, *Polymer*, 1987, **28**, 2317-2323.

[42] G. Conio, P. Corazza, E. Bianchi, A. Tealdi and A. Ciferri, *J. Polymer Sci., Part C: Polym. Letters*, 1984, **22**, 273-277.

[43] C. L. McCormick, P. A. Callais and B. H. Hutchinson Jr., *Macromolecules*, 1985, **18**, 2394-2401.

[44] T. Rosenau, A. Potthast, A. Hofinger, H. Sixta and P. Kosma, *Holzforsch.*, 2001, **117**, 1-6.

[45] A.-L. Dupont, *Polymer*, 2003, **44**, 4117-4126.

[46] E. Sjöholm, K. Gustafsson, B. Eriksson, W. Brown and A. Colmsjö, *Carbohyd. Polym.*, 2000, **41**, 153-161.

[47] S. Chrapava, D. Touraud, T. Rosenau, A. Potthast and W. Kunz, *Phys. Chem. Chem. Phys.*, 2003, **5**, 1842-1847.

[48] T. Matsumoto, D. Tatsumi, N. Tamai and T. Takaki, *Cellulose*, 2001, **8**, 275-282.

[49] J. Roehrling, A. Potthast, T. Rosenau, T. Lange, A. Borgards, H. Sixta and P. Kosma, *Biomacromol.*, 2002, **3**, 959-975.

[50] A. Potthast, T. Rosenau, R. Buchner, T. Röder, G. Ebner, H. Bruglachner, H. Sixta and P. Kosma, *Cellulose*, 2002, **9**, 41-53.

[51] T. Roeder, B. Morgenstern, N. Schelosky and O. Glatter, *Polymer*, 2001, **42**, 6765-6773.

[52] M. Terbojevich, A. Cosani, G. Conio, A. Ciferri and E. Bianchi, *Macromolecules*, 1985, **18**, 640-646.

[53] E. Bianchi, A. Ciferri, G. Conio, A. Cosani and M. Terbojevich, *Macromolecules*, 1985, **18**, 646-650.

[54] A. El-Kafrawy, *J. Appl. Polym. Sci.*, 1982, **27**, 2435-2443.

[55] B. Morgenstern, H. W. Kammer, W. Berger and P. Skrabal, *Acta. Polymer.*, 1992, **43**, 356-357.

[56] J. C. Maxwell, *A Treatise in Electricity and Magnetism*, Clarendon Press, Oxford, 1881.

[57] G. S. Greschner, *Maxwellgleichungen*, Hüthig, Basel, 1981.

[58] C. F. J. Böttcher, P. Bordewijk, *Theory of electric polarisation*, 2nd ed., Vol. 2, Elsevier, Amsterdam, 1978.

[59] H. Falkenhagen, *Theorie der Elektrolyte*, Hirzel, Leipzig, 1971.

[60] K. Ghowsi and R. J. Gale, *J. Electrochem. Soc.*, 1989, **136**, 2806-2811.

[61] J. Barthel, R. Buchner and H. Steger, *Wiss. Zeitschr. THLM* , 1989, **31**, 409-423.

[62] R. H. Cole, *Annu. Rev. Phys. Chem.* , 1977, **28**, 283-300.

[63] P. Debye, *Polar Molecules*, Dover Publ., New York, 1930.

[64] H. Pellat, *Ann. Chim. Phys.*, 1899, **18**, 150-181.

[65] K. S. Cole and R. H. Cole, *J. Chem. Phys.*, 1941, **9**, 341-351.

[66] K. S. Cole and R. H. Cole, *J. Chem. Phys.*, 1942, **10**, 98-105.

[67] D. W. Davidson and R. H. Cole, *J. Chem. Phys.*, 1950, **18**, 1417.

[68] D. W. Davidson and R. H. Cole, *J. Chem. Phys.*, 1951, **19**, 1484-1490.

[69] S. Havriliak and S. Negami, *J. Polym. Sci., Part C*, 1966, **14**, 99-117.

[70] L. Onsager, *J. Am. Chem. Soc.*, 1936, **58**, 1486-1493.

[71] E. A. S. Cavell, P. C. Knight and M. A. Sheikh, *J. Chem. Soc. Faraday Trans.*, 1971, **67**, 2225-2233.

[72] J. Barthel, H. Hetzenauer and R. Buchner, *Ber. Bunsenges. Phys. Chem.*, 1992, **96**, 1424-1432.

[73] T. G. Scholte, *Physica*, 1949, **15**, 437-449.

[74] J. G. Kirkwood, *J. Chem. Phys.*, 1939, **7**, 911-919.

[75] H. Fröhlich, *Theory of dielectrics*, 2nd ed., Oxford University Press, Oxford, 1965.

[76] P. Debye, *Polar molecules*, Dover Publ., New York, reprint of 1st edition, 1929.

[77] J. G. Powles, *J. Chem. Phys.*, 1953, **21**, 633-637.

[78] S. H. Glarum, *J. Chem. Phys.*, 1960, **33**, 639-643.

[79] T. F. Keynes and D. Kivelson, *J. Chem. Phys.*, 1971, **56**, 1057-1065.

[80] D. Kivelson and P. Madden, *Mol. Phys.*, 1975, **30**, 1749-1780.

[81] D. Kivelson and P. Madden, *J. Chem. Phys.*, 1984, **88**, 6557-6559.

[82] J. C. Dote, D. Kivelson and R. N. Schwartz, *J. Chem. Phys.* , 1981, **85**, 2169-2180.

[83] J. Barthel, R. Buchner, P.-N. Eberspächer, M. Münsterer, J. Stauber, and B. Wurm, *J. Mol. Liq.*, 1998, **78**, 83-109.

[84] U. Kaatze, *J. Solution. Chem.*, 1997, **26**, 1049-1112.

[85] J.B. Hubbard, and L. Onsager, *J. Chem. Phys.*, 1977, **67**, 4850-4857.

[86] J.B. Hubbard, *J. Chem. Phys.*, 1978, **68**, 1649-1664.

[87] J.B. Hubbard, P. Colonomos and P. G. Wolynes, *J. Chem. Phys.*, 1979, **71**, 2652-2661.

[88] W. J. Moore und D. O. Hummel, *Physikalische Chemie*, de Gruyter, Berlin, 1986.

[89] D.R. Lide (ed.), *CRC Handbook of Chemistry and Physics*, 77th ed., CRC Press, Boca Raton, 1996.

[90] O. Kratky, H. Leopold and H. Stabinger, *Z. Angew. Phys.*, 1969, **27**, 273-277.

[91] J. Barthel, R. Wachter, and H.-J. Gores, in: B.E. Conway and J.O'M. Bockris (eds.), *Modern Aspects of Electrochemistry*, vol. 13, p. 1, Plenum, New York, 1979.

[92] J. Barthel, K. Bachhuber, R. Buchner, H. Hetzenauer and M. Kleebauer, *Ber. Bunsenges. Phys. Chem.*, 1991, **95**, 853-859.

[93] R. Buchner and J. Barthel, *J. Mol. Liq.*, 1995, **63**, 55-75.

[94] T.J. Buchanan, *Proc. IEEE Part III*, 1952, **99**, 61.

[95] R. Buchner and J. Barthel, *Annu. Rep. Prog. Chem., Sect. C*, 1994, **91**, 71.

[96] R. Buchner and J. Barthel, *Annu. Rep. Prog. Chem., Sect. C*, 2001, **97**, 349-382.

[97] H. Fellner-Feldegg, *J. Phys. Chem.*, 1969, **73**, 616-623.

[98] H. Fellner-Feldegg, *J. Phys. Chem.*, 1972, **76**, 2116-2122.

[99] R. H. Cole, J. G. Berberian, S. Mashimo, G. Chryssikos, A. Burns and E. Tombari, *J. Appl. Phys.*, 1989, **66**, 793-802.

[100] R. H. Cole, *J. Phys. Chem.*, 1975, **79**, 1469-1474.

[101] R. H. Cole, S. Mashimo and P. Winsor, *J. Phys. Chem.* 1980, **84**, 786-793.

[102] C. Hoelzl *PhD. Thesis*, Regensburg 1998.

[103] R. Buchner, and J. Barthel, *Ber. Bunsenges. Phys. Chem.*, 1997, **101**, 1509-1516.

[104] C. Baar, *Master Thesis*, Regensburg, 1997.

[105] D.W. Marquardt, *J. Soc. Ind. Appl. Math.*, 1963, **11**, 431-441.

[106] J. Barthel and H.-J. Gores, *Solution Chemistry: A Cutting Edge in Modern Electrochemical Technology*, ed. G. Mamantov and A.J. Popov, *Chemistry of Nonaqueous Solutions – Current Progress*, VCH, New York, 1994.

[107] K. Weissermel and H.-J. Arpe, *Industrial Organic Chemistry*, 2nd Ed., VCH, Weinheim 1993.

[108] K. A. Krieger and M. Kilpatrick, *J. Am. Chem. Soc.*, 1937, **59**, 1878-1883.

[109] D.A. Macinnes, T. Shedlovsky and L.G. Longworth, *J. Am. Chem. Soc.*, 1932, **54**, 2758-2762.

[110] J.A.N. Friend and A. T. W. Colley, *J. Chem. Soc.*, 1931, 3148-3149.

[111] K.H. Popp, *PhD. Thesis*, Regensburg 1986.

[112] Y-Z. Wei and S. Sridhar, *J. Chem. Phys.*, 1990, **92**, 923-928.

[113] R. Buchner, J. Barthel and J. Stauber, *J. Chem. Phys. Lett.*, 1999, **306**, 57-63.

[114] T. Chen, G. Hefter and R. Buchner, *J. Phys. Chem. A*, 2003, **107**, 4025-4031.

[115] R. Buchner, G.T. Hefter and P.M. May, *J. Phys. Chem. A*, 1999, **103**, 1-9.

[116] H. Kohner, *Z. Phys. Chem. B*, 1928, **6**, 427-455.

[117] C. P. Rao, P. Balaram and C. N. R. Rao, *J. Chem. Soc. Faraday Trans. 1*, 1980, **76**, 1008.

[118] D. Balasubmarian and R. Shaikh, *Biopolymers*, 1973, **12**, 1639-1650.

[119] G. Gsaller and G. Gritzner, *Z. Phys. Chem.*, 1983, **138**, 137-155.

[120] M.J. Adams, C.B. Baddiel, G.E. Ellisand, R.G. Jones and A. J. Matheson, *J. Chem. Soc., Faraday Trans. 2*, 1974, **70**, 1114-1120.

[121] M.J. Adams, C.B. Baddiel, G.E. Ellisand, R.G. Jones and A. J. Matheson, *J. Chem. Soc., Faraday Trans. 2*, 1975, **71**, 1823-1828.

[122] E.R. Stimson and E.E. Schrier, *J. Chem. Eng. Data*, 1974, **19**, 354-358.

[123] J.F. Hinton, A. Beeler, D. Harpool and R.W. Briggs and A. Pullman, *Chem. Phys. Lett.*, 1977, **47**, 411-415.

[124] A. Gupta and C.N.R. Rao, *J. Phys. Chem.*, 1973, **77**, 2888-2896.

[125] R.H. Staley and J. L. Beauchamp, *J. Am. Chem. Soc.*, 1975, **97**, 5920-5921.

[126] B. Wurm, *Phd. Thesis*, Regensburg 1998.

[127] J. Barthel, H. Hetzenauer and R. Buchner, *Ber. Bunsenges. Phys. Chem.*, 1992, **96**, 1424-1432.

[128] R. Buchner, S.G. Capewell, G.T. Hefter and P.M. May, *J. Phys. Chem. B*, 1999, **103**, 1185-1192.

[129] J. Barthel and I. Beer, unpublished results.

[130] N. S. Poonia and A. V. Bajaj, *Chem. Rev.*, 1979, **79**, 389-445.

[131] U. Olsher, R.M. Izatt, J.S. Bradshaw and N. K. Dalley, *Chem. Rev.*, 1991, **91**, 137-164.

[132] J. Barthel, H. Krienke and W. Kunz, *Physical Chemistry of Electrolyte Solutions*, 1998 Steinkopff Verlag, Darmstadt.

[133] R.C. Paul, J.S. Banait and S. P. Narula, *Austr. J. Chem.*, 1975, **28**, 321-326.

[134] D. Das, B. Das and D.K. Hazra, *J. Solution Chem.*, 2002, **31**, 425-431.

[135] C.N.R. Rao, V. V. Bhujle, A. Goel, U. R. Bhat and A. Paul, *J. Chem. Soc. Chem. Commun.*, 1973, 161-162.

[136] a) P. Tarte, *Spectr. Acta*, 1965, **21**, 313-319. b) P. Tarte, *J. Inorg. Nucl. Chem.*, 1967, **29**, 915-923. c) P. Tarte and J. Preudhomme, *Spectr. Acta*, 1970, **26A**, 747-754.

[137] C.N.R. Rao, H.S. Randhawa, N.V.R. Reddy and D. Chakravorty, *Spectrochim. Acta, Part A*, 1975, **31**, 1283-1291.

[138] V.P. Anosov, T.N. Komogorova, I.T. Ovechenko, A.K. Dibrova and M.V. Shablygin, *Zh. Fiz. Khim.*, 1990, **64**, 124-128.

[139] V.M. Ryabikova, B.S. Krumgal´z, and K.P. Mishchenko, *Russ. J. Phys. Chem.* **45**, (1971) 1451.

[140] J.F. Hinton and E.S. Amis, *Chem. Rev.*, 1971, **71**, 627-675.

[141] C. Lassaigne and P. Baine, *J. Phys. Chem.*, 1971, **75**, 3188-3190.

[142] C. P. Rao, A. M. Rao and C. N. R. Rao, *Inorg. Chem.*, 1984, **23**, 2080-2085.

[143] W.E. Bull, S.K. Madan, and J. E. Willis, *Inorg. Chem.*, 1963, **2**, 303-306.

[144] P. Chakrabarti, K. Venkatesan and C. N. R. Rao, *Proc. R. Soc. Lond. A.*, 1981, **375**, 127-153.

[145] T. Asahara, K. Ikeda and N. Yoda, *J. Chem. Sci. A 1*, 1968, **6**, 2489-2499.

[146] T. Megyes, unpublished results.

[147] I. A. Shoshina, E. M. Borulidina, L. I. Gulyaeva, B. K. Filanovskii, M. S. Grilikhes and A. L. Rotinyan, *Sov. Electrochem.*, 1980, **16**, 1031-1033.

[148] J. Barthel, J.-H. Gores, G. Schmeer and R. Wachter, *Topp. Curr. Chem.*, 1983, **111**, 33-144.

[149] N.K. Pyper, C. G. Pike and P.P. Edwards, *Mol. Phys.*, 1992, **72**, 353-372.

[150] J.I. Kim, *Z. Phys. Chem. NF*, 1978, **113**, 129-150.

[151] J. H. Gibbs, C. Cohen, P. D. Flemming and H. Porosoff, in R. L. Kay (ed.) *The Physical Chemistry of Aqueous Systems*, Plenum, New York, 1973.

[152] J. B. Hasted, in F. Franks (ed.) *Water, a Comprehensive Treatise*, Vol. 1, Plenum, New York, 1972.

[153] E. S. Rittner, *J. Chem. Phys.*, 1951, **19**, 1031.

[154] J. Saint Germain and M. Vincendon, *Org. Magn. Res.*, 1983, **21**, 371-375.

[155] J. J. P. Stewart, *J. Comput. Mol. Design*, 1990, **4**, 1-105.

[156] A.V. Yakimanskii, A.M. Bochek, V.A. Zubkov and G.A. Petropavlovskii, *Zh. Prikl. Khim.*, 1993, **66**, 2829-2832.

[157] N.G. Tsygankova, D.D. Grinshpan and A.O. Koren, *Cellulose Chem. Technol.*, 1996, **30**, 353-357.

[158] J. O´M. Bockris and A.K.N. Reddy, *Modern Electrochemistry 1. Ionics*, 2nd ed., Plenum Press, New York, 1998.

[159] J. Barthel and R. Neueder, *Electrolyte Data Collection. Part 1 g: Conductivities, Transference Numbers, and Limiting Ionic Conductivities of Protophilic H-Bond Donor and Aprotic Solvents, I: Amides*, in: G. Kreysa (ed.), *Chemistry Data Series*, Vol. XII, Dechema, Frankfurt, 2001.

[160] D.W. James and R.E. Mayes, *J. Phys. Chem.*, 1984, **88**, 637-642.

[161] J.L. Dote and D. Kivelson, *J. Phys. Chem.* 1983, **87**, 3889-3893.

[162] W.E. Waghorne, A.J.I. Ward, T.G. Clune and B.G. Cox, *J. Chem. Soc. Faraday Trans. 1*, 1980, **76**, 1131-1137.

[163] H. Ohtaki and T. Radnai, *Chem. Rev.*, 1993, **93**, 1157-1204.

[164] Y. Marcus, *Ion Solvation*, 1986, John Willey and Sons Ltd.

[165] P.R. Smirnov and V. N. Trostin, *Russ. J. Phys. Chem.*, 1993, **67**, 1259-1263.

[166] J.E. Enderby, S. Cummings, G.J. Herdman, G.W. Neilson, P. S. Salmon and N. Skipper, *J. Phys. Chem.*, 1987, **91**, 5851-5858.

[167] J.R. Newsome, G.W. Neilson and J.E. Enderby, *J. Phys. Part C*, 1980, **13**, 923-926.

[168] R. W. Creekmore and C. N. Reilly, *J. Phys. Chem.*, 1969, **74**, 1563.

[169] J. Vorgin, P.S. Knapp, W.L. Flint, A. Anton, G. Highberger and E.R. Malinowski, *J. Chem. Phys.*, 1971, **54**, 176-181.

[170] S. H. Lee and J. C. Rasiah, a) *J. Chem. Phys.*, 1994, **101**, 6964-6974.

[171] S. H. Lee and J. C. Rasiah *J. Phys. Chem.*, 1996, **100**, 1420-1425.

[172] M. Mezei and D.L. Beveridge, *J. Phys. Chem.*, 1981, **74**, 6902-6910.

[173] E. Clementi and R. Barsotti, *Chem. Phys. Lett.*, 1978, **59**, 21-25.

[174] C.C. Pye, *Int. J. Quant. Chem.*, 2000, **76**, 62-76.

[175] A. Tongraar, K.R. Liedl and B.M. Rode, *Chem. Phys. Lett.*, 1998, **286**, 56-64.

[176] R. W. Impey, P. A. Maden and J.R. McDonald, *J. Phys. Chem.*, 1983, **87**, 5071-5083.

[177] M. R. Reddy and M. Berkowitz, *J. Chem. Phys.*, 1988, **88**, 7104-7110.

[178] G.H. Haggis, J. B. Hasted and T.J. Buchanan, *J. Chem. Phys.*, 1952, **20**, 1452-1465.

[179] A.G. Novikov, M.N. Rodnikova, V.V. Savostin and O.V. Sobolev, *J. Mol. Liq.*, 1999, **82**, 83-104.

[180] S. Obst, and H. Bradaczek, *J. Phys. Chem.*, 1996, **100**, 15677-15687.

[181] C. F. Mattina and R. M. Fuoss, *J. Phys. Chem.*, 1975, **79**, 1604-1610.

[182] M.R. Islam, I. Ahmad and A. A. Ansari, *J. Electrochem. Soc.*, 1989, **136**, 1303-1308.

[183] G. Gritzner and K.H. Stellnberger, *J. Chem. Soc. Faraday Trans.*, 1992, **88**, 3013.

[184] J. Burgess, in *Ions in solution*, Ellis Horwood Lim., Chichester 1988, p. 51-61.

[185] Y. Marcus, *J. Chem. Soc. , Faraday Trans. 1*, 1987, **83**, 339-349.

[186] R.C. Paul, J.S. Banait and S. P. Narula, *J. Electroanal. Chem.*, 1975, **66**, 111-115.

[187] R.A. Craig and R. E. Richards, *J. Chem. Soc. , Faraday Trans. 1*, 1963, **59**, 1972-1982.

[188] V. Gutmann, M. Michlmayr and G. Peychal-Heiling, *Anal. Chem.*, 1968, **40**, 619-623.

[189] R.R. Bessette and D. F. Harwood, *Analytica Chim. Acta*, 1973, **66**, 105-111.

[190] M. Ferriol, A. Siblini and G. Noyel, *J. Mol. Liq.*, 1995, **63**, 239-249.

[191] S.M. Puranik, A. C. Kumbharkhane and S. C. Mehrota, *J. Mol. Liq.*, 1991, **50**, 143-153.

[192] R.C. Petersen, *J. Phys. Chem.*, 1960, **64**, 184-185.

[193] P. Assarson and F.R. Eirich, *J. Phys. Chem.*, 1968, **72**, 2710-2719.

[194] M.I. Davis and M. E. Hernandez, *J. Chem. Eng. Data*, 1995, **40**, 674-678.

[195] A. Pal and Y.P. Singh, J. Chem. Eng. Data, 1995, **40**, 818-822.

[196] D.B. Henson and C. A. Swenson, *J. Phys. Chem.*, 1973, **77**, 2401-2406.

[197] C.M. Kinart, W.J. Kinart, A. Bald and A. Szejgis, *Phys. Chem. Liq.*, 1995, **30**, 151-157.

[198] T. Takamuku, D. Matsuo, M. Tabata, T. Yamaguchi and N. Nishi, *J. Phys. Chem. B*, 2003, **107**, 6070-6078.

[199] J. A. N. Friend and A. T. W. Colley, *J. Chem. Soc.*, 1931, 3148-3149.

[200] H. E. Moran Jr., *J. Phys. Chem.*, 1956, **60**, 1666-1667.